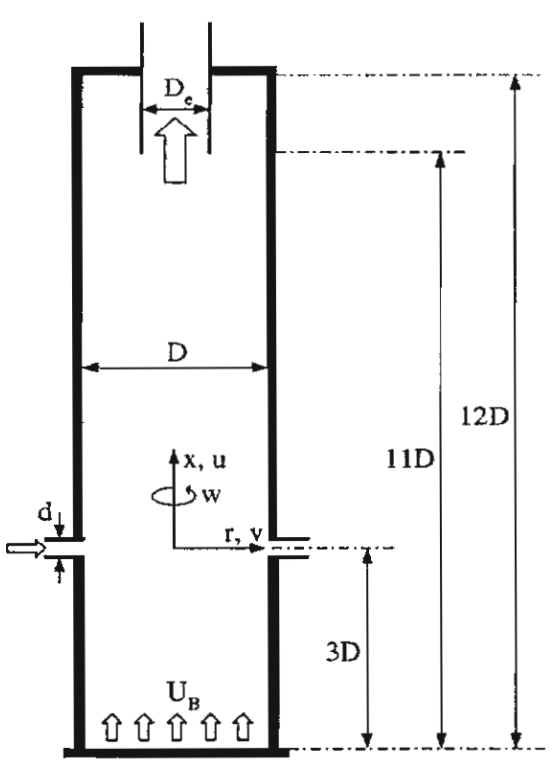
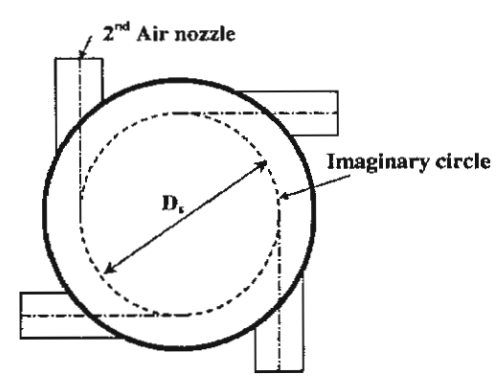
การทดลองของ Lin et. at. (1998) ไม่ได้บอกค่าความเร็วอากาศปฐมภูมิกับอากาศทุติยภูมิ ที่ทางเข้าทั้งสอง ดังนั้นเงื่อนไขทางเข้าสำหรับความเร็วในแนวสัมผัส (w) หาได้โดยการ ประมาณนอกช่วง (extrapolated) จากค่าความเร็วของผลการทดลอง ส่วนความเร็วในแนวแกน



รูปที่ 6.30 ลักษณะเตาฟลูอิดไดช์เบดแบบฉีดอากาศทุติยภูมิด้านข้าง (VFBC) ของ Lin *et. al.* (1998) และ computational domain



รูปที่ 6.31 Imaginary circle และ การจัดวาง secondary air injection nozzles

(U<sub>B</sub>) และความเร็วในแนวรัศมี (V<sub>j</sub>) หาได้จากความสัมพันธ์ระหว่างอัตราการใหลของอากาศปฐม ภูมิกับอากาศทุติยภูมิ ซึ่งหาได้จากสมการดังนี้

$$U_B = Q_r \times \frac{4w}{D_s} \times \frac{d_0^2}{D}$$
$$V_j = w \frac{\sqrt{D_s^2 + D^2}}{D_s}$$

$$l = \frac{d_0^2}{\sqrt{D_s^2 + D^2}}$$

โดยที่  $Q_r$  เป็นอัตราส่วนการฉีด ( $Q_r = Q_B/Q_j$ ,  $Q_B$  และ  $Q_j$  เป็นอัตราการไหลอากาศปฐมภูมิ และอากาศทุติยภูมิตามลำดับ),  $U_B$  เป็นความเร็วในแนวแกน,  $V_j$  ความเร็วในแนวรัศมี, / เป็น ขนาดของช่องฉีดที่ใช้ในการคำนวณ ในการทำนายจะกำหนดให้  $D=190~\mathrm{mm}$ ,  $d_0=19~\mathrm{mm}$ ,  $D_0=0.095~\mathrm{mm}$ 

ในการจำลองการไหลนี้ได้ใช้เงื่อนไขของ axisymmetry ในการคำนวณ เพื่อศึกษาเปรียบ เทียบการใช้  $k-\varepsilon$  model และ ASM ที่ใช้ numerical differencing scheme 4 แบบ คือ upwind, hybrid, QUICK และ SOU schemes ซึ่งผลลัพธ์ที่ได้จะนำไปเปรียบเทียบกับข้อมูลที่ ได้จากการทดลองของ Lin et. at. (1998) ที่ตำแหน่ง x=4D, 5D, 6D, 7D, 8D, 9D และ 10D

การศึกษาความเป็นอิสระของกริต (grid independent) ต่อผลการทำนายความเร็วตามแนว แกนและตามแนวสัมผัส ซึ่งทำการคำนวณที่จำนวนกริดเท่ากับ 60x25, 70x25, 80x30, 90x35 และ 100x40 จากการวิเคราะห์พบว่าจำนวนกริดมีผลต่อการทำนายการไหลพอสมควร แต่ค่าที่ ได้ก็ไม่แตกต่างกันมากดังนั้นในการคำนวณจะเลือกใช้กริดขนาด 80x30 ก็เพียงพอ

การทำนายการไหลในกรณี  $Q_r = 2$  และ  $D_s/D = 1.0$  เมื่อทำการประมาณนอกช่วงความเร็ว ฉีดในแนวสัมผัสจากผลการทดลองจะได้ w = 9 m/s และคำนวณความเร็วที่ทางเข้าของอากาศ ปฐมภูมิ,  $U_B = 0.8$  m/s และความเร็วการฉีดอากาศทุติยภูมิในแนวรัศมี,  $V_j = 4.3587$  m/s ส่วน ขนาดของช่องฉีด, I = 4.359 mm

#### 6.5.1 การทำนายการไหลโดย k-arepsilon model

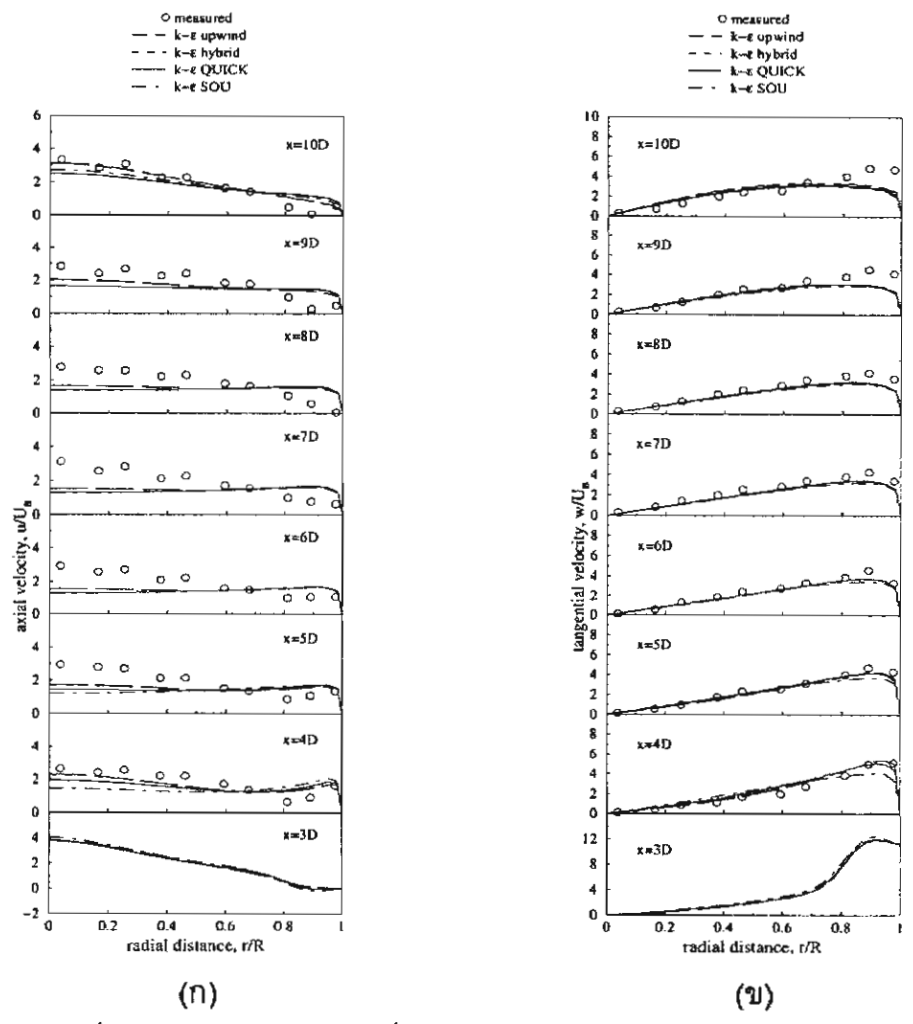
จากการจำลองการใหลโดย  $k-\varepsilon$  model ร่วมกับ scheme ต่างๆ ผลลัพธ์ที่ได้ถูกแสดงใน รูปของความเร็วดามแนวแกนและความเร็วตามแนวสัมผัสรวมถึง contour plot และ vector plot

ผลของความเร็วตามแนวแกนและความเร็วตามแนวสัมผัส ได้แสดงในรูปที่ 6.32(ก) และ 6.32(ข) ซึ่งจากรูปแสดงให้เห็นการเปลี่ยนแปลงของความเร็วจากระยะกึ่งกลางถึงผนัง รูปที่ 6.3 (ก) แสดงการเปลี่ยนแปลงของความเร็วตามแนวแกน จากรูปพบว่าในตำแหน่ง x = 3D ถึง 8D ค่าที่คำนวณได้ทั้ง 4 schemes พบว่าคำตอบที่ได้จาก upwind และ hybrid schemes สามารถ ทำนายได้ใกล้เคียงกับข้อมูลจากการทดลองมากกว่า QUICK และ SOU schemes โดยเฉพาะ ในช่วง r/R ตั้งแต่ 0 ถึง 0.6

การเบ่ลี่ยนแปลงของความเร็วตามแนวสัมผัสแสดงในรูป 6.32(ข) จากรูปการทำนายของ ทั้ง 4 schemes มีลักษณะเดียวกับการทำนายในแนวแกน แต่ค่าที่ได้จาก upwind และ hybrid schemes จะทำนายได้ดีในตำแหน่ง x = 4D ถึง 7D ส่วนตำแหน่งที่เหลือ QUICK และ SOU schemes ทำนายได้ดีกว่า ซึ่งจากภาพรวมทั้งหมดเห็นว่าทุก scheme ทำนายค่าได้ใกล้เคียง กับข้อมูลจากการทดลอง

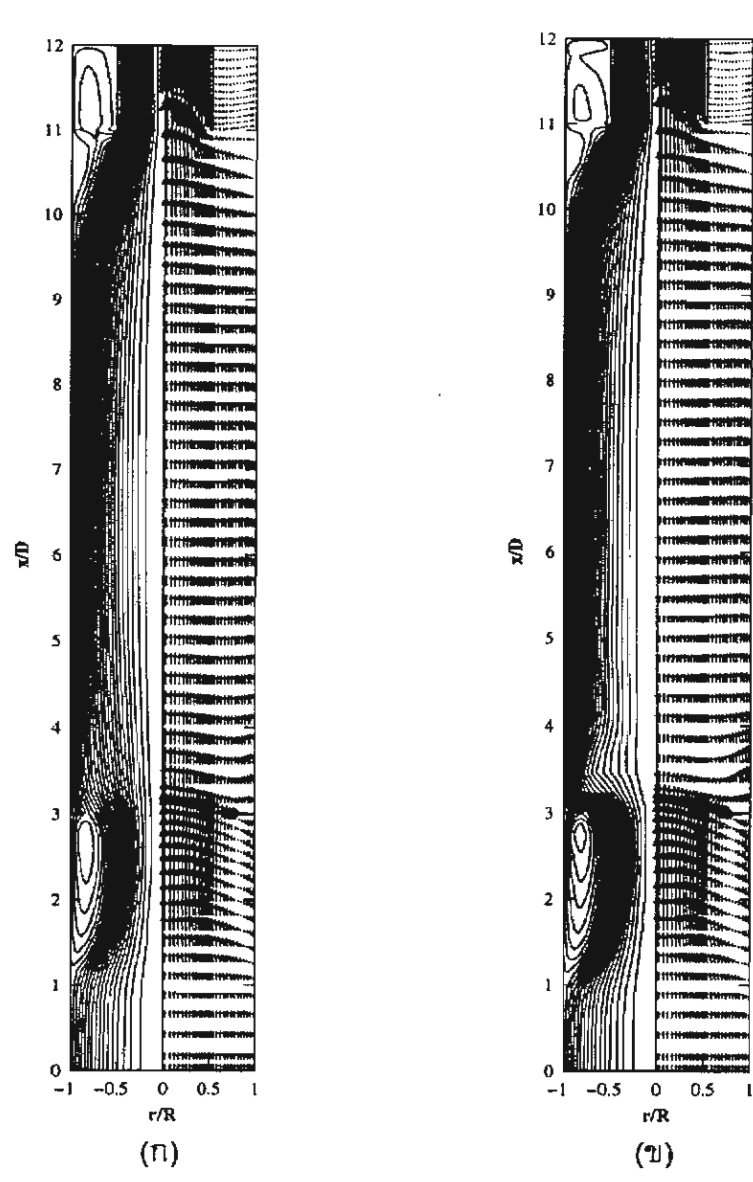
Contour plot ของ stream function และ vector plot ที่ทำนายโดย upwind และ SOU schemes ได้แสดงในรูปที่ 6.33(ก) และ 6.33(ข) ตามลำดับ จาก contour plot ของรูปที่ 6.33

(n) สังเกตว่ามี recirculation เกิดขึ้นเลย 3 ตำแหน่งด้วยกัน ที่บริเวณด้านล่างช่องฉีด 2 ตำแหน่ง และปลายทางออกที่อยู่ระหว่างปล่องกับผนังอีก 1 ตำแหน่ง ขณะที่ contour plot ของ รูปที่ 6.33(ข) จะสังเกตเห็น recirculation ได้ถึง 6 ตำแหน่งด้วยกัน



รูปที่ **6.32** การเปลี่ยนแปลงของความเร็วที่ทำนายโดย  $k-\varepsilon$  model (ก) ความเร็วตามแนว แกน (ข) ความเร็วตามแนวสัมผัส

จาก vector plot รูปที่ 6.33(ก) สามารถสังเกตเห็น recirculation วงใหญ่ด้านล่างของช่อง ฉีดที่พบใน contour plot ชัดเจนยิ่งขึ้นโดยเกิดขึ้นที่บริเวณ x/D = 1.8 ถึง 3 และ r/R = 0.7 ถึง 1.0 และ recirculation วงเล็กที่ตำแหน่ง x/D = 2.9 และ r/R = 0.95 ส่วน vector plot ที่ด้าน ปลายทางออกบริเวณปล่องกับผนังเดามีขนาดเล็กมาก ใน vector plot ของรูปที่ 6.33(ข) สังเกต เห็นการเปลี่ยนแปลงขนาดและทิศทางของความเร็วได้อย่างชัดเจนการจำลองการใหลโดย  $k-\varepsilon$  model ซึ่งทำการเปรียบเทียบประสิทธิภาพของ scheme ต่างๆ อาจสรุปได้ว่า upwind และ hybrid schemes ทำนายได้ดีใกล้เคียงกับผลการทดลองที่สุดบนความเร็วทั้งในแนวแกน และแนวสัมผัส



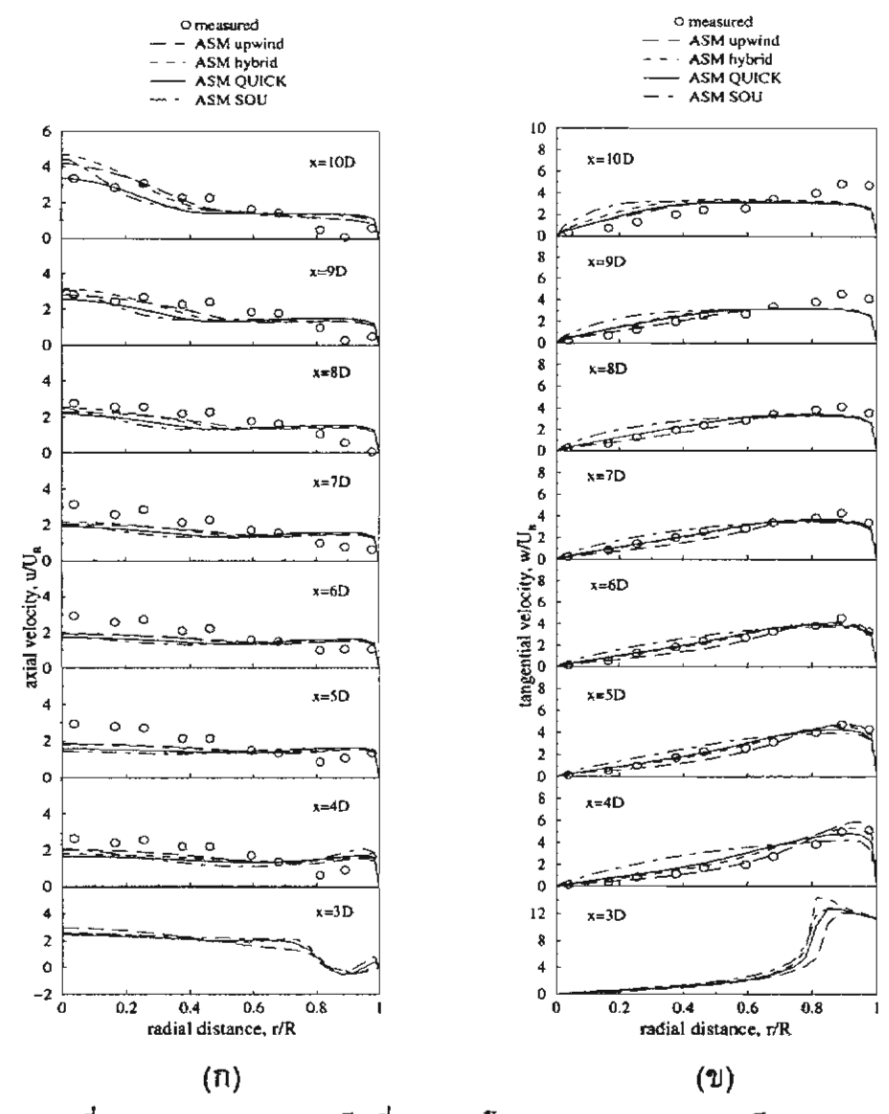
รูปที่ 6.33 Contour plot ของ stream function กับ vector plot ของความเร็ว ทำนายโดย  $k-\varepsilon$  model ที่ใช้ (ก) upwind scheme และ (ข) SOU scheme

#### 6.5.2 การทำนายการไหลโดย Algebraic Stress model (ASM)

การจำลองโดยใช้ ASM ร่วมกับ scheme ต่างๆ ได้นำมาแสดงในรูปของความเร็วตามแนว แกน, ความเร็วตามแนวสัมผัส, contour plot และ vector plot

รูปที่แสดงให้เห็นการเปลี่ยนแปลงของความเร็วจากระยะกึ่งกลางถึงผนังของความเร็วตาม แนวแกนและความเร็วตามแนวสัมผัสในรูปที่ 6.34(ก) และ 6.34(ข) ตามลำดับ

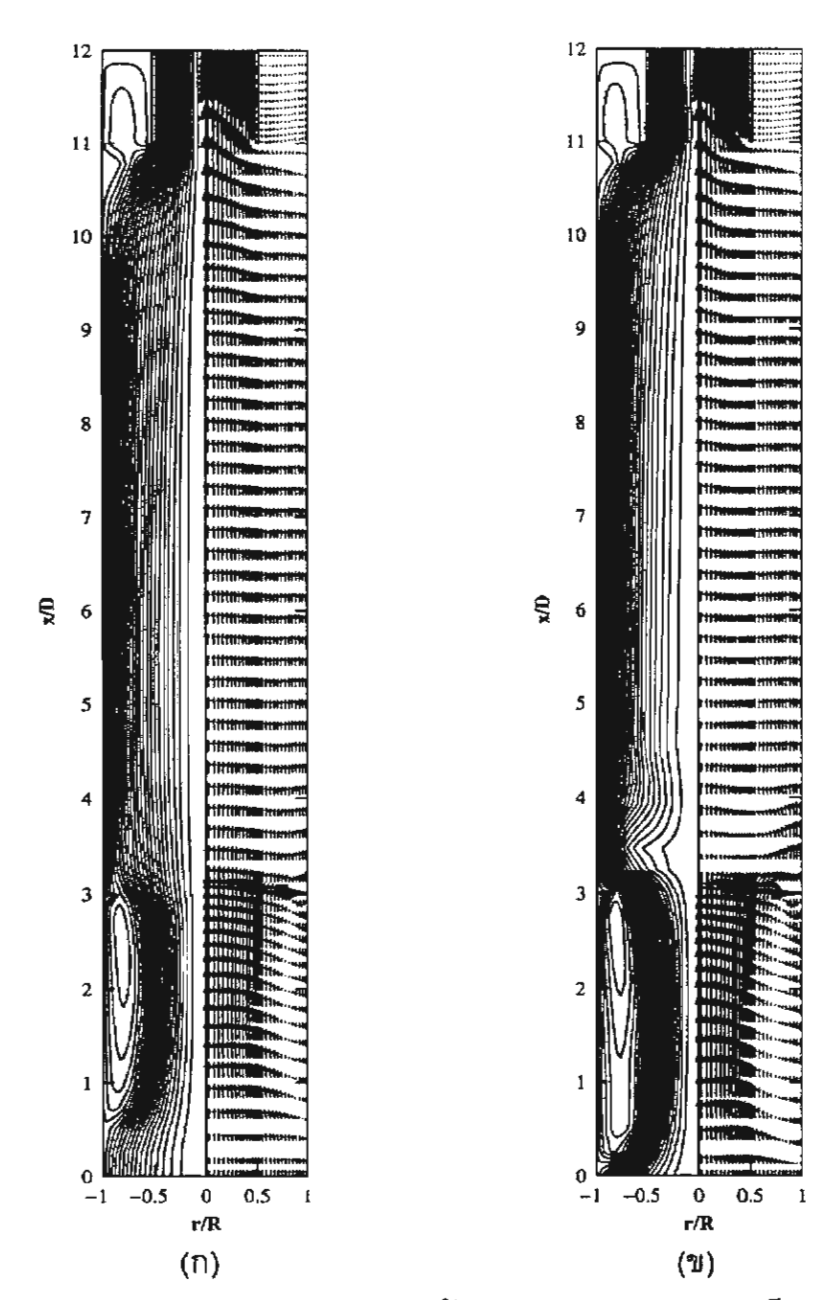
รูปที่ 6.34(ก) ซึ่งแสดงการเปลี่ยนแปลงของความเร็วตามแนวแกน พบว่าในดำแหน่ง x = 3D ถึง 8D ค่าที่คำนวณได้จาก SOU scheme มีค่าที่ไกล้เคียงกับผลการทดลองมากกว่าโดย เฉพาะในตำแหน่งที่ใกล้กับช่องฉีด ในบริเวณ r/R ประมาณ 0 ถึง 0.5 ส่วนความเร็วในแนวแกน สัมผัสในรูปที่ 6.34(ข) พบว่า upwind และ hybrid schemes ทำนายได้ใกล้เคียงกว่า SOU scheme อย่างชัดเจนในช่วง r/R ประมาณ 0 ถึง 0.6



รูปที่ 6.34 การเปลี่ยนแปลงของความเร็วที่ทำนายโดย ASM (ก) ความเร็วตามแนวแกน (ข) ความเร็วตามแนวสัมผัส

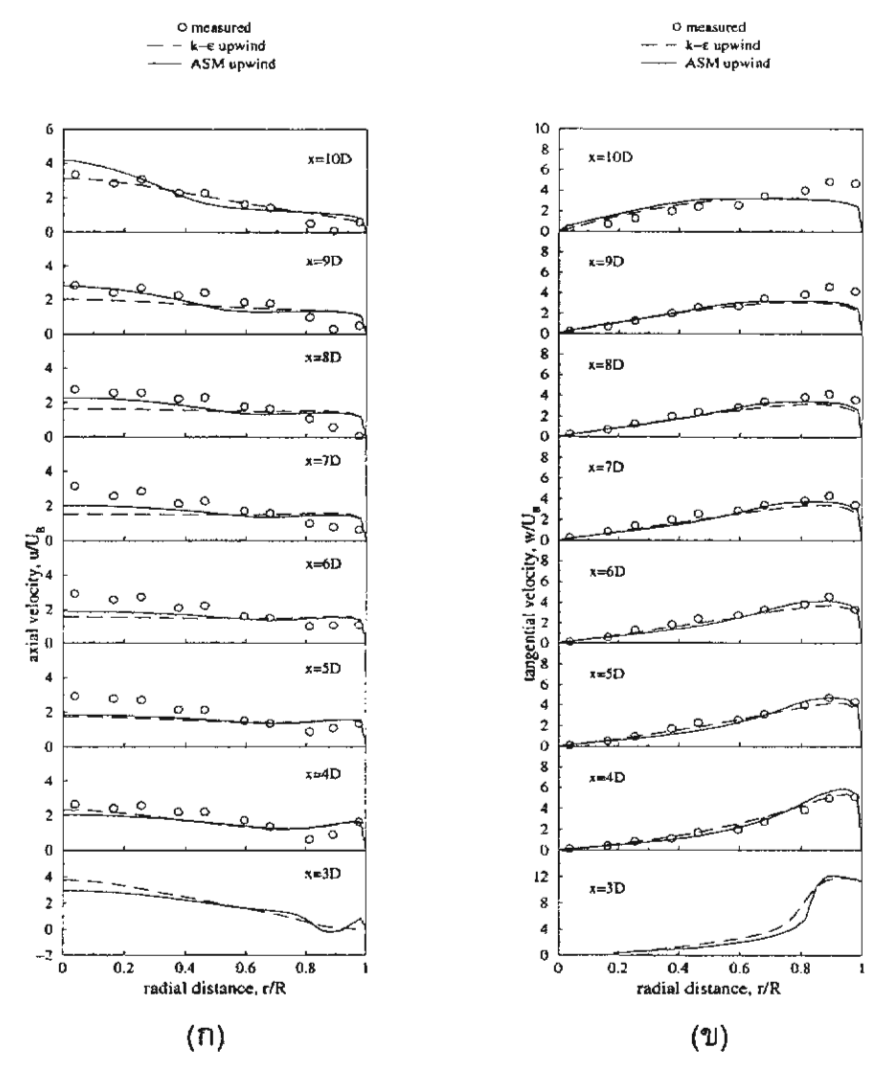
Contour plot และ vector plot ที่ทำนายโดย upwind และ SOU schemes ได้แสดงในรูปที่ 6.35(ก) และ 6.35(ข) ตามลำดับ จาก contour plot ของรูปทั้งสอง สังเกตว่า การทำนายโดย SOU scheme จะเกิด recirculation ที่ตำแหน่งใต้และเหนือช่องฉีด ในขณะที่ผลจาก upwind กลับไม่แสดงให้เห็น recircultion ที่ตำแหน่งดังกล่าว จาก vector plot รูปที่ 6.35(ก) ไม่สามารถ เห็นการไหลย้อนกลับซึ่งก็ยืนยัน ผลที่พบในcontour plot ชัดเจนยิ่งขึ้น ส่วนใน vector plot ของ รูปที่ 6.35(ข) จะสังเกตการไหลย้อนกลับของ vector ความเร็วได้อย่างชัดเจนที่ตำแหน่งใต้ช่อง ฉีด

การจำลองการไหลโดย ASM ซึ่งทำการเปรียบเทียบความสามารถของ scheme ต่างๆ คือ upwind, hybrid, QUICK และ SOU สรุปได้ว่า upwind และ hybrid scheme ให้ผลการทำนาย ความเร็วทั้งในแนวแกนและแนวสัมผัสได้ใกล้เคียงกับผลการทดลอง



รูปที่ 6.35 Contour plot ของ stream function กับ vector plot ของความเร็ว ทำนายโดย ASM ที่ใช้ (ก) upwind scheme และ (ข) SOU scheme

รูป 6.36(ก) และ 6.36(ข) เป็นรูปที่เปรียบเทียบผลการทำนายโดย  $k-\varepsilon$  model กับ ASM ของความเร็วในแนวแกนและความเร็วในแนวสัมผัสตามลำดับ จากรูปที่ 6.36(ก) ซึ่งเป็น ความเร็วในแนวแกนที่ใช้ upwind scheme ในการคำนวณของทั้ง 2 models พบว่า ค่าที่ทำนาย โดย ASM นั้นใกล้เคียงกับผลการการทดลองมากกว่า  $k-\varepsilon$  model ส่วนการเปรียบเทียบ model ในการทำนายความเร็วในแนวสัมผัสในรูปที่ 6.36(ข) ซึ่งใช้ upwind scheme มีผลการ เบ้รียบเทียบเหมือนกับในแนวแกนคือ ASM ทำนายใกล้เคียงกับผลการการทดลองมากกว่า  $k-\varepsilon$  model



รูปที่ 6.36 กราฟเปรียบเทียบการทำนายระหว่าง  $k - \varepsilon$  model กับ ASM (ก) ความเร็วตาม แนวแกน (ข) ความเร็วตามแนวสัมผัส

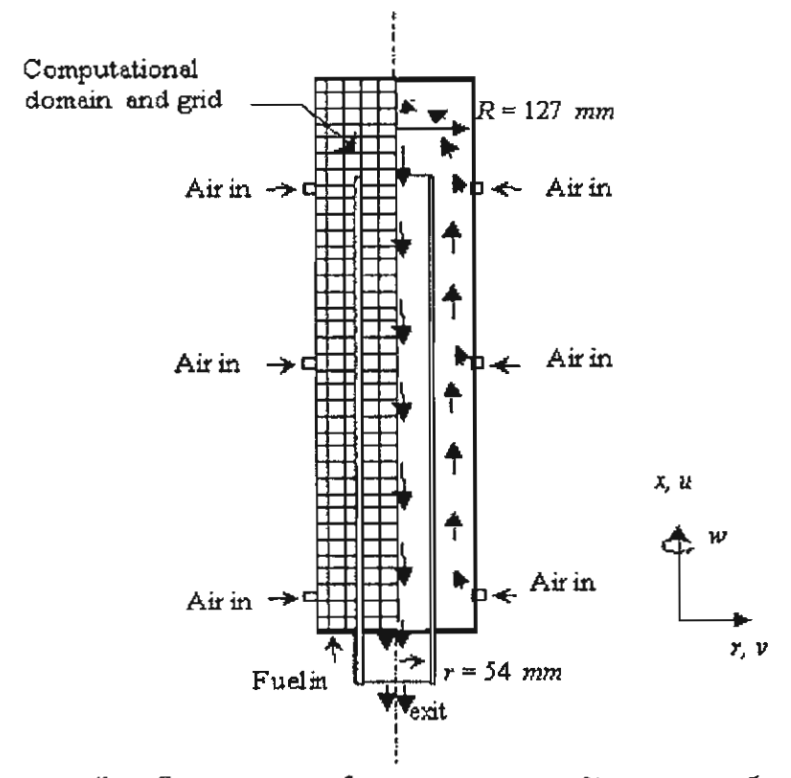
# 6.6 เตาเผาวอร์เทคของ Nieh and Zhang (1992)\*\*\*\*

เตาวอร์เทล (vortex combustor, VC) เป็นเตาที่ถูกพัฒนาขึ้นมาโดยที่ใช้เทลนิลของไหล แบบหมุนวนความเร็วสูงช่วยในการเผาไหม้ การไหลแบบหมุนวนความเร็วสูงได้ถูกนำมาใช้ใน งานทางด้านอุตสาหกรรมเป็นจำนวนมาก เช่น เตาเผา หัวเผา เครื่องยนต์สันดาปภายใน เครื่อง ยนต์กังหันก๊าซ และอุปกรณ์แลกเปลี่ยนความร้อนต่างๆ ในระบบการเผาไหมันั้น การหมุนวนได้ ถูกนำมาใช้เพื่อเพิ่มความเสถียรของเปลวไฟ เพิ่มการผสมคลุกเคล้าของเชื้อเพลิงและอากาศ และช่วยเพิ่มการถ่ายเทความร้อน นอกเหนือจากช่วยเพิ่มเวลาอยู่ในเตาของเชื้อเพลิง (fuel residence time) และช่วยลดมลพิษที่เกิดจากการเผาไหม้นี้ เพราะว่าการหมุนวนช่วยเหนียวนำ

ได้นำเสนอใน Regional Conference on Energy Technology Towards a Clean Environment เชียงใหม่ และ จะนำเสนอใน Intersociety Energy Conversion Engineering Conference, USA.

ให้เกิดการใหลวนไปมาในบริเวณกึ่งกลางของเตา (central recirculation zone) เป็นผลให้เกิด ความปั่นป่วนอย่างรุนแรงขึ้นในแต่ละชั้นระหว่างการไหลวนไปมาและการไหลของชั้นภายนอก ซึ่งช่วยทำให้เปลวไฟในเตาเสถียรยิ่งขึ้น โครงสร้างของความปั่นป่วนในการไหลแบบหมุนวน ความเร็วสูงนี้โดยทั่วไปมีความสัมพันธ์ที่ซับซ้อนมาก การไหลวนไปมา (recirculation) อันเป็น ผลจากการหมุนวนสามารถนำไปสู่ การเพิ่มประสิทธิภาพการสันดาป ลดมลภาวะที่ปล่อยอก (NO<sub>x</sub>, เขม่า, สารคาร์บอนที่เผาไหม้ไม่หมด) ลดความยาวของเปลวเพลิงและเป็นผลให้เตาเผา มีขนาดเล็กลง เพิ่มความเสถียรของการสันดาป ซึ่งเตาวอร์เทคนี้ถูกออกแบบมาเพื่อแก้ปัญหา ต่างที่เกิดขึ้นในเตาที่กล่าวในข้างตัน โดยเตาวอร์เทคนั้นจะรวมข้อดีของเตาไซโคลน, เตาถ่าน หินผง (pulverized coal), ห้องสันดาปของเครื่องยนต์กังหันก๊าซ และเตา fluidized bed เข้าด้วย กันเพื่อแก้ปัญหาในเรื่องของ slag, เขม่า, ขึ้เถ้า รวมถึงการเพิ่มเวลาในการเผาไหม้เพื่อการเผา ใหม้ที่ดีขึ้น และที่แน่นอนย่อมนำไปสู่ขนาดที่เล็กลงกว่าเตาที่กลำวมาแล้ว

การใหลแบบหมุนวนอย่างรุนแรงในเตาเผาวอร์เทคถูกนำมาพิจารณาในงานวิจัยนี้ โดยมี โครงสร้างของเตาเผาดังแสดงในรูปที่ 6.37 ซึ่งประกอบไปด้วยท่อตรงกลางที่มีขนาดเส้นผ่าศูนย์ กลางเท่ากับ 0.11 m โดยมีศูนย์กลางร่วมกับห้องเผาใหม้ทรงกระบอกที่มีความสูง 0.66 m และ มีขนาดเส้นผ่าศูนย์กลางเท่ากับ 0.25 m ขนาดความสูงของท่อตรงกลางที่วางในห้องเผาใหม้ เท่ากับ 0.51 m อากาศถูกฉีดเข้าไปในห้องเผาใหม้ในแนวสัมผัสผ่านหัวฉีด 3 ชุดและใหลออก ผ่านท่อตรงกลาง ค่า swirl number ที่วัดได้เท่ากับ 13.9 ข้อมูลจากการทดลองวัดที่ตำแหน่ง x = 0.051, 0.112, 0.173, 0.234, 0.295, 0.358, 0.42 0.483, 0.544, และ 0.605 m. ข้อกำหนดของ เตาเผาได้สรุปไว้ในตารางที่ 1 ด้านล่าง



รูปที่ 6.37 การจัดการไหล,โดเมนและกริดในการคำนวณสำหรับเตาเผาวอร์เทค

**ตารางที่ 6.1** โครงสร้างและเงื่อนไขการไหลสำหรับเตาเผาวอร์เทค

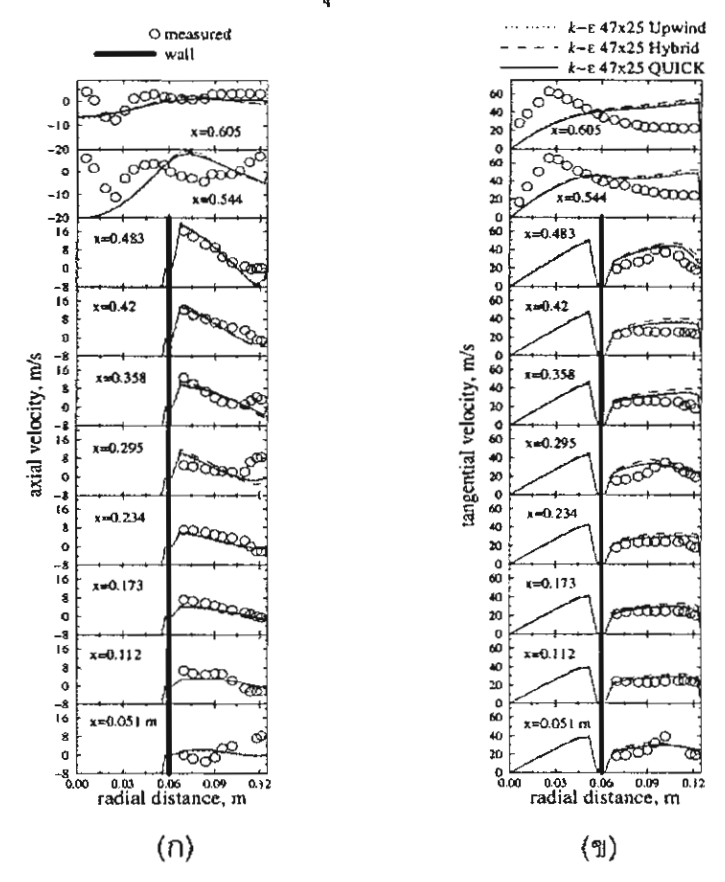
Parameter	Magnitude		
Vortex chamber geometry			
chamber inner dia., m	0.25		
chamber height, m	0.66		
centre tube outer dia., m	0.13		
centre tube inner dia., m	0.11		
centre tube height, m	0.51		
Multiple air injection			
nozzle height distribution, m	0.051	0.295	0.483
flow rate distribution, <i>m</i> <sup>3</sup> / <i>h</i>	226	226	226
tangential velocity, m/s	24.6	24.6	24.6
air temperature, K	300	300	300

สำหรับการจำลองการใหลในเตาเผาวอร์เทค เชื้อเพลิงก๊าซมีเทน (CH<sub>4</sub>) ถูกใช้แทนแกลบ เพื่อทำให้การจำลองง่ายขึ้น เชื้อเพลิงก๊าซจะถูกฉีดใต้เตาเผาไปยังด้านล่างของเตา เพื่อที่จะ ศึกษาอิทธิพลทางเข้าของการฉีดเชื้อเพลิงต่อคุณสมบัติการใหลที่มีการเผาใหม้เมื่อฉีดอากาศคง ที่ จึงได้ทำการแบ่งประเภทของการฉีดเชื้อเพลิงเป็น 2 แบบ คือการฉีดเชื้อเพลิงในแนวแกนและ การฉีดเชื้อเพลิงทำมุม (30องศาจากแนวสัมผัส)

# 6.6.1 การทำนายการไหลในเตาเผาที่ไม่มีปฏิกิริยาเผาไหม้

อิทธิพลของจำนวนกริดต่อรูปร่างความเร็วที่ทำนายได้ถูกตรวจสอบโดยการเปรียบ เทียบเมื่อใช้จำนวนกริดขนาดต่าง ๆกัน พบว่าจำนวนกริดขนาด 40x20 หรือจำนวนกริดที่ ละเอียดกว่า เพียงพอที่จะรับรองได้ว่าค่าจากการจำลองการไหลไม่ได้รับอิทธิพลจากจำนวนกริด ที่ใช้ การกระจายความเร็วในแนวแกนและแนวสัมผัสแสดงในรูปที่ 6.38(n) และ 6.38(v) ตาม ลำดับ จากการใช้ schemes ทั้งสามเมื่อเปรียบเทียบกับผลการทดลองพบว่ามีค่าที่ทำนายได้ เหมือนกัน ซึ่งแสดงว่าทุก schemes สามารถใช้ได้ในการคำนวณ ซึ่งต่อไปจะใช้เพียง upwind scheme ในการคำนวณถัดไป ตามรูปที่ผ่านมาแสดงให้เห็นว่าผลจากการทำนายโดย  $k-\varepsilon$  model มีความแตกต่างจากผลการทดลองโดยเฉพาะบริเวณด้านบนของเตา ตัวอย่างเช่น  $k-\varepsilon$  model ไม่สามารถทำนาย แถบของ central toroidal recirculation และการเคลื่อนที่แบบ combined forced and free vortex ในส่วนบนของเตาเผา (ที่ x=0.544 และ 0.605 m) อย่าง

ไรก็ตามในการวิจัยนี้ ยังคงใช้  $k-\varepsilon$  model ในการทำนายแนวโน้มของลักษณะการไหลที่มีการ เผาไหม้ในเดาเผาวอร์เทคเนื่องจากความไม่ยุ่งยากในการใช้นั่นเอง

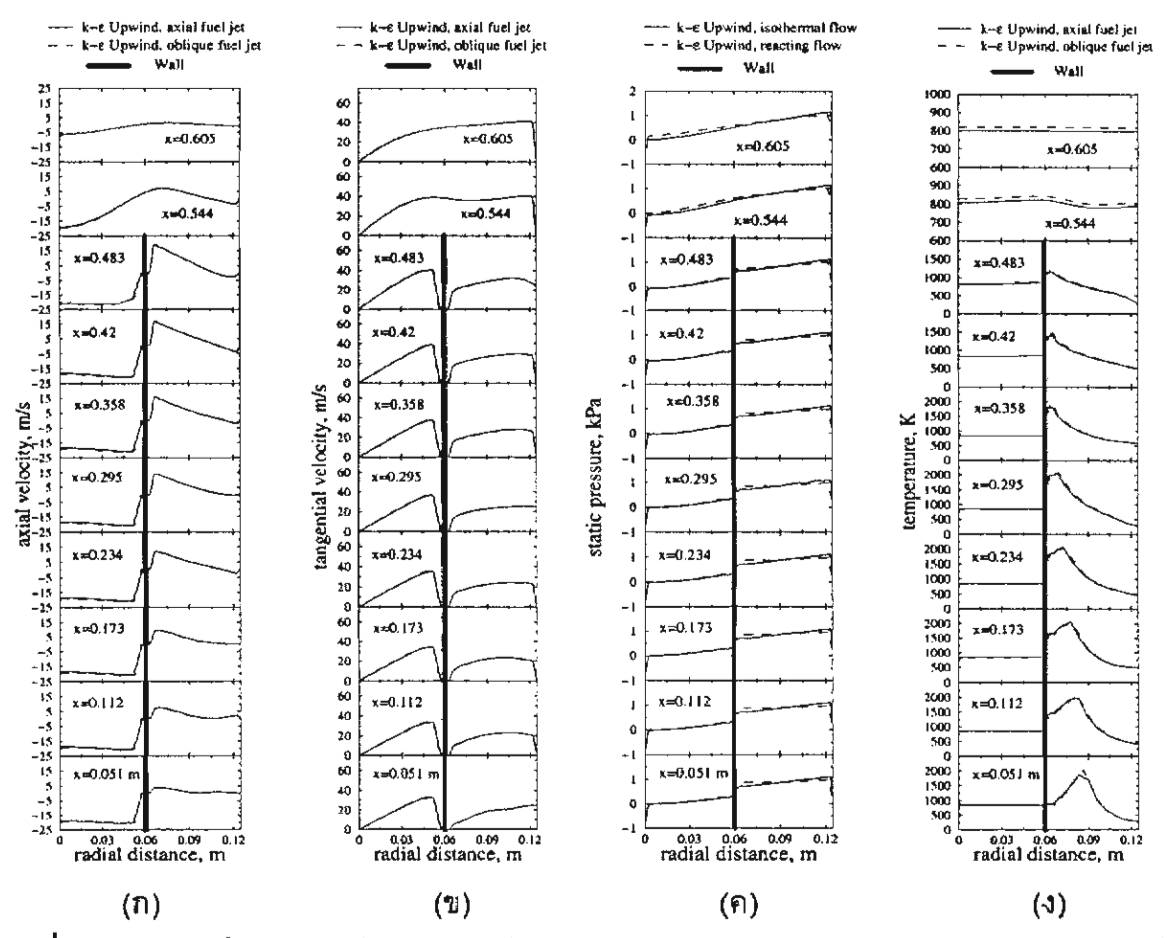


รูปที่ 6.38 เปรียบเทียบผลจากการทดลองกับผลจากการทำนายโดยใช้ schemes ที่แตกต่างกัน (ก) ความเร็วตามแนวแกนและ (ข) ความเร็วตามแนวสัมผัส

# 6.6.2 การทำนายการไหลในเตาเผาที่มีปฏิกิริยาเผาไหม้

การศึกษาอิทธิพลของทางเข้าในการฉีดเชื้อเพลิงต่อสนามการไหลและอุณหภูมิ โดยมีการ ฉีดเชื้อเพลิง 2 แบบคือแบบแรกทำได้โดยการวางหัวฉีดเชื้อเพลิงขนานกับแนวแกนของเตาเผา เรียกว่า การฉีดเชื้อเพลิงตามแนวแกน ส่วนแบบที่สองทำได้โดยการวางแนวของหัวฉีดทำมุม 30 องศากับเส้นสัมผัสที่ทางเข้าของเชื้อเพลิง รูปร่างของความเร็วตามแนวแกน, ความเร็วตาม แนวสัมผัส, ความดันสถิตย์และอุณหภูมิที่คำนวณได้สำหรับการฉีดเชื้อเพลิงทั้ง 2 แบบถูกแสดง ในรูปที่ 6.39(ก), 6.39(ข) และ 6.39(ค) ตามลำดับ สังเกตว่าการฉีดเชื้อเพลิงทั้งสองแบบไม่มีผล ต่อคุณสมบัติการไหลเฉลี่ย ตัวอย่างเช่นการกระจายความเร็วและความดันดังจะเห็นได้จากรูปที่ 6.39(ก), 6.39(ข) และ 6.39(ค)

เมื่อเปรียบเทียบกับแบบจำลองที่ไม่มีการเผาไหม้ ความเร็วตามแนวแกนที่ทางออกในกรณี นี้มีค่าสูงกว่า (ประมาณ 3 เทำ) สำหรับรูปร่างของอุณหภูมิพบว่าการฉีดเชื้อเพลิงแบบทำมุมทำ ให้อุณหภูมิด้านบนของเตาสูงขึ้น ขณะที่อุณหภูมิบริเวณวงแหวนมีค่าเหมือนกันดังแสดงในรูปที่ 3d ซึ่งแสดงให้เห็นว่าเมื่อต้องการอุณหภูมิภายในเตาที่มีความสม่ำเสมอ รูปแบบทางเข้าของเชื้อ เพลิงควรที่จะฉีดไปในเตาในแนวสัมผัส

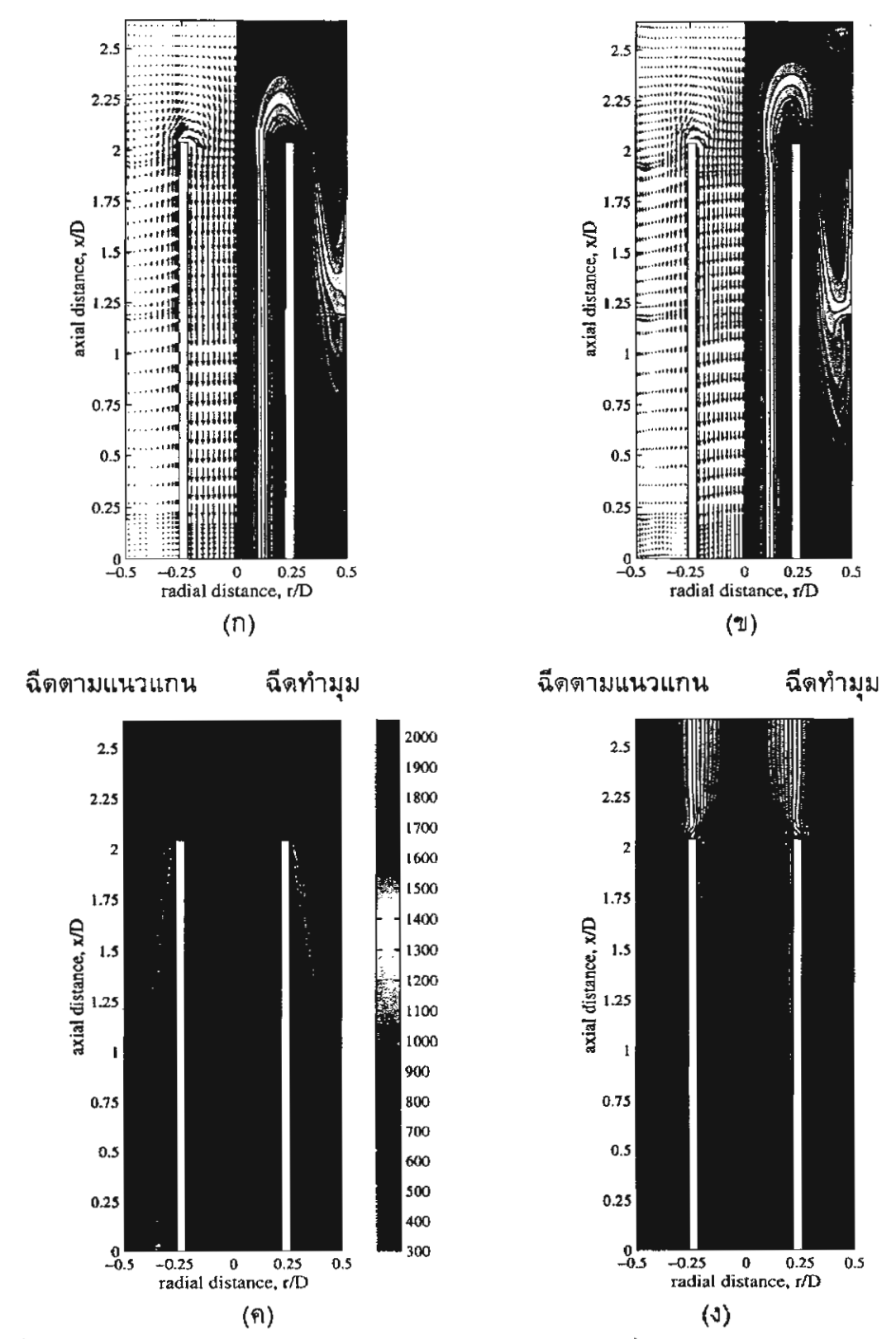


รูปที่ 6.39 รูปร่างในแนวรัศมีของความเร็ว (n) ตามแนวแกนและ (ข) แนวสัมผัส (ค) ความดัน สถิตย์และ (ง) อุณหภูมิที่คำนวณโดยใช้การฉีดเชื้อเพลิงที่แตกต่างกัน

Streamlines และ vectors ของความเร็วแสดงในรูปที่ 6.40(ก) ขณะที่รูปที่ 6.40(ข) เป็นกรณี ที่ไม่มีการเผาไหม้เพื่อเปรียบเทียบกัน ในรูปที่ 6.40(ก) และ 6.40(ข) มีอยู่ด้วยกันสองซีกคือซีก ด้านซ้ายเป็น vector ของความเร็ว โดยที่ซีกด้านขวาเป็น streamlines สำหรับ vector plots ของความเร็วสังเกตว่ารูปแบบการไหลเหมือนกันทั้งสองแบบ รูปร่างความเร็วในท่อตรงกลางที่ ทางออกในกรณีมีการเผาไหม้ค่อนข้างสม่ำเสมอ ความเร็วมีความหนาแน่นในบริเวณใกล้กับ ผนังท่อตรงกลางดังแสดงในรูปที่ 6.40(ก) และ 6.40(ข) สำหรับ streamlines จะเห็นการหมุนวน ที่มีขนาดใหญ่และความรุนแรงกว่าเมื่อสังเกตในการไหลที่มีการเผาไหม้

Contour piots ของอุณหภูมิและความดันแสดงในรูปที่ 6.40(ค) และ 6.40(ง) ตามลำดับ เช่น เดียวกันในรูปซีกด้านซ้ายเป็นกรณีฉีดเชื้อเพลิงตามแนวแกนขณะที่ซีกด้านขวาเป็นกรณีฉีดเชื้อ เพลิงทำมุม ใน contour plot ของอุณหภูมิพบว่าการฉีดเชื้อเพลิงทั้งสองแบบให้ผลที่แทบเหมือน กันแต่การฉีดเชื้อเพลิงทำมุมอุณหภูมิบริเวณแกนกลางเกือบจะสม่ำเสมอกันดังเห็นได้ในรูปที่

6.40(ก) จาก Contour ของความดันสถิตย์ในรูปที่ 6.40(ง) จะเห็นได้อย่างชัดเจนว่าผลที่ได้มี ความเหมือนกัน



รูปที่ 6.40 vector และ streamlines ของความเร็ว (ก) การไหลที่มีปฏิกิริยาการเผาไหม้ (ข) การ ไหลที่อุณหภูมิคงที่; contour plots ของ (ค) อุณหภูมิและ (ง) ความดันที่ทำนายได้

#### 6.7 สรุป

ผลการจำลองการไหลในเดาเผาซึ่งเป็นการเปรียบเทียบระหว่าง k-arepsilon model กับ ASM ทั้ง หมดสามารถสรุปได้ดังต่อไปนี้

- 1. Recirculation มีผลต่อจำนวนกริดที่น้อยที่สุดในการคำนวณอย่างมาก
- 2. ASM สามารถทำนายการไหลได้ดีกว่า  $k-\varepsilon$  mode! โดยเห็นอย่างชัดเจนบนความเร็วตาม แนวสัมผัส รวมถึงการใช้ ASM ทำให้ลักษณะรูปร่างของความเร็วตามแนวแกน และ ความเร็วตามแนวรัศมีที่ทำนายได้เปลี่ยนไปจาก  $k-\varepsilon$  mode! เล็กน้อย
- ลักษณะของการใหลนั้นขึ้นอยู่กับรูปร่างของเตาเป็นอย่างมากกว่าผลของ swirt number
   หรือการฉีดอากาศ
- 4. ผลของ numerical differencing scheme ที่ใช้นั้นมีค่อนข้างสูงต่อการไหลที่มี recirculation รวมถึงการใช้ ASM ต่อการไหลที่มี recirculation ควรเลือกใช้ scheme ที่ใช้การประมาณ เป็นเส้นตรง (first-order scheme)

สำหรับผลการทำนายการไหลภายในเตาฟลูอิดไดซ์เบดแบบฉีดอากาศทุติยภูมิด้านข้าง ผล จากการเปรียบเทียบ model ที่ใช้พบว่า ASM ทำนายได้ดีกว่า  $k-\varepsilon$  model และจากผลการ ทำนายโดยการใช้ numerical differencing scheme ด่างๆ พบว่า upwind และ hybrid schemes ประมาณค่าได้ใกล้เคียงกับผลการทดลองมากกว่า QUICK และ SOU schemes ทั้ง ในแนวแกนและแนวสัมผัส

ผลการทำนายที่มีความผิดพลาดส่วนหนึ่งน่าจะเป็นผลมาจากการไหลจริงที่เกิดขึ้นเป็นการ ไหลแบบ 3 มิติ ซึ่งในการทำนายการไหลในเตาฟลูอิดไดซ์เบดแบบฉีดอากาศทุติยภูมิด้านข้างนี้ พิจารณาการไหลแค่ 2 มิติแบบสมมาตรในแนวแกน (axisymmetric)

การคำนวณเชิงตัวเลขที่ทำนายการไหลปั่นป่วนแบบหมุนวนอย่างรุนแรงและลักษณะการ เผาไหม่ในเตาเผาวอร์เทคโดยใช้  $k-\varepsilon$  model ผลการคำนวณสำหรับการไหลที่ไม่การทำปฏิ กริยาถูกเปรียบเทียบกับค่าที่ได้จากการทดลอง ผลของจากการวิเคราะห์สามารถสรุปได้ดังต่อ ไปนี้

สำหรับการใหลในเดาเผาที่ไม่มีปฏิกิริยาเผาไหม้ การไหลของก๊าชในเตาเผาจะเป็นการไหล ปั่นป่วนซึ่งมีการหมุนวนอย่างรุนแรง, เกิด recirculation และ เป็นการไหลแบบ nonisotropic โดยอยู่ภายใต้อิทธิพลของความเร็วตามแนวสัมผัสเป็นส่วนใหญ่

สำหรับการไหลในเตาเผาที่มีปฏิกิริยาเผาไหม้ การคำนวณแสดงให้เห็นว่ารูปแบบการไหล เหมือนกับแบบจำลองการไหลในเตาเผาที่มีปฏิกิริยาเผาไหม้แต่ขนาดความเร็ว,แถบ recirculation มีมากกว่า

#### บทที่ 7

# สรุปผลงานวิจัยและข้อเสนอแนะ

## 7.1 สรุปผลงานวิจัย

จากการจำลองการใหล่ปั่นป่วนแบบหมุนวนในเตาเผาทั้งหมดโดยใช้  $k-\varepsilon$  model และ ASM ร่วมกับ numerical differencing scheme ทั้งหมด 4 ชนิด คือ upwind, hybrid, QUICK และ SOU พบว่าการจำลองการใหล่มีความสอดคล้องกับข้อมูลจากการทดลองเป็นอย่างดี โดย ASM นั้นสามารถทำนายได้ดีกว่า  $k-\varepsilon$  model อย่างเห็นได้ชัด แต่การใช้ ASM นั้นพบว่าจำ เป็นจะต้องมีการเลือกใช้ numerical differencing scheme ให้เหมาะสมโดยเฉพาะบนการใหล่ที่ มี recirculation ควรเลือกใช้ numerical differencing scheme ที่ใช้การประมาณแบบเส้นตรงจะ มีความเหมาะสมที่สุด รวมถึงลักษณะของการใหล่มีผลจากรูปร่างของเตามากกว่า swirl number (S) หรือการฉีดอากาศ

ผลการทำนายการไหลภายในเตาฟลูอิดไดซ์เบดแบบฉีดอากาศทุติยภูมิด้านข้างในแนว สัมผัสโดยเปรียบเทียบระหว่าง  $k-\varepsilon$  model กับ ASM ที่  $\mathbf{Q}_r=2$  และ  $\mathbf{D}_s/\mathbf{D}=1.0$ , ผลจากการ เปรียบเทียบ model ที่ใช้พบว่า ASM ทำนายได้ดีกว่า  $k-\varepsilon$  model และผลของ scheme ที่ใช้ พบว่า upwind และ hybrid schemes ประมาณคำความเร็วในแนวแกนและแนวสัมผัสได้ใกล้ เคียงมากกว่า QUICK และ SOU schemes

ส่วนการทำนายการไหลในเดาเผาวอร์เทคโดยใช้  $k-\varepsilon$  model สำหรับการไหลในเตาเผาที่ ไม่มีปฏิกิริยาเผาไหม้ การไหลของก๊าซในเตาเผาจะเป็นการไหลปั่นป่วนซึ่งมีการหมุนวนอย่าง รุนแรง, เกิด recirculation และ เป็นการไหลแบบ nonisotropic สำหรับการไหลในเตาเผาที่มี ปฏิกิริยาเผาไหม้ ผลจากการทำนายแสดงให้เห็นว่ารูปแบบการไหลเหมือนกับการทำนายการ ไหลในเตาเผาที่มีปฏิกิริยาเผาไหม้แต่ขนาดความเร็ว,แถบ recirculation จะมากกว่า

### 7.2 ข้อเสนอแนะในการศึกษาวิจัยต่อไป

- ควรทำการศึกษาเปรียบเทียบรูปร่างของเตาเผาแบบต่างๆต่อลักษณะการไหล
- 2. ควรมีลองการใช้ Reynolds stress model ทำนายการไหลในลักษณะเดียวกัน เพื่อทำ การเปรียบเทียบรวมถึงถึงศึกษาพฤติกรรมที่เกิดขึ้น
- ควรมีการพัฒนา model ของการเผาใหม้ต่อจากงานวิจัยนี้จาก 2 มิติ เป็น 3 มิติ เพื่อให้ งานสมบูรณ์มากขึ้นต่อไป

# บทที่ 8

# ผลที่ได้จากโครงการวิจัย

โครงการวิจัยนี้มีเป้าหมายหลัก คือ ต้องการศึกษาและเข้าใจอย่างลึกซึ้งเกี่ยวกับพฤติ กรรมการไหลในเตาเผาที่ใช้กันในภาคอุตสาหกรรม โดยใช้แบบจำลองทางคณิตศาสตร์มาช่วย อย่างไรก็ตามเนื่องจากข้อจำกัดบางประการทำให้ไม่สามารถจำลองการไหลได้เต็มรูปแบบ คือ สามมิติ จึงใช้ข้อสมมติฐานของการไหลแบบสมมาตรมาช่วยทำให้ลดรูปจาก 3 มิติ เป็น 2 มิติ ได้ เป็นการลดความยุ่งยากได้พอควร แต่ก็สูญเสียความแม่นยำบางส่วนไป

ผลจากโครงงานวิจัยนี้สามารถจำแนกได้ดังต่อไปนี้

- ผลงวนดีพิมพ์ในวารสารวิชาการนานาชาติ
   ปัจจุบันยังไม่มีการตีพิมพ์ แต่กำลังร่างอยู่ คาดว่าจะมีการตีพิมพ์ในช่วงประมาณ 6 เดือน
   ข้างหน้า เพราะว่ากำลังเก็บข้อมูลเพิ่มบางส่วนเพื่อความสมบูรณ์ของบทความ โดยจะตี
   พิมพ์ในวารสารนานาชาติดังต่อไปนี้
  - 1.1 JSME International J. of Fluids and Thermal Engineering
  - 1.2 ASEAN Journal on Science & Technology for Development
- 2. การนำผลงานวิจัยไปใช้ประโยชน์ ถึงแม้ว่างานวิจัยนี้จะไม่สามารถนำไปประยุกต์ใช้ในเชิงพาณิชย์ได้ แต่ก็มีประโยชน์อย่าง มากในเชิงวิชาการ เพราะสามารถสร้างนักวิจัยใหม่ ในระดับปริญญาโท ได้ถึง 4 คน และ กำลังจะจบปริญญาโทอีก 2 คน นอกจากนี้ยังสร้างความร่วมมือกับนักวิจัยในต่างประเทศ เพื่อแลกเปลี่ยนความรู้ทางวิชาการ (ดูภาคผนวก ข)
- ผลงานตีพิมพ์ (ทั้งหมดอยู่ในภาคผนวก ก)
  - 3.1 การเสนอผลงานในที่ประชุมวิชาการระดับนานาชาติ จำนวน 5 บทความ ก็คือ
    - 3.1.1 Pongjet Promvonge, "Simulation of a Turbulent Channel Flow with Injection Through a Slit", The Sixth Asian International Conference on Fluid Machinery, 18-21 July, 2000, Johor Bahru, Malaysia. (หน้า ก1)
    - 3.1.2 P. Promvonge, L. Vongsarnpigoon and K. Silapabanleng "A Low Emission Annular Vortex Combustion Firing Rice Husk Fuel: Part I—Numerical Simulation", The First Regional Conference on Energy Technology Towards a Clean Environment, 1-2 December 2000, Chiang Mai, Thailand. (หน้า ก9)
    - 3.1.3 P. Promvonge, L. Vongsarnpigoon and N. piriyarungroj "A Low Emission Annular Vortex Combustion Firing Rice Husk Fuel: Part II–Experimental Investigation", The First Regional Conference on Energy Technology

- Towards a Clean Environment, 1-2 December 2000, Chiang Mai, Thailand. (หน้า ก16)
- 3.1.4 P. Promvonge, L. Vongsarnpigoon and K. silapabanleng "Computation of Isothermal Confined Swirling Flow in a Combustor", 4<sup>th.</sup> SEA Regional Conference On Higher Engineering Education Network (RECHEEN 2000), 15-17 November 2000, Kuala Lumpur, Malaysia. (หนัว ก22)
- 3.1.5 P. Promvonge and K. silapabanleng "Experimental Study of Combustion Characteristics in a Rice Husk Fired Vortex Combustor", Proceedings of IECEC'01 36<sup>th.</sup> Intersociety Energy Conversion Engineering Conference, July 29-August 2, 2000, Savannah, Georgia (หน้า ก29)

# 3.2 การเสนอผลงานในที่ประชุมวิชาการระดับชาติ จำนวน 5 บทความ

- 3.2.1 Pongjet Promvonge and Kulthon Silapabanleng, "Simulation of Turbulent Flow through a Circular Orifice" Proceeding of 13<sup>th</sup> National Mechanical Engineering Conference, December 1999, Vol. 2, pp. 172-176.(หน้า ก36)
- 3.2.2 P. Promvonge, L. Vongsarnpigoon and K. silapabanleng "Numerical Simulation of Isothermal Swirling Turbulent Flow in a Combustor", The Fifth Annual National Symposium on Computational Science and Engineering, 19-20 June 2001, Bangkok Convention Center (BCC), Central Plaza. (หน้า ก42)
- 3.2.3 พงษ์เจต พรหมวงศ์ และ ปริญญา รวมภักดีกุล, "การจำลองการไหลปั่นป่วน แบบหมุนวนในเตาเผา" สัมมนาวิชาการวิศวกรรมเครื่องกลแห่งประเทศไทย ครั้งที่ 13, 2-3 ธันวาคม พ.ศ. 2542, เล่มที่ 1, หน้า 160-165 (หน้า ก52)
- 3.2.4 พงษ์เจต พรหมวงศ์ ชินรักษ์ เชียรพงษ์ และ สมชาย ศรีพัฒนะพิพัฒน์ "การ ศึกษาเชิงตัวเลขของการใหลแบบปั่นป่วนในช่องที่มีการฉีดด้านข้าง" สัมมนา วิชาการวิศวกรรมเครื่องกลแห่งประเทศไทยครั้งที่ 14, 2-3 พฤศจิกายน 2543, หน้า 66-72 (หน้า ก59)
- 3.2.5 พงษ์เจต พรหมวงศ์ ปริญญา รวมภักดีกุล และ กุลธร ศิลษ์บรรเลง "การ คำนวณการไหลหมุนวนแบบอุณหภูมิคงที่ในเตาเผาโดย Algebraic Reynolds Stress Model" สัมมนาวิชาการวิศวกรรมเครื่องกลแห่งประเทศไทยครั้งที่ 14, 2-3 พฤศจิกายน 2543, หน้า 47-52 (หน้า ก67)

#### 3.3 วารสารวิชาการในประเทศ จำนวน 4 บทความ

- 3.3.1 พงษ์เจต พรหมวงศ์ และ ยุทธนา พลอยฉาย "การทำนายการไหลแบบปั่นป่วน ในช่องขนานที่มีครีบ" วารสารพระจอมเกล้าลาดกระบังปีที่ 8 ฉบับที่ 3, ธันวาคม 2543, หน้า 1-6 (หน้า ก74)
- 3.3.2 ปริญญา รวมภักดีกุล นิยม ศรีศิริสิทธิกุล และ พงษ์เจต พรหมวงศ์ "การศึกษา เชิงตัวเลขของการไหลแบบปั่นป่วนในเตา" วารสารพระจอมเกล้าลาดกระบังปีที่ 8 ฉบับที่ 3, ธันวาคม 2543, หน้า 13-18 (หน้า ก81)
- 3.3.3 ศุภชัย เลื่อนลอย นิวัติ พิริยะรุ่งโรจน์ และ พงษ์เจต พรหมวงศ์ "อิทธิพล ความชื้นของแกลบต่อคุณลักษณะการเผาใหม้" วารสารพระจอมเกล้าลาดกระ บังปีที่ 9 ฉบับที่ 1, เมษายน 2544 (หน้า ก88)
- 3.3.4 สมศักดิ์ โพธิ์ถวิลเกียรติ์ นิวัติ พิริยะรุ่งโรจน์ และ พงษ์เจต พรหมวงศ์ "อิทธิพล ของขนาดของแกลบต่อคุณลักษณะการเผาไหม้" วารสารพระจอมเกล้าลาดกระ บังปีที่ 9 ฉบับที่ 1, เมษายน 2544 (หน้า ก94)

# เอกสารอ้างอิง

- Ahmed, S.A. 1997a. "An Isothermal Experimental investigation of Turbulence Transport Through an Abrupt Axisymmetric Expansion." **Proc. Instn. Mech. Engrs.**Vol.212 Part G: 45-55.
- Ahmed, S.A. 1997b. "Three Component Velocity Measurements of an Isothermal Confined Swirling Flow." **Proc. Instn. Mech. Engrs.** Vol.211 Part G: 113-122.
- Ahmed, S.A. and Nejad, A.S. 1992. "Premixed, Turbulent Combustion of Axisymmetric Sudden Expansion Flows." Int. J. Heat and Fluid Flow. Vol.13 No.1: 15-21.
- Boysan, F. et. al. 1982. "A Fundamental Mathematical Modelling Approach to Cyclone Design." Trans. Inst. Chem. Eng. Vol. 60: 222-230.
- Chen, C.J. and Jaw, S.Y. 1997. Fundamentals of Turbulence Modeling. London.: Taylor&Francis.
- Ehalil, E.E. et. al. 1975. "The Calculation of Local Flow Properties in Two-Dimensional Furnaces." Heat Mass Transfer. Vol.18: 775-791.
- El-Mahallawy, F.M. and Habib, M.A. 1978. "Study of Mixing of Two Coaxial Swirling Jets in a Cold Model Furnace." 35-47. in Khalil, K.H. et. al. Flow, **Mixing and Heat**Transfer in Furnace. London: Pergamon Press
- Fraser, S.M. et. al. 1997. "Computation and Experimental Investigations in a Cyclone Dust Seperator." **Proc. Instn. Mech. Engrs.** Vol.211 Part E: 247-257.
- Gaski, T.B. et. al. 1996. Simulation and Modelling of Turbulent Flows. New York.:

  Oxford University Press.
- Gaski, T.B. and Peyret, R. Editor. 1986. Handbook of Computational Fluid Mechanics. London.: Academic Press Ltd.
- Halthore, R.N. and Gouldin, F.C. July 1986. "Laser Scatter Measurement for Gas Densities in a Swirling Flow Combustor." AIAA J. Vol.24 No.7: 1129-1136.
- Hogg, S. and LeschZiner, M.A. January 1989. "Computation of Highly Swirling Confined Flow with a Reynold Stress Turbulence Model." AIAA J. Vol.27 No.1: 57-63.
- Holzapfel, F. et. al. September 1999. "Quintuple Hot-wire Measurements of the Turbulence Structure in Confined Swirling Flows." Trans. ASME J. of Fluid Engineering. Vol. 121: 517-525.

- Hwang, C.C. et. al. March 1993. "A Comparison of the Linear and Nonlinear k-l Turbulence Models in Combustors." **Trans. ASME J. of Fluid Engineering.** Vol.115: 93-102.
- Jones, W.P. and Pascau, A. September 1989. "Calculation of Confined Swirling Flows with a Second Moment Closure." Trans. ASME J. of Fluid Engineering. Vol.111: 248-255.
- Kim, K.Y. and Chung, M.K. March 1988. "Calculation of a Strongly Swirling Turbulent Round Jet with Recirculation by an Algebraic Stress Model." Heat and Fluid Flow J. Vol.9 No.1: 62-68.
- Kitoh, O. 1990. "Experimental study of Turbulent Swirling Flow in a Straight Pipe." Fluid Mechanic J. Vol.25: 445-479.
- Launder, B.E. et. al. 1975. "Progress in the Development of a Reynold Stress Turbulence Closure." J. Fluid Mechanics. Vol.68: 537-566.
- Lin, C.A. and Lu, C.M. July 1994. "Modeling Three-Dimensional Gas Turbine Combustor Model Flow Using Second-Moment Closure." **AIAA J.** Vol.32 No.7: 1416-1422.
- Lin, C.H. et. al. 1997. "Evaluation of the Combustion Efficiency and Emission of Pollutants by Coal Particles in a Vortexing Fluidized Bed." Combustion and Flame. Vol. 110: 163-172.
- Lin, C.H. et. al. 1998. "A Study on the Swirling Flow Flied in the Freeboard of a Vortexing Fluidized Bed Combustor." **JSME international Journal, Series B.** Vol. 41: 538-545.
- Lixing, Z. 1993. Theory and Numerical Modeling of Turbulent Gas-Particle Flows and Combustion. China.: Science Press and CRC Press.
- Lockwood, F.C. et. al. 1974. "An Experimental and Theoretical Investigation of Turbulent Mixing in a Cylindrical Furnace." Combustion and Flame. Vol.23: 283-293
- Nieh, S. and Yang, G. 1986. "Modeling of Solid Flows in a Fluidized Bed with Secondary Tangential Air Injection in the Freeboard." AIChE Annual Meeting, Paper No. 41K.
- Patankar, S.V. 1980. Numerical Heat Transfer and Fluid Flow. Washington D.C.: Hemisphere.
- Promvonge, P. and Vongsarnpigoon, L. March-June 1998. "A Simplified Algebraic Reynolds Stress Model for Calculating Confined Swirling Flows." Eng. Trans. A

- Research Publication of Mahanakorn University of Technology. Vol.1 No.2 :150-161.
- Rhode, D.L. et. al. April 1983. "Mean Flowfields in Axisymmetric Combustor Geometries with Swirl." AIAA J. Vol.21 No.4: 593-600.
- Rodi, W.A. 1976. "New Algebraic Relations for Calculating the Reynolds Stresses." Z. Angew. Math. Mech. (ZAMM). Vol.56: T219-T221.
- Ronald, M.C.S. et. al. 1984. An Experimental Investigation of Gas Jets in Confined Swirling Air Flow. NASA CR 3832.
- Serag-Eldin, M.A. and Spalding, D.B. July 1979. "Computations of Three-Dimensional Gas-turbine Combustion Chamber Flows." Journal of Engineering for Power. Vol.101: 327-336.
- Sloan, D.G. et. al. 1986. "Modeling of Swirl in Turbulent Flow System." Progr. Energy Combust. Sci. Vol.12: 163-250.
- Speziale, C.G. 1987. "On Non-Linear k-l and  $k-\varepsilon$  models of Turbulence." **J. of** Fluid Mechanics. Vol.178: 459-475.
- Speziale, C.G. 1991. "Annual Review of Fluid Mechanics." Annual Review Inc. Vol.23: 107-157.
- Verteeg, H.K. and Malalasekera, W. 1995. An Introduction to Computational Fluid

  Dynamics: The Finite Volume Method. English.: Longman Scientific & Technical,

  Longman Group Limited.
- Willcox, C.D. 1993. Turbulence Modelling for CFD. California.: DCW Industries Inc.
- Xia, J.L. et. al. July 1999. "Study of Swirling Flow in a Combustion Chamber."

  Proceedings of the 3<sup>rd</sup> ASME/JSME Joint Fluids Engineering Conference.
- Zhang, J. et. al. 1992. "A New Version of Algebraic Stress Model for Simulating Strongly Swirling Turbulent Flows." J. Numerical Heat Transfer. Vol.22 Part B: 49-62.

ภาคผนวก ก บทความตีพิมพ์



# THE SIXTH ASIAN INTERNATIONAL CONFERENCE ON FLUID MACHINERY

# **PROCEEDINGS**

18 - 21 JULY 2000

THE PUTERI PAN PACIFIC HOTES

JOHOR BAHRU

JOHOR BAHRU JOHOR, MALAYSIA

<u>o</u>

ACULTY OF THE HANG AFT NOTINE RING

**a** 

INSTITUTION OF ENGINEERS MALAYSIA (IEM)

# SIMULATION OF A TURBULENT CHANNEL FLOW WITH INJECTION THROUGH A SLIT

#### Pongjet Promvonge

Department of Mechanical Engineering, Faculty of Engineering, King Mongkut's Institute of Technology Ladkrabang, Bangkok 10520, THAILAND. Email: kppongje@kmitl.ac.th

#### ABSTRACT

The paper presents the simulation of a turbulent channel flow with injection through a slit. A Finite Volume approach with a non-uniform and staggered grid system is employed in the present simulation. To account for the turbulence nature of the flow, an algebraic Reynolds stress model (ASM) and the standard k- $\varepsilon$  turbulence model are incorporated in the time-averaged governing equations. Effect of numerical diffusion on the calculated results is also investigated by comparing between a second-order-differencing scheme for the convection transport and a first-order one. The influences of injection through the slit on mean flow properties in a fully developed turbulent channel flow are investigated and compared with available measurements. The computation reveals that use of ASM leads to slightly accurate results than that of the standard k- $\varepsilon$  turbulence model.

#### 1. INTRODUCTION

The injection of a side-jet into a cross-flow is encountered in several engineering applications, such as transpiration cooling of turbine blades, the mixing process for the combustor cooling, the transition from hover to forward flight of a V/STOL aircraft, the entrainment of jet pump and drag reduction. Injection of fluid from a wall to the flow is a way to control wall turbulence. When the jet is injected into a cross-flowing stream, there is a complicated interaction between the jet and the cross-flow. Its nature of this kind of flow is still not well understood and need to clarify how mean flow and turbulence characteristics are affected by the fluid injection. There have been many reports published on the jet in a turbulent cross-flow. Andreopoulos [1] presented an investigation of velocity fluctuation statistics in the jet-pipe flow normal to a crossstream for different ratios of jet-to-crossflow velocities. Sumitani and kasagi [2] studied turbulent channel flow with uniform injection and suction on the two opposite channel walls by a direct numerical simulation (DNS) and obtained various statistic characteristics on turbulence. Kato et al. [3] presented a method to reduce turbulent frictional drag by injection of high viscosity fluid into the boundary layer. The flow characteristics in a two-dimensional channel with nonuniform injection using both laser-Doppler velocimetry measurements and DNS for comparison can be found in Liou et al. [4]. Sano [5] investigated experimentally the turbulent channel flow with various side-jet injection flow rates. The brief survey presented above reveals that there has been no report of numerical investigation on the mean flow properties in a channel flow with side injection with an algebraic Reynolds stress model

This article deals with the numerical simulation of a fully developed turbulent channel flow with a side-jet injection of Sano [5] by utilizing the ASM and various numerical schemes. The process of recovery to equilibrium state from non-equilibrium state is investigated numerically by predicted wall static pressure and velocity profiles.

#### 2. MATHEMATICAL FORMULATION

#### 2.1 Governing Equations

The phenomenon under consideration is governed by the steady two-dimensional axisymmetric form of the continuity and the time-averaged incompressible Navier-Stokes equations. In the Cartesian tensor system these equations can be written in the following form:

$$\frac{\partial}{\partial x_i}(\rho u_i) = 0 \tag{1}$$

$$\frac{\partial(\rho u_i u_j)}{\partial x_i} = -\frac{\partial \rho}{\partial x_i} + \frac{\partial}{\partial x_j} (\bar{t}_{ij} + \tau_{ij}) \tag{2}$$

where  $\rho$ ,  $u_i$ , p and  $x_i$  are the density, mean velocity tensor, mean pressure and coordinate tensor respectively. The mean viscous stress tensor is approximated as:

$$\tilde{t}_{ij} = \mu \left( \frac{\partial u_i}{\partial x_j} + \frac{\partial u_j}{\partial x_i} \right) \tag{3}$$

where  $\mu$  is laminar viscosity. The time-averaged Reynolds stress tensor,  $\tau_{ij} = -\rho u_i u_j$ , in the above equation is not known and thus, models are needed to express it in terms of the solution variables. In the present study, two turbulence models are used, namely the k- $\varepsilon$  model and an algebraic stress model (ASM). The k- $\varepsilon$  model has been reviewed in references [6] and it will be described briefly. The standard k- $\varepsilon$  model version relates the turbulent eddy viscosity to the turbulence kinetic energy k and the dissipation rate  $\varepsilon$  through Boussinesq's approximation as:

$$\tau_{ij} = -\frac{2}{3}\delta_{ij}(\rho k) + \mu_i(\frac{\partial u_i}{\partial x_j} + \frac{\partial u_j}{\partial x_i})$$
 (4)

where  $\mu_t = \rho C_{\mu} k^2 / \varepsilon$  is the turbulent eddy viscosity and  $\varepsilon$  is the dissipation rate of turbulence kinetic energy (TKE). The modelled equation of the TKE, k is given by:

$$\frac{\partial}{\partial x_j} \left( \rho u_j k \right) = \frac{\partial}{\partial x_j} \left( \frac{\mu_e}{\sigma_k} \frac{\partial k}{\partial x_j} \right) + G - \rho \varepsilon \tag{5}$$

in which  $\mu_e = \mu_t + \mu$  is effective viscosity. Similarly the dissipation rate of TKE is given by the following equation:

$$\frac{\partial}{\partial x_{j}} \left( \rho u_{j} \varepsilon \right) = \frac{\partial}{\partial x_{j}} \left( \frac{\mu_{e}}{\sigma_{\varepsilon}} \frac{\partial \varepsilon}{\partial x_{j}} \right) + \frac{\varepsilon}{k} \left( C_{\varepsilon 1} G - C_{\varepsilon 2} \rho \varepsilon \right) \tag{6}$$

where G is the rate of generation of the TKE while  $\rho \varepsilon$  is its destruction rate. G is given by:

$$G = \mu_e \left[ \left( \frac{\partial u_i}{\partial x_j} + \frac{\partial u_j}{\partial x_i} \right) \frac{\partial u_i}{\partial x_j} \right]$$
 (7)

The boundary values for the turbulent quantities near the wall are specified with the wall function method [7].  $C_{\mu} = 0.09$ ,  $C_{e1} = 1.44$ ,  $C_{e2} = 1.92$ ,  $\sigma_k = 1.0$ , and  $\sigma_{\epsilon} = 1.3$  are empirical constants [6] in the turbulence transport equations. Reynolds-averaged transport equations can be solved for  $\tau_{ij}$ , [6] the modelled equations for which are:

$$\frac{\partial \tau_{ij}}{\partial t} + \frac{\partial (u_k \tau_{ij})}{\partial x_k} = -G_{ij} - \Phi_{ij} + D_{ij} + \varepsilon_{ij}$$
(8)

where

$$G_{ij} = \text{local production} = \rho P_{ij} = -\left(\rho \overrightarrow{u_i u_k} \frac{\partial u_j}{\partial x_k} + \rho \overrightarrow{u_j u_k} \frac{\partial u_i}{\partial x_k}\right)$$

$$\Phi_{ij} = \text{local pressure strain} = -C_1 \frac{\rho \varepsilon}{k} \left( \overrightarrow{u_i u_j} - \frac{2}{3} k \delta_{ij} \right) - C_2 \left( G_{ij} - \frac{2}{3} G \delta_{ij} \right)$$

$$D_{ij} = \text{net diffusive transport} = -\frac{\partial}{\partial x_k} \left( (\frac{\mu_e}{\sigma_T}) \frac{\partial \overrightarrow{u_i u_j}}{\partial x_k} \right)$$

$$\varepsilon_{ij} = \text{local dissipation tensor} = \frac{2}{3} \rho \varepsilon \delta_{ij}$$

in which  $C_1 = 2.5$ , and  $C_2 = 0.55$  are model constants.

#### 2.2 Algebraic Reynolds Stress Model (ASM)

For simplicity in solving the six Reynolds stresses, Rodi's approximation [8] is used in this study and the Reynolds stress transport can be expressed in algebraic form as follows:

$$\frac{D\tau_{ij}}{Dt} - D_{ij} = \frac{\tau_{ij}}{\rho k} (\frac{Dk}{Dt} - D_k) \tag{9}$$

Substitution of eqs. (5) and (8) into eq. (9) gives the desired algebraic expression for  $\tau_{ii}$ :

$$-G_{ij} - \Phi_{ij} + \frac{2}{3} \delta_{ij} \rho \varepsilon = \frac{\tau_{ij}}{\rho k} (G - \rho \varepsilon)$$
 (10)

The ASM expressions can thus be rewritten as:

$$\rho \overrightarrow{u_i u_j} = \frac{2}{3} \delta_{ij} \rho k + \frac{\lambda k}{\varepsilon} \left( G_{ij} - \frac{2}{3} \delta_{ij} G \right)$$
(11)

where the empirical constant  $\lambda$ , was found to be 0.135, [9] is defined as:

$$\lambda = \frac{1 - C_2}{C_1 - 1 + \frac{G}{\rho \varepsilon}} \tag{12}$$

#### 2.3 Common Form for the Equations

All the governing equations can be re-organised and expressed in a standard form that includes the convection, diffusion, and source terms for 2-D axisymmetric flows as follows:

$$\frac{\partial}{\partial x}(\rho u\phi) + \frac{\partial}{\partial y}(\rho v\phi) - \frac{\partial}{\partial x}\left(\Gamma_{\phi x}\frac{\partial \phi}{\partial x}\right) - \frac{\partial}{\partial y}\left(\Gamma_{\phi y}\frac{\partial \phi}{\partial y}\right) = S_{\phi}$$
(13)

where  $\phi$  may stand for any variable including the velocity components,  $\Gamma_{\phi_X}$  and  $\Gamma_{\phi_Y}$  are the exchange coefficients for  $\phi$ , and  $S_{\phi}$  is the source term.

#### 2.4 Solution Procedure

In the present computation, the time-averaged Navier-Stokes equations, the TKE equation, and the TKE dissipation rate equation are solved numerically by a control-volume finite-difference method [10] together with the turbulence model equations, equation (4) for the k- $\varepsilon$  model or equation (11) for the ASM. All equations are in a generalised form of equation (13). The SIMPLE algorithm is utilised for pressure-velocity de-coupling and iteration [10, 11]. The first-order upwind (FOU) and the second-order upwind (SOU) [12] schemes were used for discretising convection and diffusion transports on a staggered grid cell. The under-relaxation iterative TDMA line-by-line sweeping technique is used for solving the resultant finite-difference equations. The computation was carried out using a personal computer (Pentium III-450 MHz). About 7,000 iterations were needed to achieve satisfactory convergence for each calculation case, which requires about 1.0 hr of computer time.

#### 3. CHANNEL FLOW WITH SIDE-INJECTION OF SANO [5]

A flow in channel with a side jet of Sano [5] was employed in the present simulation. A schematic configuration of the channel is shown in Fig. 1 below. The channel with a length of about 3,050-mm has a width (h) of 30-mm and the slit width (L) for injection is 10 mm. Profile measurements of axial velocity, wall-static pressure, Reynolds stresses, and wall shear stresses were provided and measured by using a constant-temperature-type hot-wire anemometer. The mean velocity  $u_{in}$  at the channel inlet was set at 10.0 m/s while side-injection flow rate,  $Q = vL/hu_{in}$  where v = injection velocity, was set at three values: 0.067, 0.133 and 0.2. The measurements were made at eight stations, namely, x = 70, 110, 150, 250, 350, 500, 700, and 950 mm from the slit.

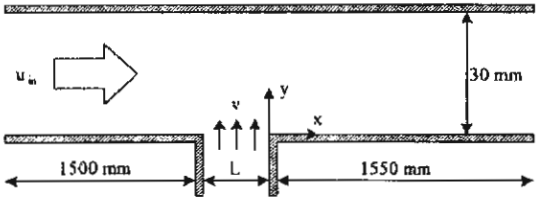


Fig. 1 Geometry of channel with side-jet injection.

#### 4. RESULTS AND DISCUSSION

The comparisons between the predicted results by the k- $\epsilon$  turbulence model and the ASM with different numerical schemes and the measured data of the flow are presented in Figs. 2 through 7. The predicted axial velocities are compared with the measurements, where solid or dash curves are represented for the calculated results while open circles for the measured data. The computational results are based on an 80x40 non-uniform grid with refinement in the vicinity of the slit. Grid independence of the numerical results was verified with a 120x60 finer grid. It is found that the differences for both the base grid and the finer grid in local flow properties are marginal. This suggests that grid independent solutions can be obtained with an 80x40 grid, which is used throughout the computations.

#### 4.1 Effects of Numerical Schemes

The axial mean velocity profiles predicted with the k- $\varepsilon$  model and the FOU and SOU schemes are compared with the measured data in Figs. 2 and 3 for side-injection flow rates of 0.067 and 0.2 respectively. A closer examination reveals that predictions with both the schemes generally are in good agreement with the measurements. However, in prediction with the SOU scheme in Fig. 3, under-predicted results are seen in the vicinity of the slit while excellent agreement is found in the upper wall region in comparison with experimental data. Overall, use of the SOU leads to slight improvement so the FOU is sufficient for computation of this flow.

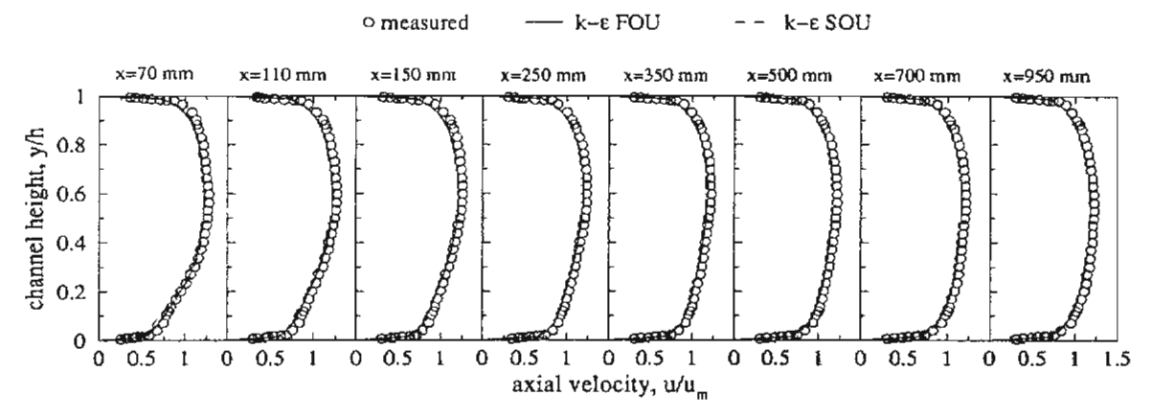


Fig. 2 Effects of numerical schemes on streamwise velocity profiles with measurements for Q = 0.067

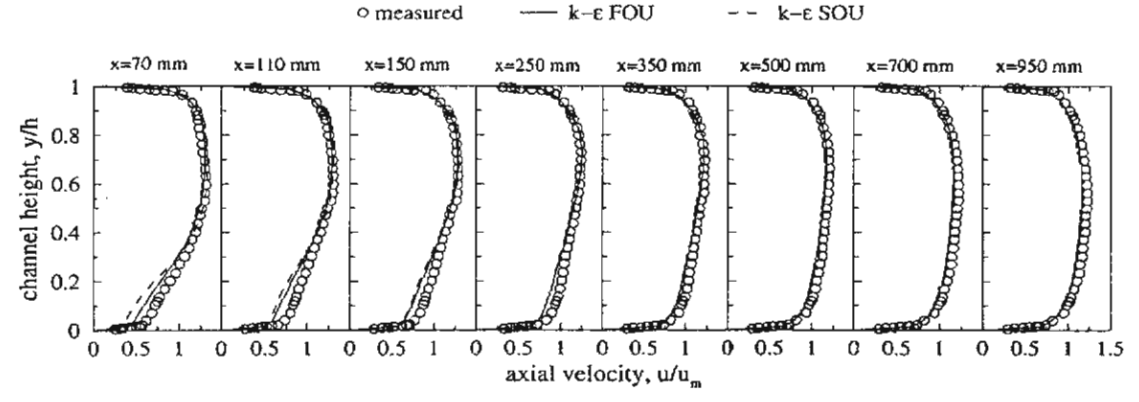


Fig. 3 Effects of numerical schemes on streamwise velocity profiles with measurements for Q = 0.2

#### 4.2 Flow Field

Velocity Field. Predictions using the k- $\varepsilon$  model and the ASM are compared with experimental data in Figs. 4, 5 and 6 for the injection flow rates of 0.067, 0.133 and 0.2 respectively. It is found that for lower injection flow rate, Q = 0.067, the predicted profiles of streamwise mean velocity are in excellent agreement with measurements for both turbulence models as depicted in Fig. 4. However, increase in side-injection flow rate leads to significant deviations between predicted and measured results in the vicinity of side-jet port but both predicted and measured profiles agree well after station x=350-mm as can be seen in Figs. 5 and 6. Close examination

reveals that as the flow proceeds toward the injection slit, the mean velocity profiles gradually becomes nonuniform and asymmetrical near the wall and returns to uniform and symmetric after advancing in the downstream direction. The ASM gives slight under-prediction close to the injection port while the k- $\varepsilon$  model predicts slightly better. But for further downstream from the slit, results predicted by both turbulence models are similar and agree very well with measurements.

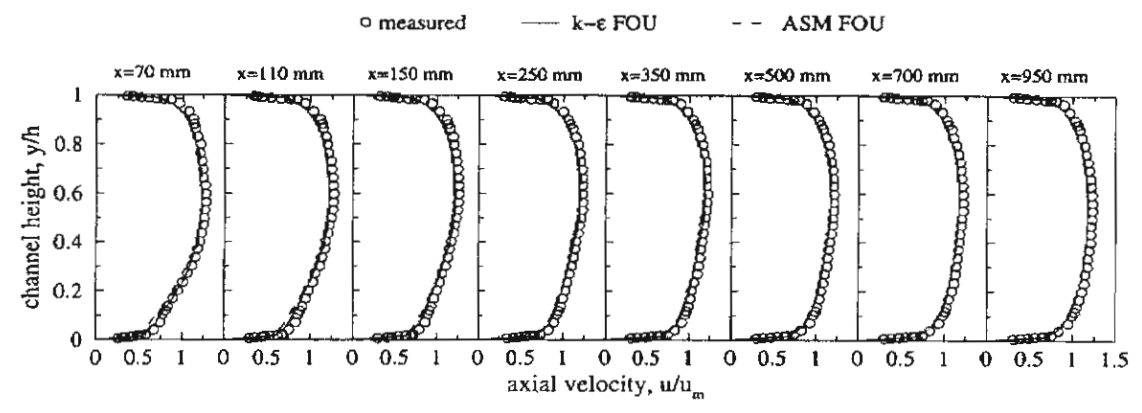


Fig. 4 Comparison of predicted streamwise velocity profiles with measurements for Q = 0.067

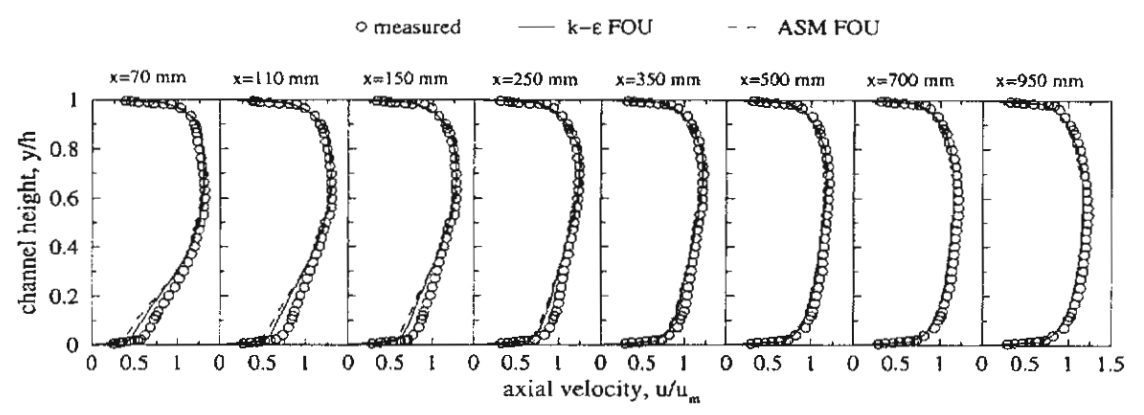


Fig. 5 Comparison of predicted streamwise velocity profiles with measurements for Q = 0.133

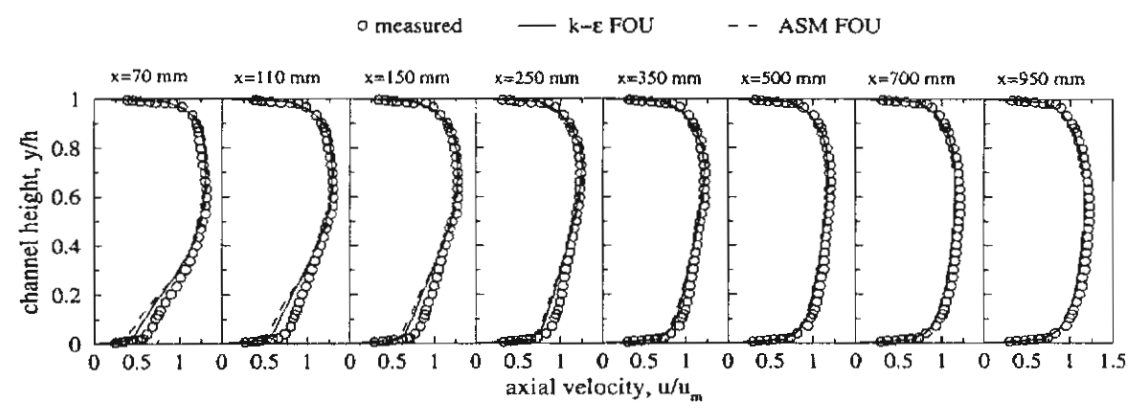


Fig. 6 Comparison of predicted streamwise velocity profiles with measurements for Q = 0.2

Pressure Field. Figure 7 compares the non-dimensional profiles of static pressure along the upper and lower walls using the FOU scheme with the measurements. It is found that the pressure profiles for the lower wall are nearly similar to those for the upper wall except for the

vicinity of the slit. A close look reveals that there is a high-pressure drop across the side-jet port for both walls. This suggests that injection to the flow suffers substantially from a pressure loss. Predictions with both turbulence models show favourable agreement only in the downstream region of the slit. However, for upstream of the slit, the calculated wall pressures for both walls rise faster than the experiment shows. At upstream regions from the slit, the ASM results mimic experimental data better while the k- $\epsilon$  model ones are over-predicted especially at high flow rates of injection. Again, use of the ASM results in slight improvement for this flow.

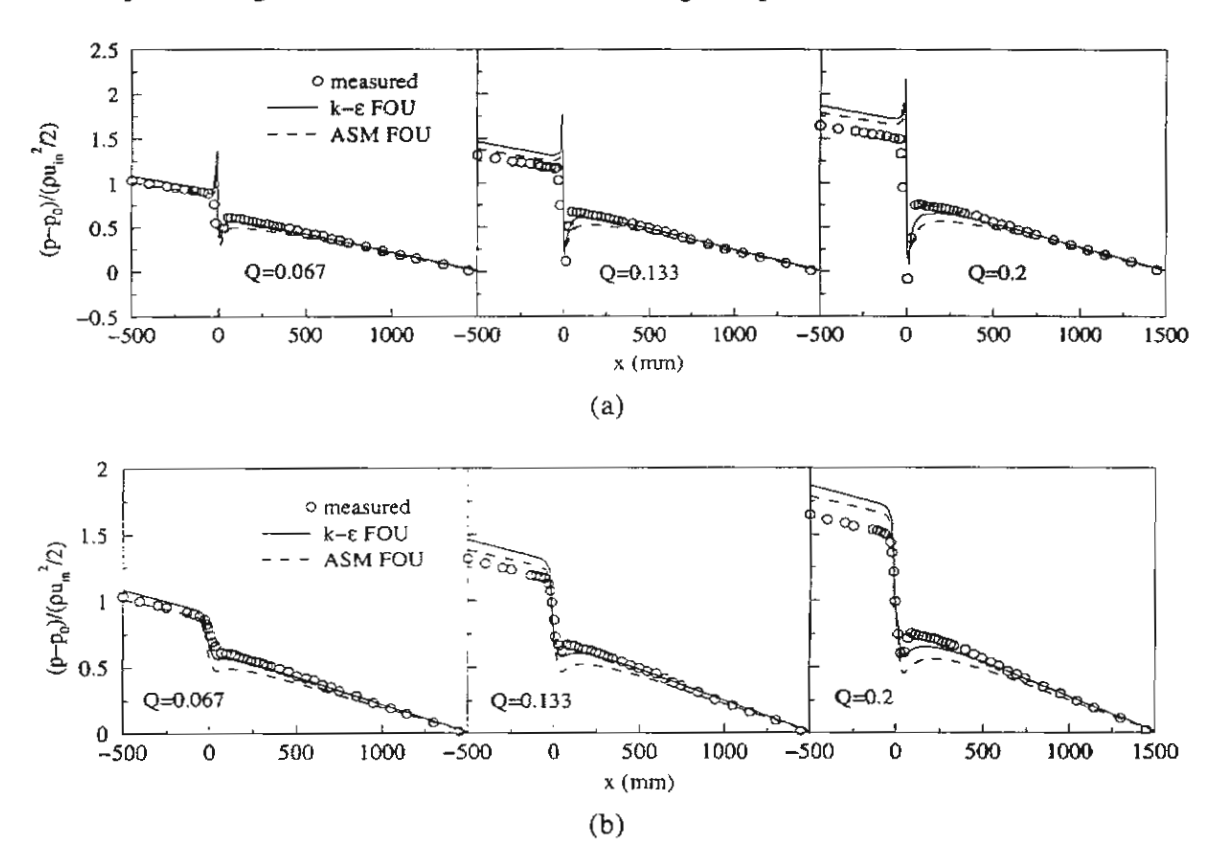


Fig. 7 Comparison of predicted wall static pressure distributions with measurements under different side-injection flow rates, Q, for (a) lower wall and (b) upper wall (p<sub>0</sub> = exit pressure).

#### 5. CONCLUDING REMARKS

Simulations of turbulent channel flow with side-injection have been carried out by utilizing the k- $\epsilon$  model and ASM with two numerical schemes. The prediction of mean flow properties was compared with measurements. The conclusions from the investigation can be drawn as follows:

- 1. The predicted axial velocity and wall-static pressure profiles by the FOU and SOU schemes for both turbulence models are generally in good agreement with measurements.
- 2. ASM with the FOU scheme shows small improvement over the k-ε model.
- The FOU and SOU schemes give slightly under-predicted in the vicinity of the slit for the lower wall but slightly over-predicted results for the upper wall in comparison with measurements.
- 4. The higher side-injection flow rate leads to substantial under-prediction in the vicinity of the side-jet slit.

#### 6. ACKNOWLEDGEMENTS

The authors would like to gratefully acknowledge the Thailand Research Fund for financial support of this research.

#### 7. REFERENCES

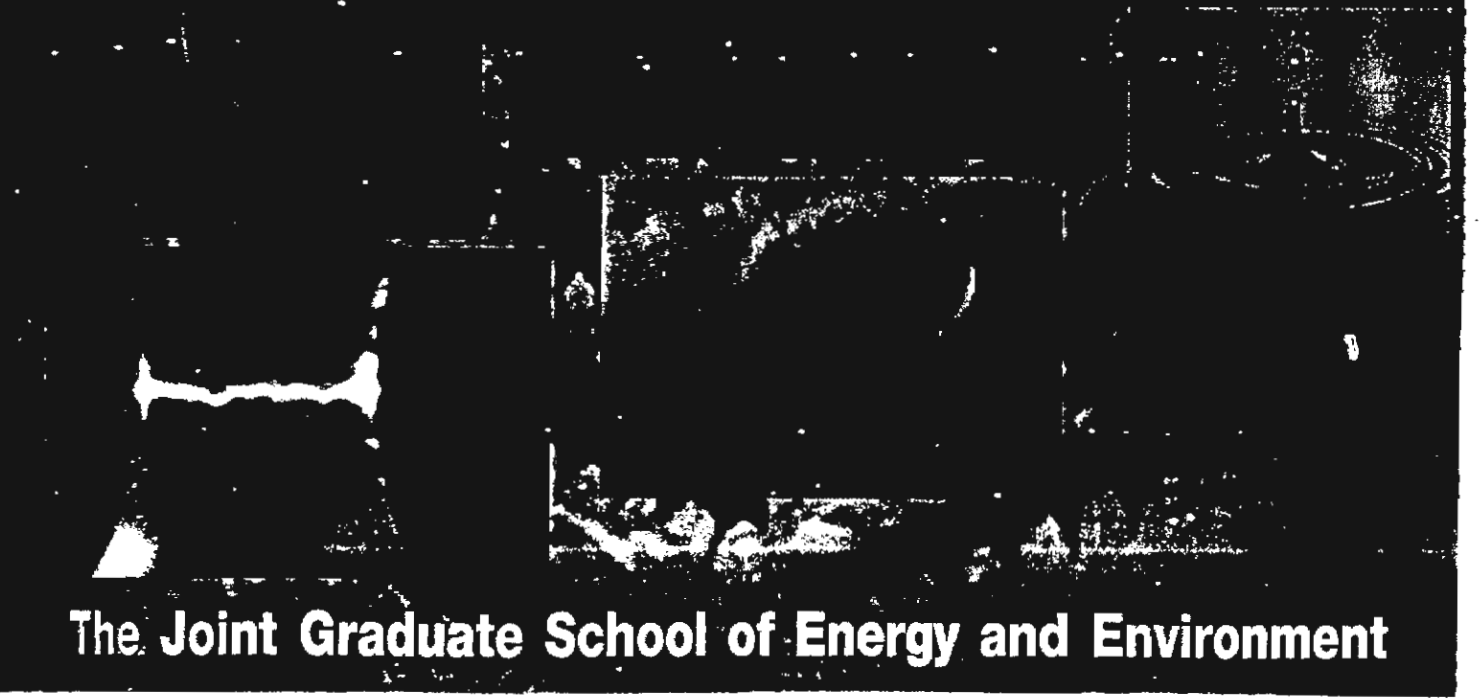
- 1. Andreopoulos, J., Measurements in a Jet-Pipe Flow Issuing Perpendicularly into a Cross Stream, ASME J. of Fluids Engineering, Vol. 104, pp. 493-499, 1982.
- 2. Sumitani, Y. and Kasagi, N., Direct Numerical Simulation of Turbulent Transport with Uniform Wall Injection and Suction, AIAA J., Vol. 33, No. 7, pp. 1220-1228, 1995.
- 3. Kato, H., Fujii, Y., Yamaguchi, H., and Miyanaga, M., Frictional Drag Reduction by Injecting High-Viscosity Fluid into Turbulent Boundary Layer, Trans. ASME, J. Fluids Engineering, Vol. 115, 1993.
- Liou, T.M., Lien, W.Y. and Tsai, G.S., Experimental and Computation Studies of Fluid Flow in a Two-dimensional Porous-walled Channel, 9<sup>th</sup> Symposium on Turbulent Shear Flows, 5-4, 1993.
- 5. Sano, M., Mean Flow and Turbulence Characteristics in a Turbulent Channel Flow with Injection through a Slit, Proceedings of the 3<sup>rd</sup> ASME/JSME Joint Fluids Engineering Conference, Paper No. FEDSM99-7283, 18-23 July, San Francisco, California, 1999.
- 6. Wilcox, C.D., Turbulent Modelling for CFD, DCW Industries, Inc., California, 1993.
- 7. Patankar, S.V. and Spalding, D.B., Heat and Mass Transfer in Boundary Layers, Intertext Books, London, 1970.
- 8. Rodi, W.A., New Algebraic Relations for Calculating the Reynolds Stresses, Z. Angew. Math. Mech. (ZAMM), vol. 56, pp. T219-T221, 1976.
- 9. Promvonge, P., Numerical Simulation of Turbulent Compressible Vortex-Tube Flow, Proceedings of the 3<sup>rd</sup> ASME/JSME Joint Fluids Engineering Conference, Paper No. FEDSM99-6972, 18-23 July, San Francisco, California, 1999.
- 10.Patankar, S.V., Numerical Heat Transfer and Fluid Flow, Hemisphere, Washington, D.C., 1980.
- 11. Versteeg, H.K. and Malalasekera, W., An Introduction to Computational Fluid Dynamics: The Finite Volume Method, Longman Scientific & Technical, Longman Group Limited, Essex, England, 1995.
- 12. Shyy, W., Thakur, S., and Wright, J., Second Order Upwind and Central Difference Schemes for Recirculating Flow Computation, AIAA J., Vol.30, No.4, pp.931-932, 1992.



The First Regional Conference on Energy Technology Towards a Glean Environment

1st-2nd December 2000 The Empress Hotel, Chiang Mai, Thailand

Efficient Energy and Clean Environment A Review of The Past and a Look at the Next Decade



#### A Low Emission Annular Vortex Combustor Firing Rice Husk Fuel: Part I – Numerical Simulation

#### P. Promvonge<sup>1</sup>, L. Vongsarnpigoon<sup>2</sup>, S. Sripattanapipat<sup>1</sup> and K. Silapabanleng<sup>3</sup>

- Department of Mechanical Engineering, Faculty of Engineering, King Mongkut's Institute of Technology Ladkrabang, Bangkok 10520, Thailand. Email: <a href="mailto:kppongje@kmitl.ac.th">kppongje@kmitl.ac.th</a>
- Department of Mechanical Engineering, Faculty of Engineering, Mahanakorn University of Technology, Bangkok 10530, Thailand.
- 3. Department of Mechanical Engineering, Faculty of Engineering, Chulalongkorn University, Bangkok 10330, Thailand.

#### **Abstract**

The paper presents the simulation of the strongly swirling turbulent flow and combustion characteristic in an annular vortex combustor (VC) for burning rice husk. Computations, based on a staggered finite volume method, were carried out by utilising the standard k- $\epsilon$  turbulence model for the closure of the second-order correlation moments in the governing equations. Cold flow and mixture fraction combustion models for gas fuel were used to investigate the effects of various operating parameters on the mean flow properties in the VC. Some of calculated results are compared with available measurements.

#### Introduction

To help increase rice husk utilisation in an efficient, clean manner, a novel non-slagging vortex combustor (VC) was recently developed and investigated for drying/heating application purposes. The VC technique first developed for coal fuel [1] is evolved from the basic understanding of swirling gasparticle flows and combustion in vortex chambers [2]. Its integrates many advantages from cyclone combustor, fluidized bed combustor, multistage combustion and pulverized coal-fired combustor; while eliminates most of their inherent disadvantages. This combustor is featured with two vertical, concentric tubes with multiple air injection. Due to the strong swirl and low temperature combustion environments, the VC has demonstrated to pose many inherent advantages: vigorous gas-particle turbulence, long particle residence time, high combustion intensity, and broad fuel flexibility.

As schematically shown in Fig. 1, primary air is provided into the lower chamber (or the bottom), together with solid fuel. Secondary air is tangentially injected into the annular chamber of the VC through the nozzles arranged at various strategic levels to form a strong swirl. Combustion occurs primarily in the annular space. Then, hot flue gas spirally ascends to the top before leaving through the exhaust center tube. The combined effects of centrifugal, gravitational, and fluid drag forces give rise to fuel particles to be trapped along the height of the combustor. As particles are burned they continually reduce in mass and size until completely burned out. The majority of ash particles become light or small enough to be entrained by the flue gas and exit the combustor as flyash. Some may remain in the combustor bottom as dry ash. Hence, it is necessary to know the detailed aerodynamic structure and the distinct flow characteristics of the VC. However, little study pertaining to its flow properties has been made and numerical study of combusting rice husk flow in the VC has never come across due to its difficulty in modelling.

This article deals with the numerical results of the isothermal and combusting gas flows in a VC of Nieh and Zhang [1], along with only the measured cold flow results for comparison. This investigation is to help expand the technical database, better understand the involved physical processes, and guide the design and operation of the vortex combustor.

#### **Mathematical Modelling and Solution Procedure**

Governing Equations for Flow Model: The phenomenon under consideration is governed by the steady two-dimensional axisymmetric form of the continuity and the time-averaged incompressible

Navier-Stokes equations. In the Cartesian tensor system these equations can be written in the following form:

$$\frac{\partial}{\partial x_i} (\rho u_i) = 0 \tag{1}$$

$$\frac{\partial(\rho u_i u_j)}{\partial x_j} = \frac{\partial}{\partial x_i} + \frac{\partial}{\partial x_i} (\bar{t}_{ij} + \tau_{ij})$$
 (2)

where  $\rho$ ,  $u_i$ , p and  $x_i$  are the density, mean velocity tensor, mean pressure and coordinate tensor respectively. The mean viscous stress tensor is approximated as:

$$\bar{t}_{ij} = \mu \left( \frac{\partial u_i}{\partial x_j} + \frac{\partial u_j}{\partial x_i} \right) \tag{3}$$

where  $\mu$  is laminar viscosity and  $\tau_{ij} = -\rho u_i u_j$  is the time-averaged Reynolds stress tensor. The standard k- $\varepsilon$  model relates the turbulent eddy viscosity to the turbulence kinetic energy k and the dissipation rate  $\varepsilon$  through Boussinesq's approximation as:

$$\tau_{ij} = -\frac{2}{3}\delta_{ij}(\rho k) + \mu_i(\frac{\partial u_i}{\partial x_i} + \frac{\partial u_j}{\partial x_i})$$
 (4)

where  $\mu_t = \rho C_{\mu} k^2 / \varepsilon$  is the turbulent eddy viscosity and  $\varepsilon$  is the dissipation rate of turbulence kinetic energy (TKE). The modelled equation of the TKE, k is given by:

$$\frac{\partial}{\partial x_j} \left( \rho u_j k \right) = \frac{\partial}{\partial x_j} \left( \frac{\mu_e}{\sigma_k} \frac{\partial k}{\partial x_j} \right) + G - \rho \varepsilon \tag{5}$$

in which  $\mu_e = \mu_i + \mu$  is effective viscosity. Similarly the dissipation rate of TKE is given by the following equation:

$$\frac{\partial}{\partial x_{j}} \left( \rho u_{j} \varepsilon \right) = \frac{\partial}{\partial x_{j}} \left( \frac{\mu_{e}}{\sigma_{\varepsilon}} \frac{\partial \varepsilon}{\partial x_{j}} \right) + \frac{\varepsilon}{k} \left( C_{\varepsilon 1} G - C_{\varepsilon 2} \rho \varepsilon \right) \tag{6}$$

where G is the rate of generation of the TKE while  $\rho \varepsilon$  is its destruction rate. G is given by:

$$G = \mu_e \left[ \left( \frac{\partial u_i}{\partial x_j} + \frac{\partial u_j}{\partial x_i} \right) \frac{\partial u_i}{\partial x_j} \right]$$
 (7)

The boundary values for the turbulent quantities near the wall are specified with the wall function method [3].  $C_{\mu} = 0.09$ ,  $C_{\epsilon 1} = 1.44$ ,  $C_{\epsilon 2} = 1.92$ ,  $\sigma_k = 1.0$ , and  $\sigma_{\epsilon} = 1.3$  are empirical constants [4] in the turbulence transport equations.

Gaseous Phase Combustion: The combustion model is based upon the assumption of single chemical reaction with fast chemistry with respect to the turbulent time scale. The mass fractions of fuel, oxidant and products are only functions of the mixing rate. In a combustion system, a fuel stream flows into the chamber at a rate of f kg/s and an oxidant stream at a rate of f kg/s. They mix in the combustion chamber to form a mixture which flows out at a rate of 1.0 kg/s. For adiabatic, steady flow, the fuel and oxidant enthalpies can be related to f as follows [5]:

$$f = \frac{h - h_{ox}}{h_{fu} - h_{ox}} \qquad \text{or} \qquad f = \frac{\left(C_p T + m_{fu}\right) - \left(C_p T\right)_{ox}}{\left(C_p T + H\right)_{fu} - \left(C_p T\right)_{ox}} \tag{8}$$

where f called the mixture fraction, is between 0.0 and 1.0, H and  $m_j$  are the heat of combustion and mass fraction of species j. From the partial differential equation of f, the flame temperature (T) can be

obtained. Thus, the density  $\rho$ , is calculated from ideal gas equation,  $\rho = MP/\overline{R}T$  in which  $1/M = \sum (m_j/M_j)$ ,  $\overline{R}$  is the universal gas constant and M is the mean mixture molar mass.

Common Form for the Equations: All the governing equations can be re-organised and expressed in a standard form that includes the convection, diffusion, and source terms for 2-D axisymmetric flows as follows:

$$\frac{\partial}{\partial x}(\rho u\phi) + \frac{\partial}{\partial y}(\rho v\phi) - \frac{\partial}{\partial x}\left(\Gamma_{\phi x}\frac{\partial \phi}{\partial x}\right) - \frac{\partial}{\partial y}\left(\Gamma_{\phi y}\frac{\partial \phi}{\partial y}\right) = S_{\phi} \tag{9}$$

where  $\phi$  may stand for any variable including the velocity components,  $\Gamma_{\phi_x}$  and  $\Gamma_{\phi_y}$  are the exchange coefficients for  $\phi$ , and  $S_{\phi}$  is the source term.

Solution Procedure: In the present computation, the time-averaged Navier-Stokes equations, the TKE equation, the TKE dissipation rate equation and the mixture fraction equation are solved numerically by a control-volume finite-difference method [6] together with the turbulence model equations. All equations are in a generalised form of equation (9). The SIMPLE algorithm is utilized for pressure-velocity de-coupling and iteration [6, 7]. The first-order upwind, hybrid and the QUICK [8] schemes were used for discretising convection and diffusion transports on a staggered grid cell. The under-relaxation iterative TDMA line-by-line sweeping technique is used for solving the resultant finite-difference equations. The computation was carried out using a personal computer (Pentium III-550 MHz). About 20,000 iterations were needed to achieve satisfactory convergence for each calculation case, which requires about 2.0 hr of computer time.

#### **Vortex Combustor Flow**

A strongly swirling flow in a VC [1] was selected and its schematic diagram of the VC is shown in Fig. 1. It comprised a 0.11 m diameter central tube, concentrically placed inside a cylindrical chamber of 0.66 m height and 0.25 m diameter. The center tube was set 0.51 m into the chamber. Air injected into the chamber tangentially through 3 sets of nozzles spirally ascended through the annular space and exhausted through the central tube. The measured swirl number (S) was 13.9. Experimental data of mean velocities are provided at ten axial locations, namely, x = 0.051, 0.112, 0.173, 0.234, 0.295, 0.358, 0.42 0.483, 0.544, and 0.605 m. The specifications of the combustor are summarised in Table 1 below.

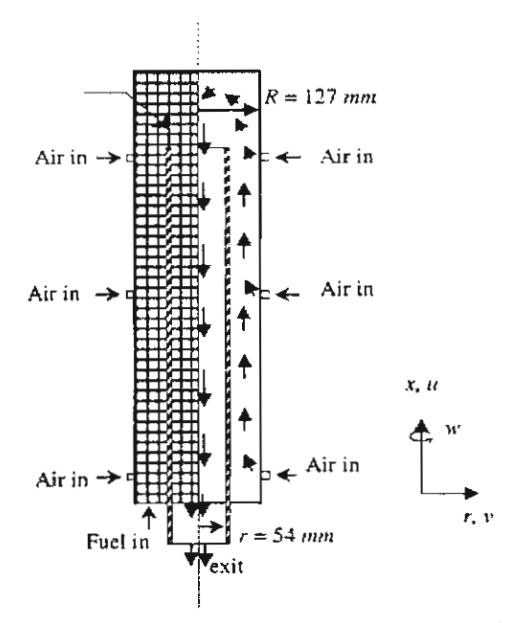


Fig. 1 Flow arrangement, computational domain and grid for the VC [1].

**Table 1** Geometry and flow conditions for the vortex chamber [1].

Parameter	Magnitude			
Vortex chamber geometry chamber inner dia., m chamber height, m centre tube outer dia., m centre tube inner dia., m centre tube height, m		0.25 0.66 0.13 0.11 0.51		
Multiple air injection nozzle height distribution, m flow rate distribution, m <sup>3</sup> /h tangential velocity, m/s air temperature, K	0.051 226 24.6 300	0.295 226 24.6 300	0.483 226 24.6 300	

For modelling of the combusting VC flow, methane (CH<sub>4</sub>) gas fuel was employed instead of rice husk because of simplicity. The gas fuel was injected at the bottom into the lower chamber. To study the effect of inlet fuel injection on combusting flow properties for keeping air injection constant, two types of the injection were made. One was the axial injection and the other was the oblique fuel jet (30-degree from a tangential line).

#### **Results and Discussion**

**Prediction of Cold VC Flow:** The influence of grid mesh distribution on the predicted velocity profiles is investigated by comparison with measurements for different grid densities. It is found that a grid size of 40x20 or finer is sufficient to ensure grid-independence of results. The axial and tangential velocity variations in Figs. 2a and 2b, respectively, for various numerical schemes along with the measurements show that, except for minor differences, all three schemes for the convective terms yield almost the same results. This indicates that any of the numerical schemes can be used to calculate the flow with adequate accuracy and thus, only upwind scheme was carried out throughout. These figures indicate that the predictions with the k- $\varepsilon$  model resulted in poorer agreement with the experimental data especially in the top cylindrical region. For example, the k- $\varepsilon$  model fails to predict the central toroidal recirculation zone and the combined forced and free vortex motion in the upper region of the combustor (at x = 0.544 and 0.605 m). However, in the present study, the k- $\varepsilon$  model was still used for giving a trend of the combusting flow characteristics in the VC since it is robust and easy for use.

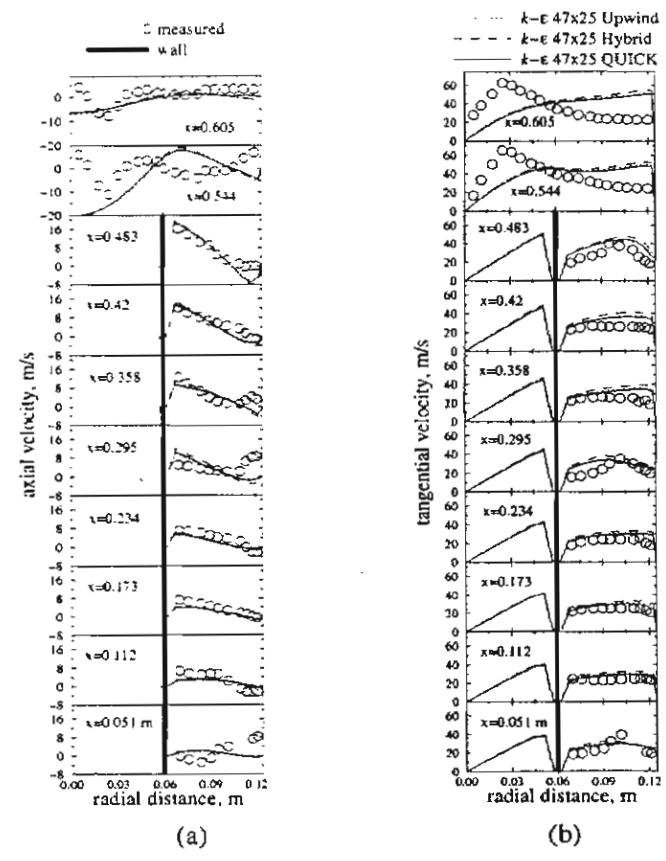


Fig. 2 Comparison of measurements with predictions using different schemes, (a) axial and (b) tangential velocities.

Prediction of Reacting VC Flow: The influence of inlet fuel injection on the flow and temperature fields was studied by using two different inlet fuel injection types. The first type was made by setting the fuel inlet nozzle to obtain a fuel jet parallel to the axial axis, called the axial fuel jet. The second type was set to obtain an oblique fuel jet with an inclination angle of 30° along the tangential line at

the fuel inlet. The predicted axial velocity, tangential velocity, static pressure and temperature profiles for both fuel injections are depicted in Fig. 3a, 3b, 3c and 3d, respectively. It is worth noting that both fuel injections have no effect on the mean flow properties such as velocities and pressure as can be seen in Fig. 3a, 3b and 3c. When compared to the cold flow model, the axial velocity at the outlet for this case is higher (about 3 times). For the temperature profiles, It is found that the oblique fuel injection leads to a higher temperature in the upper chamber while gives the same temperature in the annular region as shown in Fig. 3d. This indicates that inlet fuel should be tangentially injected into the chamber when uniform temperature inside the VC is needed.

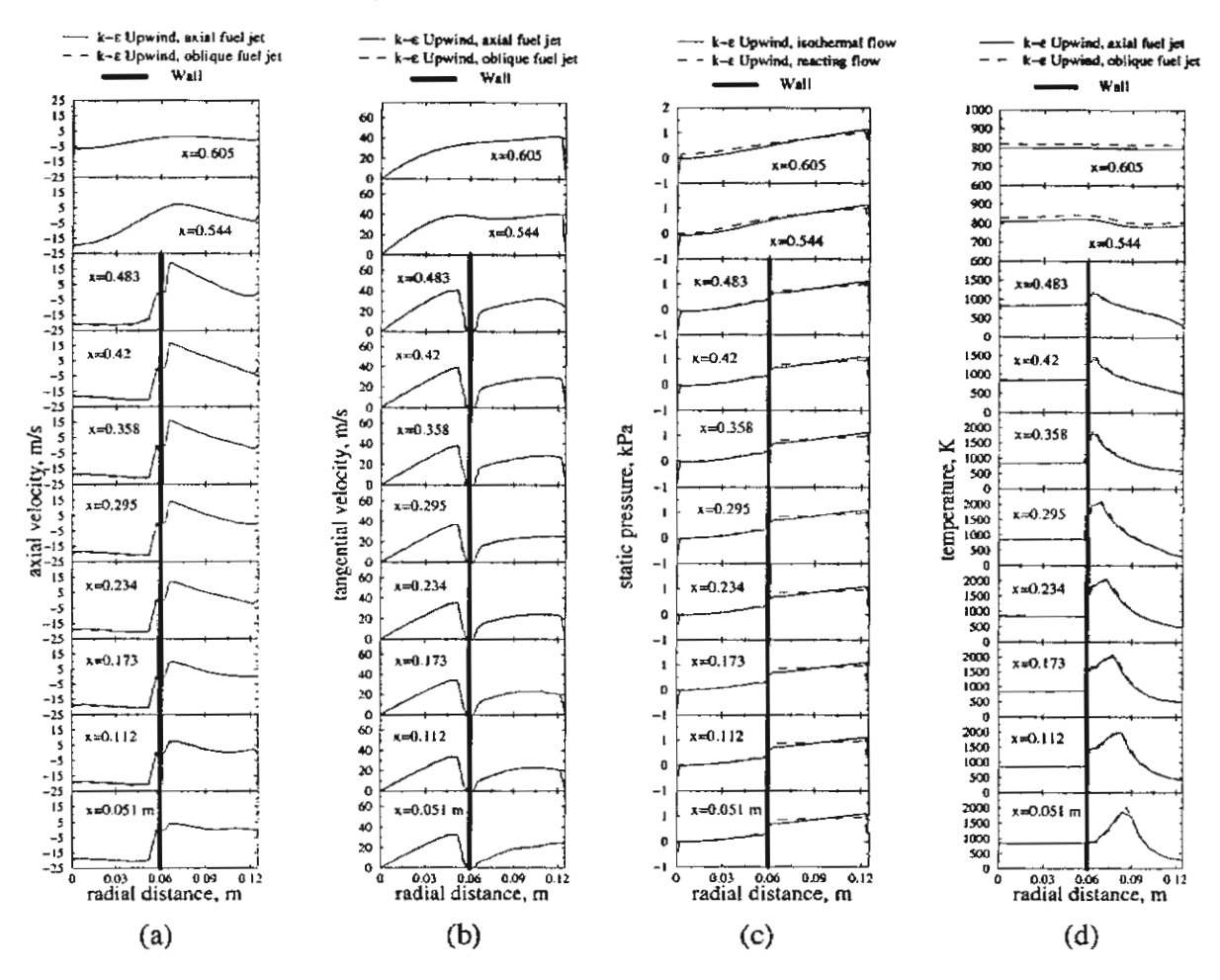


Fig. 3 Radial profiles of (a) axial and (b) tangential velocities (c) static pressure, and (d) temperature calculated with different fuel injections.

Streamlines and velocity vectors are presented in Fig. 4a while Fig. 4b is for the cold flow for comparison. In Figs. 4a and 4b, each has two parts: the left half contains the velocity vectors whereas the right half contains the streamlines. For the vector plots of velocity, it should be note that the flow patterns are similar for both flow models. The velocity profile in the exhaust center pipe region for the reacting flow is relatively uniform. The velocity is more concentrated in the vicinity of the center pipe walls for both models as can be seen in Fig. 4a and 4b. For streamlines, the stronger and wider recirculation zone is observed for the reacting flow.

The contour plots of temperature and pressure are exhibited in Figs. 4c and 4d respectively. Also, in the figures the left half is for the axial fuel injection while the right half for oblique fuel injection. For the temperature contours, it is found that both inlet fuel injections yield almost similar results but the oblique fuel injection performs a nearly uniform temperature along the core region as can be seen in Fig. 4c. From the contours of static pressure in Fig. 4d, it is clear that both fuel injections give identical results.

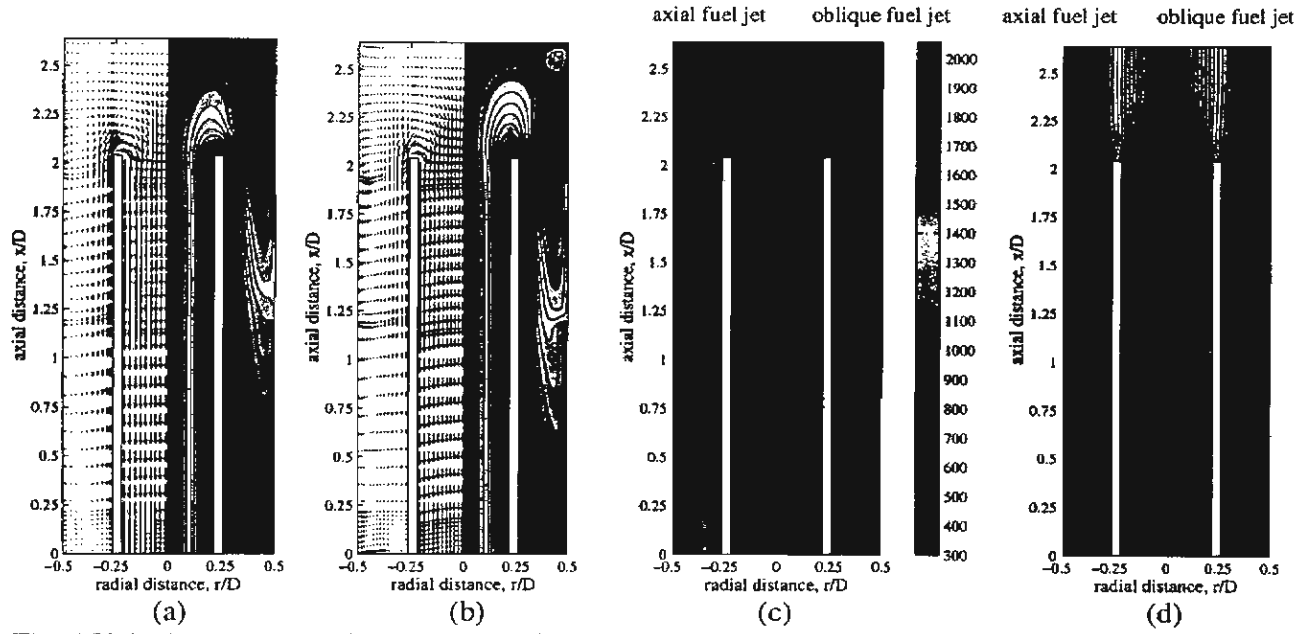


Fig. 4 Velocity vectors and streamlines of (a) reacting flow and (b) isothermal flow; contour plots of (c) predicted temperature and (d) pressure.

#### **Conclusions**

Numerical investigations have been carried out to predict a strongly swirling turbulent flow and combustion characteristic in a vortex combustor using the k- $\varepsilon$  model. The present numerical results for the cold flow are compared with available experimental data. Major findings can be summarised as follows: For the cold flow, the gas flow in the combustor is characterised as a strongly swirl, recirculating, and nonisotropic turbulent flow with a dominant tangential velocity component. Local recirculating flows occur near the injecting nozzles, at the chamber bottom, at the top of the center tube, and in the vortex core. For the reacting flow model, the computation shows that the flow pattern is similar to the cold flow model but the magnitude of velocity, recirculation zone are greater.

#### Acknowledgements

The authors would like to acknowledge with appreciation the Thailand Research Fund (TRF) for financial support of this research.

#### References

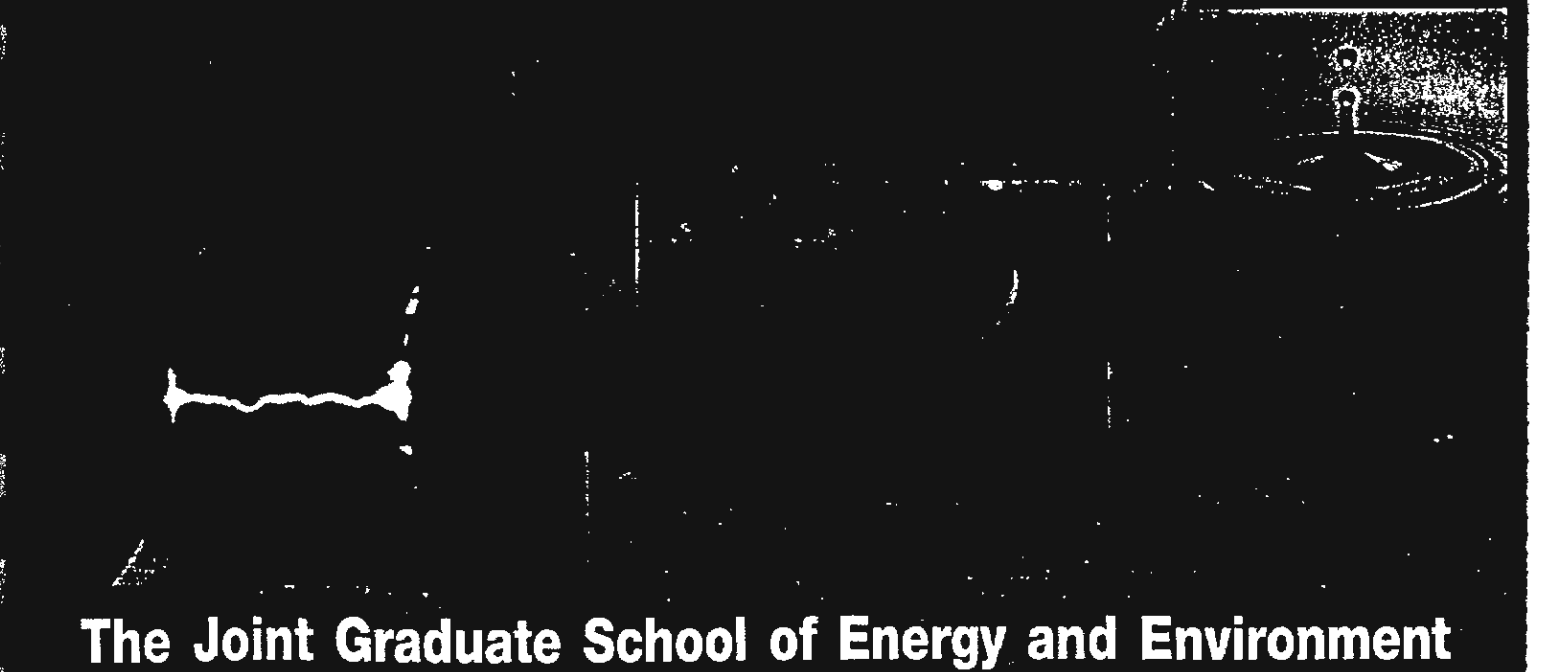
- [1]. Nieh, S. and Zhang, J. (1992), Simulation of the Strongly Swirling Aerodynamic Field in a Vortex Combustor, Trans. ASME J. of Fluids Engineering, Vol.114, Sept.
- [2]. Gupta, A.K., Lilley, D.G., and Syred, N. (1984), Swirl Flows, Abacus Press, Turnbridge Wells, England.
- [3]. Patankar, S.V. and Spalding, D.B. (1970), Heat and Mass Transfer in Boundary Layers, Intertext Books, London.
- [4]. Sloan, D.G., Smith, P.J., and Smoot, L.D. (1986), Modeling of Swirl in Turbulent Flow System, Progr. Energy Combust. Sci., vol. 12, pp. 163-250.
- [5]. Turns, S. R., An Introduction to Combustion, McGraw-Hill, 1996.
- [6]. Patankar, S.V. (1980), Numerical Heat Transfer and Fluid Flow, Hemisphere, Washington, D.C.
- [7]. Wilcox, C.D. (1993), Turbulent Modelling for CFD, DCW Industries, Inc., California.
- [8]. Leonard, B.P. (1979), A Stable and Accurate Convective Modelling Procedure Based on Quadratic Upstream Interpolation, Comp. Meth. Appl. Mech. Eng., 19, pp.59-98.



la Phret Rochall Combarcade Lina più Noll. Popy La la la la la la la la marcade

The Empress Hotel, Citiang Mai, Theiland

Efficient Energy and Clean Environment A Review of The Past and a Look at the Next Decade



#### A Low Emission Annular Vortex Combustor Firing Rice Husk Fuel: Part II – Experimental Investigation

#### P. Promvonge<sup>1</sup>, L. Vongsarnpigoon<sup>2</sup> and N. Piriyarungroj<sup>1</sup>

- 1. Department of Mechanical Engineering, Faculty of Engineering, King Mongkut's Institute of Technology Ladkrabang, Bangkok 10520, Thailand. Email: <a href="mailto:kppongje@kmitl.ac.th">kppongje@kmitl.ac.th</a>
- 2. Department of Mechanical Engineering, Faculty of Engineering, Mahanakorn University of Technology, Bangkok 10530, Thailand.

#### **Abstract**

This paper presents the study of flow and combustion characteristics of rice husk fuel in an annular vortex combustor (VC). The temperature distributions for selected locations inside the combustor and the fly ash and smoke from its flue gas were measured and observed respectively. Measurements were made by setting constant mass flow rate of rice husk to be 0.3 kg/min and by varying the equivalence ratio,  $\Phi$ , to be 0.8, 1.0 and 1.2. The ratio of volumetric flow rates of the primary air to the secondary air,  $\lambda$ , was set to be 4 and 1.5. The experiment shows the maximum temperature of about 1300 K in the annular chamber with less smoke of flue gas. Besides, the sizes of flyash particles from the exhaust stack can be controlled by the flow rate ratios of the primary air to the secondary air,  $\lambda$ . The VC shows an excellent performance, high stabilization and ease of operation in firing the fine rice husk and its important feature is that some small ashes remain in the bottom of the VC.

**Keywords:** annular vortex, vortex combustor, rice husk, biomass.

#### Introduction

The conventional sources of energy have been depleting at an alarming rate and the price of conventional energy is going up. Thus, the focus on alternative renewable sources of energy has been increasing and biomass is one of them that has been getting continued and increased attention. In general, paddy rice is one of the mostly produced crops throughout the world. Since it is not possible to take the whole of it as food, about 22% by weight of this paddy rice is generated as a waste, known as rice husk. It is estimated that over 60 million tons of rice husk are generated each year worldwide. Thailand generates 4.4-4.6 million tons of rice husk annually, which their thermal potentials are equivalent to 1.46-1.53 million tons of crude oil. About 10% of rice husk are utilized as a source of heat energy in Thailand. It is creating waste management problem, especially in the rice milling sites. The characteristic of rice husk is presented in Table 1. Therefore, an attempt to energy recovery from this rice husk waste by combustion technique may be worthwhile. With this the burning of rice husk by an annular vortex combustor (VC) can be considered.

There have been many reports published on various combustors using biomass materials or coals as a fuel. Tuatawin and Watcharaapapaibul [1] studied the performance of a concentric-vortex furnace firing rice husk. The relation between air-fuel ratio and efficiency of the furnace was reported. Jittrepit [2] and Nanumchok [3] presented an experimental investigation of combustion characteristics in a cyclone combustor for burning sawdust. The combustion characteristics in a fluidized bed furnace using rice husk fuel for fluidized bed paddy dryer can be found in Chujinda [4]. Srisawas [5] also presented an improvement of Chujinda's furnace. An extensive study of a vortex combustor for burning dry ultrafine coal and coal water fuel was reported by Nieh and Fu [6]. For above combustors burning rice husk fuel, effects of ash inside the combustors on combustion efficiency including its problem in elimination were reported.

This article deals with a preliminary study of combustion characteristics and temperature distributions in a vortex combustor burning rice husk fuel. Effect of feeding secondary air on flame

stability, temperature control in the combustor, ashes and smokes from the exhaust stack are studied and observed for a future reference in improving the performance of the combustor.

Table 1 Composition of rice husk [4]	
Carbon	36.8 %
Hydrogen	5.8 %
Oxygen	37.4 %
Nitrogen	0.14 %
Sulfur	0.1 %
Moisture	7.8 %
Ash	18.9 %
Density, kg/m <sup>3</sup>	100.
Gross heat of combustion, kcal/kg	3,308.
Stoichiometric air	3.2731 kg/kg fuel

#### **Experimental Setup**

The rice husk particles were milled and grinded, sieved up to about 1-mm size (between 1.19 and 1.41 mm), and stored in the laboratory under dry condition (9.2% of moisture content). The arrangement of experimental system of the combustor is shown in Fig. 1 below. The combustor is a concentric cylindrical pipe made of steel while of stainless steel for the exhaust center pipe. It is 0.755-m high and 0.195-m inside diameter with multiple injection nozzles of 0.005-m dia. each for the secondary air  $(Q_s)$  as depicted in Fig. 2. The exhaust center pipe is 0.078 m in diameter.

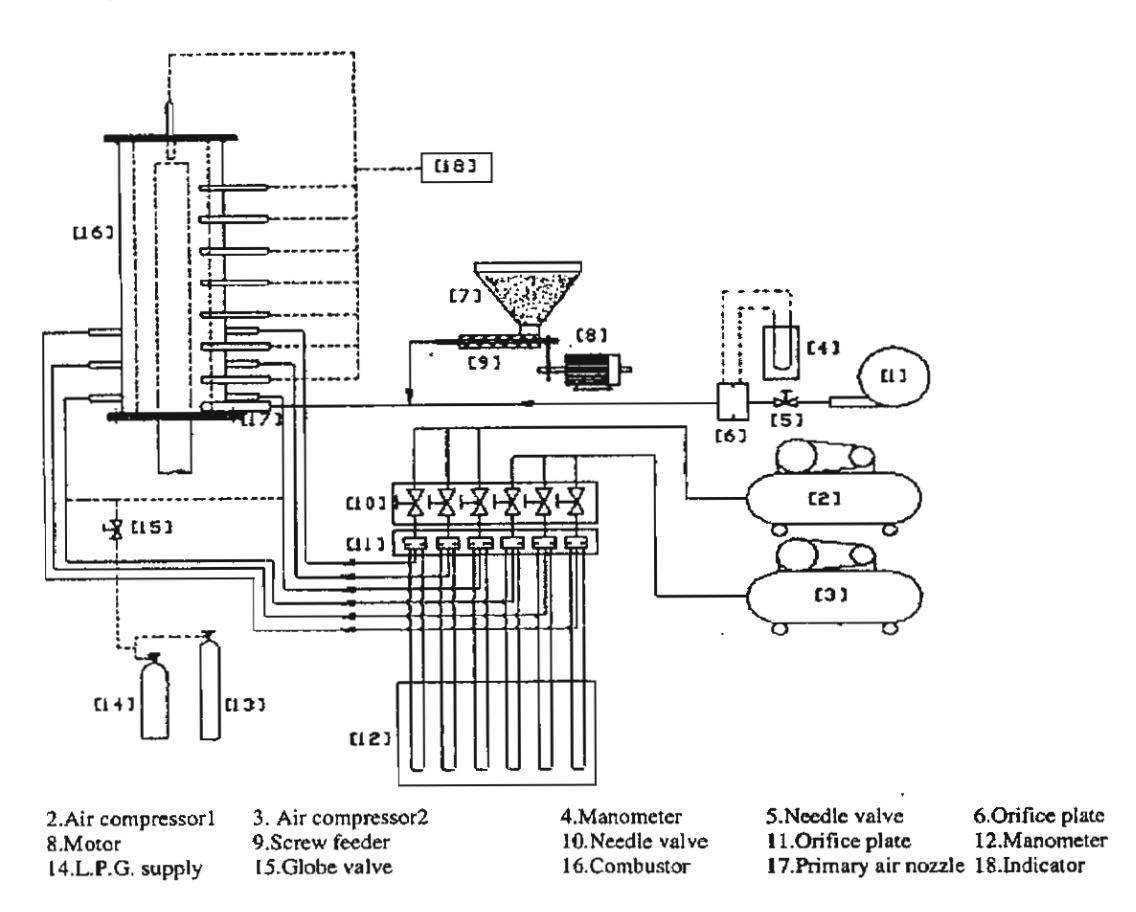


Fig. 1 Schematic diagram of experimental setup of combustion system.

1.Blower

7. Hopper

13.Oxygen

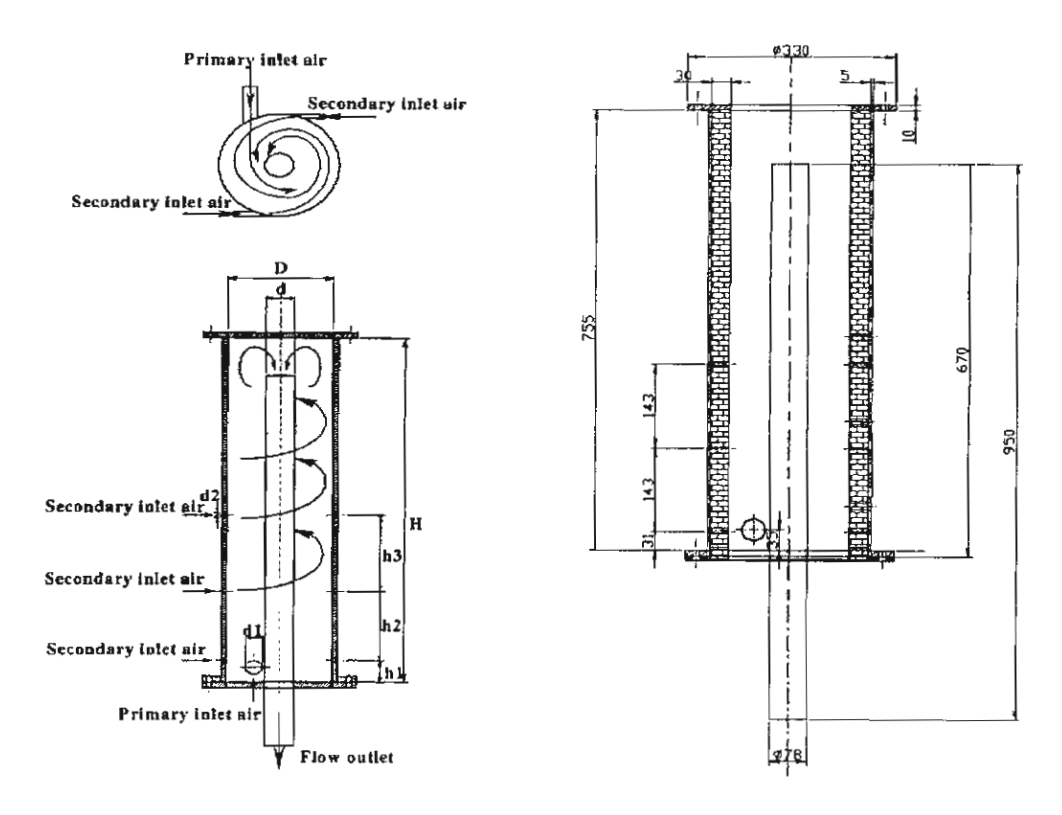


Fig. 2 Configuration of vortex combustor (unit in mm.)

The combustor was operated over a temperature range from 800-1000 K. A blower and two compressors were used for providing both primary and secondary combustion airs. Rice husk fuel was fed through a screw feeder and injected to the bottom chamber by pneumatic conveying via the primary air  $(Q_p)$ . Start up process was commenced by heating up the VC with LPG torch inserted at the lower air nozzle slot. The preheating took about 20 minutes for the chamber to raise its temperature to be about 680 K. Then feeding commenced through the hopper, slowly with the rice husk until 0.3 kg/min and kept constant. When the temperature in the chamber reached 950 K, stop of preheating with LPG was made. A thick, black smoke was seen at the beginning and slowly thinned out by adjusting the air/fuel (A/F) ratio. Excess air at various levels for equivalence ratio of 0.8, 1.0 and 1.2 was tried for each of  $\lambda$ . The temperatures were monitored at various selected locations with chromel-alumel (type K) thermocouples while volumetric flow rates of primary and secondary airs were measured by using orifice meters. All data collection was taken at steady state condition.

#### Results and Discussion

The VC was originally designed to accommodate various types of coal fuels as sources of heat. The VC responded significantly to the various fuels as expected. For rice husks, the level of equivalence ratio (or excess air) was varied to optimize the temperature inside the VC. The measurements of temperature were made at seven axial locations namely, x = 0.1, 0.2, 0.3, 0.4, 0.5, 0.6 and 0.7 m.

#### **Effects of Equivalence Ratios**

The radial profiles of temperature inside the VC for  $\Phi = 0.8$  (rich),  $\Phi = 1.0$  (stoich.) and  $\Phi = 1.2$  (lean) are presented in Figs. 3a, 3b and 3c respectively. The feed-rate of fine rice husk with 9.2% moisture content was 0.3 kg/min and kept constant throughout.

For  $\Phi = 0.8$ , Fig. 3a, it is found that the temperature profiles for all locations generally are not uniform. The temperature in the vicinity of the center pipe is higher than that near the chamber walls. Maximum temperature of about 1400 K takes place in the top of chamber while lower temperature can be seen near the chamber wall. Unburned fuel and black smoke emission from the exhaust stack were

observed for this case. This indicates the incomplete combustion (high CO concentration) or combustion reaction takes place very slowly.

Fig. 3b shows the temperature distributions for  $\Phi = 1.0$ . It can be seen that except for few early stations, the temperature profiles are nearly uniform for all stations especially at the top chamber. The maximum temperature around 1300 K is found in the top annular space whereas the minimum temperature in the vicinity of the chamber walls at early stations. This shows insufficient turbulence at the bottom chamber, which was due to too many rice husks, resulting in inadequate mixing and consequently the presence of fuel rich zones within the bottom space. This case yielded a less black smoke emission from the exit pipe.

The temperature distribution for  $\Phi = 1.2$  is depicted in Fig. 3c. It is worth noting that the temperature profiles similar to the case for  $\Phi = 1.0$ , are nearly uniform for all stations. The peak temperature of some 1200 K is also seen in the top annular space while lowest temperature at the bottom one. The peak one for every station is found in the middle between the chamber and center pipe walls. The maximum temperature for this case has the lowest value among the three cases, as expected, since an increase in the excess air leads to decreasing temperature in the combustion system. White and thin smoke emission and small size of flyash particles are visible. This points out that complete combustion takes place for this case.

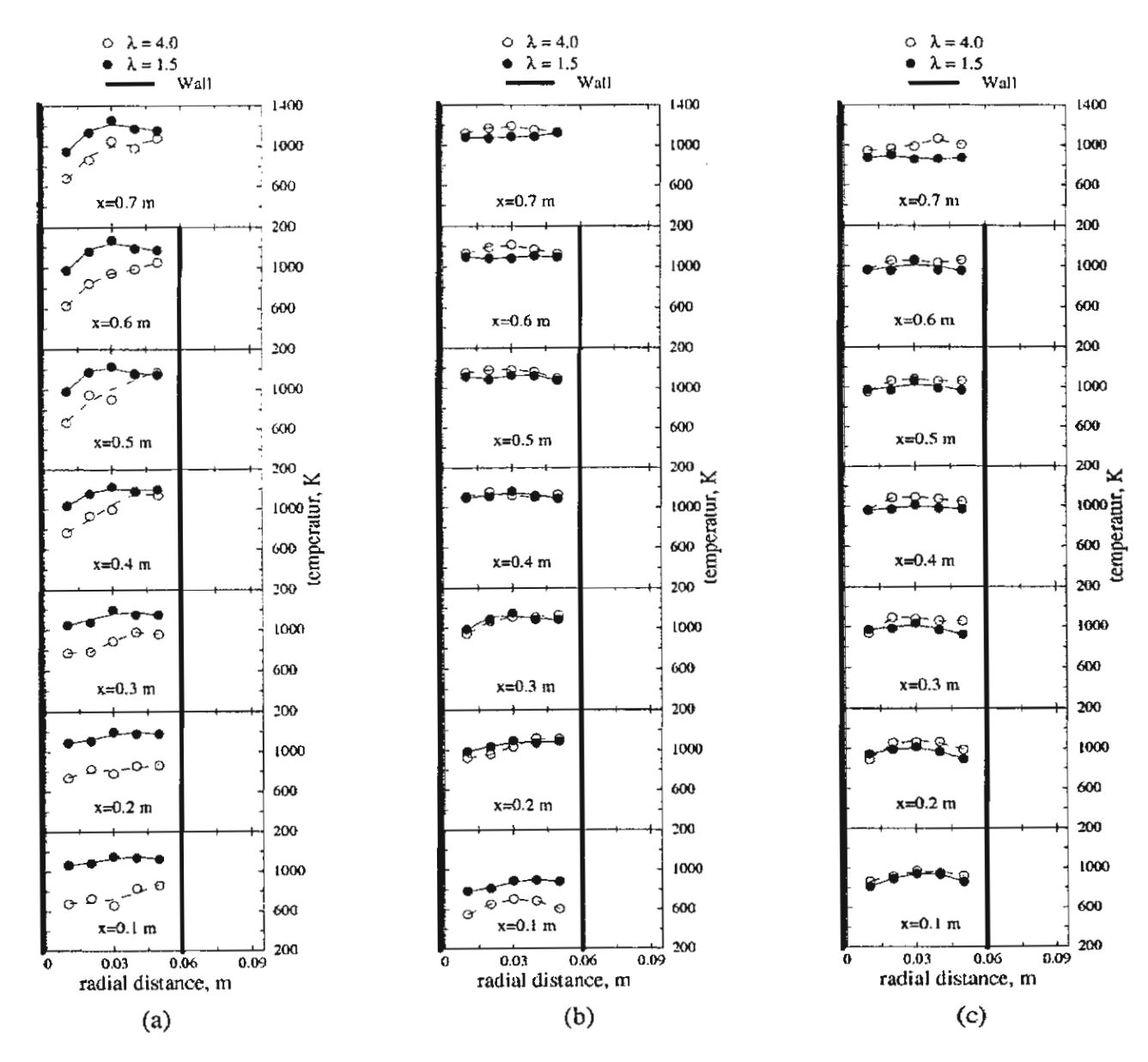


Fig. 3 Temperature distributions inside the combustor, (a)  $\Phi = 0.8$ , (b)  $\Phi = 1.0$ , and (c)  $\Phi = 1.2$ .

#### Effects of Volumetric flow rate ratios of Primary to Secondary Airs ( $\lambda$ )

The ratio of volumetric flow rate of the primary air to the secondary air, defined as  $\lambda = Q_p/Q_s$ , is an indication of the strength of the vortex of the flow. The decrease in value of  $\lambda$  results in the higher tangential velocity component (strong vortex). This means that the impact of swirling phenomenon of the secondary air on the flow and temperature fields becomes more pronounced as the value of  $\lambda$  is reduced. Comparison of the temperature distributions between  $\lambda = 4$  and  $\lambda = 1.5$  for various equivalence ratios is presented in Fig. 3.

For  $\Phi=0.8$ , it is obvious that adjusting of  $\lambda=1.5$  leads to a flatter and higher temperature distribution curve than that of  $\lambda=4$ . This indicates that the use of a small value of  $\lambda$  can improve the temperature distributions in the VC for the rich mixture as can be seen in Fig. 3a. When  $\Phi=1.0$ , it is interested to note that the influence of  $\lambda$  on the temperature profiles shows only the first two stations at the bottom while no effect of  $\lambda$  on the temperature profiles is found at other stations as illustrated in Fig. 3b. As  $\Phi=1.2$ , it is worth noting that no effect of  $\lambda$  on the temperature distributions is seen at all stations as exhibited in Fig. 3c. It is concluded that for the value of  $\Phi$  above 1.0, use of a small value of  $\Lambda$  results in no significant effect on temperature profiles in the VC but enhances swirling intensity instead. However, the increased swirling intensity leads to an abatement of particle elutriation, and to enlargement of the region of recirculating zone.

#### **Conclusions**

The measurements of temperature distributions and the observation of flue gas emission have been conducted during the combustion of fine rice husk in the VC. The conclusions derived from the results of these experiments are as follows: combustion of rice husk with equivalence ratio between 1.0 and 1.2 using the VC yields good combustion efficiency, flame stabilization, low emission and reliable furnace condition. For equivalence ratio  $\geq 1.0$ , the increase in secondary air has no significant effect on the temperature distributions inside but helps reduce the size of flyash particles.

#### Acknowledgements

The authors would like to acknowledge with appreciation, the Thailand Research Fund (TRF) for the financial support in part and the Mechanical Engineering Department, Mahanakorn University of Technology (MUT) for their support in this effort and the MUT undergraduate students for data collection.

#### References

- [1]. Tuatawin, T and Watcharaapapaibul, S., Bachelor Thesis, Mechanical Engineering Department, King Mongkut's University of Technology Thonburi, Bangkok, 1991.
- [2]. Jittrepit, P., Master Thesis, Mechanical Engineering Department, King Mongkut's Institute of Technology North Bangkok, Bangkok, 1992.
- [3]. Nanumchok, S., Master Thesis, Mechanical Engineering Department, King Mongkut's Institute of Technology North Bangkok, Bangkok, 1996.
- [4]. Chujinda, A., Master Thesis, Department of Energy Technology, King Mongkut's University of Technology Thonburi, Bangkok, 1997.
- [5]. Srisawas, B., Master Thesis, Department of Energy Technology, King Mongkut's University of Technology Thonburi, Bangkok, 1998.
- [6]. Nieh, S. and Fu, T.T., Proceeding of The 5<sup>th</sup> International Coal Conference, 1988, Pittsburgh, pp. 761-768.

### THE FACULTY OF ENGINEERING UNIVERSITY OF MALAYA







## 4th. SEA Regional Conference On Higher Engineering Education Network (RECHEEN 2000) 15-17 November 2000 Kuala Lumpur, Malaysia.

THEME: ADVANCED RESEARCH IN SCIENCE, ENGINEERING AND TECHNOLOGY

15 September 2000

Pongjet Promvonge, Lerkiat Vongsampigoon & Kulthorn Silapabanleng Dept. of Mech. Eng, King Mongkut's Inst of Tech. Ladkrabang, Bankok,, Thailand

Title of Paper

: Computation of isothermal confined swirling flow in a

combustor

Dear Pongjet Promvonge,

I am pleased to inform you that your paper entitled as above has been accepted for the conference. Please prepare your paper based on the author's kit enclosed and return to me by 5 <sup>th</sup> October 2000.

Thank you and see you at the conference.

Best regards.

.,

Prof. M. Mahmoud Moghavvemi Chairman Technical Committee

## COMPUTATION OF ISOTHERMAL CONFINED SWIRLING FLOW IN A COMBUSTOR

#### Pongjet Promvonge

Dept. of Mechanical Engineering, Faculty of Engineering, King Mongkut's Institute of Technology Ladkrabang, Bangkok 10520, Thailand. Email: kppongje@kmitl.ac.th

#### Lerkiat Vongsampigoon

Dept. of Mechanical Engineering, Faculty of Engineering, Mahanakorn University of Techonology, Bangkok, Thailand.

Kulthorn Silapabanleng
Dept of Mechanical Engineering, Faculty of Engineering,
Chulalongkorn University, Bangkok 10330, Thailand.

Abstract: The paper presents the simulation of strongly swirling confined flow in a combustor with an algebraic Reynolds stress model (ASM). The k-\varepsilon turbulence model was also employed in the present simulation for comparison. For the flows compared, the predicted results of gas tangential and axial velocities based on this model are in good agreement with measurements. The computation shows that the ASM is superior to the k-\varepsilon model in capturing the stabilising effect of the swirl.

Keywords: swirl, turbulent flow, algebraic stress model.

#### I. INTRODUCTION

Swirl flows have been of considerable interest over the past decades because of their occurrence in industrial applications, such as furnaces, utility boilers, internal combustion engines, gas turbine combustors and dust collectors [2, 5]. Swirl has been used in combustion systems to enhance the flame stability, the mixing and heat transfer besides prolonging the fuel residence time and abating the pollutants. This is because under appropriate conditions, swirl can be employed to induce a central recirculation zone. The recirculating flow generates additional turbulence in the shear layer between the reverse flow and the surrounding forward flow and helps stabilize the flame in combustors. Swirling turbulent flows are physically complex in nature due to the effect of a swirlturbulence interaction. The turbulence structure in swirling turbulent flows is generally highly non-isotropic and nonhomogeneous.

Computation of swirling flows is a difficult and challenging task. Large velocity gradients appear in these flows, so numerical problems and turbulence modelling play a significant role in their analysis. The commonly used, the k- $\epsilon$  model may not be suitable for simulating swirling turbulent flows [3, 6, 7]. It is also found that the use of modified k- $\epsilon$  models or even the non-linear k- $\epsilon$  model [13] leads to no significant improvement of the predictions in swirling flows. The second-order moment closure models, i.e., the Reynolds stress model (RSM) and the algebraic Reynolds stress model provide better methods for the simulation of swirling turbulent flows [6, 7]. The

RSM is regarded as a most logical approach to the turbulence closure problem, which does not need any ad hoc modification for extra strain rates. However, in the prediction of swirling flows with the RSM, it is necessary to solve a total of 11 governing differential equations of elliptic type: a continuity equation, three momentum equations, an \(\epsilon\)-equation, and six equations for the Reynolds stresses. This leads to much extra computational effort to solve six Reynolds stress transport equations simultaneously [6, 7] and much attention needs to be paid to numerical stability and inlet boundary conditions. It is for this reason that a simplified algebraic Reynolds stress turbulence model [16] in axisymmetric cylindrical coordinates is employed for simulating strongly swirling flows.

In this paper, the formulation of the present model, the procedure of numerical solution based on the present ASM and the validation results of the proposed model are described in detail. The validation was conducted through successive comparisons of the calculated gas tangential, radial and axial velocities with the test data measured in a cold flow combustor.

#### II. MATHEMATICAL FORMULATION

#### 2.1 Governing Equations

The phenomenon under consideration is governed by the steady two-dimensional axisymmetric form of the continuity and the time-averaged incompressible Navier-Stokes equations. In the Cartesian tensor system these equations can be written in the following form:

$$\frac{\partial}{\partial x_i} (\rho u_i) = 0 \tag{1}$$

$$\frac{\partial (\rho u_i u_j)}{\partial x_i} = \frac{\partial \rho}{\partial x_i} + \frac{\partial}{\partial x_i} (\bar{t}_{ij} + r_{ij})$$
 (2)

where  $\rho$ ,  $u_i$ , p and  $x_i$  are the density, mean velocity tensor, mean pressure and coordinate tensor respectively. The mean viscous stress tensor,  $\overline{t_{ii}}$ , is approximated as:

$$\bar{t}_{ij} = \mu \left( \frac{\partial u_i}{\partial x_j} + \frac{\partial u_j}{\partial x_i} \right)$$
 (3)

where  $\mu$  is laminar viscosity. The time-averaged Reynolds stress tensor,  $\tau_{ij} = -\rho u_i u_j$ , in the above equation is not known and thus, models are needed to express it in terms of the solution variables. In the present study, two turbulence models are used, namely the k- $\varepsilon$  model and an algebraic stress model (ASM). The k- $\varepsilon$  model has been reviewed in references [4, 15] and it will be described briefly. The standard k- $\varepsilon$  model version relates the turbulent eddy viscosity to the turbulence kinetic energy k and the dissipation rate  $\varepsilon$  through Boussinesq's approximation as:

$$\tau_{ij} = -\frac{2}{3}\delta_{ij}(\rho k) + \mu_t(\frac{\partial u_i}{\partial x_j} + \frac{\partial u_j}{\partial x_i})$$
 (4)

where  $\mu_t = \rho C_{\mu} k^2 / \varepsilon$  is the turbulent eddy viscosity and  $\varepsilon$  is the dissipation rate of turbulence kinetic energy (TKE). The modelled equation of the TKE, k is given by:

$$\frac{\partial}{\partial x_j} (\rho u_j k) = \frac{\partial}{\partial x_j} \left( \frac{\mu_e}{\sigma_k} \frac{\partial k}{\partial x_j} \right) + G - \rho \varepsilon \tag{5}$$

in which  $\mu_e = \mu_t + \mu$  is effective viscosity. Similarly the dissipation rate of TKE is given by the following equation:

$$\frac{\partial}{\partial x_j} \left( \rho u_j \varepsilon \right) = \frac{\partial}{\partial x_j} \left( \frac{\mu_e}{\sigma_\varepsilon} \frac{\partial \varepsilon}{\partial x_j} \right) + \frac{\varepsilon}{k} \left( C_{\varepsilon 1} G - C_{\varepsilon 2} \rho \varepsilon \right) \tag{6}$$

where G is the rate of generation of the TKE while  $\rho \varepsilon$  is its destruction rate. G is given by:

$$G = \mu_e \left[ \left( \frac{\partial u_i}{\partial x_j} + \frac{\partial u_j}{\partial x_i} \right) \frac{\partial u_i}{\partial x_j} \right]$$
 (7)

The boundary values for the turbulent quantities near the wall are specified with the wall function method [10].  $C_{\mu} = 0.09$ ,  $C_{\epsilon 1} = 1.44$ ,  $C_{\epsilon 2} = 1.92$ ,  $\sigma_k = 1.0$ , and  $\sigma_{\epsilon} = 1.3$  are empirical constants [4, 15] in the turbulence transport equations. Reynolds-averaged transport equations can be solved for  $\tau_{ij}$ , [4, 15] the modelled equations for which are:

$$\frac{\partial \tau_{ij}}{\partial t} + \frac{\partial (u_k \tau_{ij})}{\partial x_k} = -G_{ij} - \Phi_{ij} + D_{ij} + \varepsilon_{ij}$$
 (8)

where

$$\begin{split} G_{ij} &= \text{local production} = \rho P_{ij} = - \left( \rho \overline{u_i u_k} \frac{\partial u_j}{\partial x_k} + \rho \overline{u_j u_k} \frac{\partial u_i}{\partial x_k} \right) \\ \Phi_{ij} &= \text{local pressure strain} = -C_1 \frac{\rho \varepsilon}{k} \left( \overline{u_i u_j} - \frac{2}{3} k \delta_{ij} \right) \\ &- C_2 \left( G_{ij} - \frac{2}{3} G \delta_{ij} \right) \\ D_{ij} &= \text{net diffusive transport} = -\frac{\partial}{\partial x_k} \left( \frac{\mu_\varepsilon}{\sigma_T} \right) \frac{\partial \overline{u_i u_j}}{\partial x_k} \end{split}$$

 $\varepsilon_{ij} = \text{local dissipation tensor} = \frac{2}{3} \rho \varepsilon \delta_{ij}$ 

in which  $C_1 = 2.5$ , and  $C_2 = 0.55$  are model constants.

#### 2.2 Algebraic Reynolds Stress Model (ASM)

For simplicity in solving the six Reynolds stresses, Rodi's approximation [11] is used in this study and the Reynolds stress transport can be expressed in algebraic form as follows:

$$\frac{D\tau_{ij}}{Dt} - D_{ij} = \frac{\tau_{ij}}{Ok} (\frac{Dk}{Dt} - D_k)$$
(9)

Substitution of eqs. (5) and (8) into eq. (9) gives the desired algebraic expression for  $\tau_{ii}$ :

$$-G_{ij} - \Phi_{ij} + \frac{2}{3} \delta_{ij} \rho \varepsilon = \frac{\tau_{ij}}{\rho k} (G - \rho \varepsilon)$$
 (10)

The ASM expressions can thus be rewritten as:

$$\rho \overrightarrow{u_i u_j} = \frac{2}{3} \delta_{ij} \rho k + \frac{\lambda k}{\varepsilon} \left( G_{ij} - \frac{2}{3} \delta_{ij} G \right)$$
 (11)

where the empirical constant  $\lambda$ , was found to be 0.135, [16] is defined as:

$$\lambda = \frac{1 - C_2}{C_1 - 1 + \frac{G}{\rho \varepsilon}} \tag{12}$$

#### 2.3 Common Form for the Equations

All the governing equations can be re-organised and expressed in a standard form that includes the convection, diffusion, and source terms for 2-D axisymmetric flows as follows:

$$\frac{\partial}{\partial x}(\rho u\phi) + \frac{\partial}{\partial y}(\rho v\phi) - \frac{\partial}{\partial x}\left(\Gamma_{\phi x}\frac{\partial \phi}{\partial x}\right) - \frac{\partial}{\partial y}\left(\Gamma_{\phi y}\frac{\partial \phi}{\partial y}\right) = S_{\phi}$$
 (13)

where  $\phi$  may stand for any variable including the velocity components,  $\Gamma_{\phi_{\chi}}$  and  $\Gamma_{\phi_{y}}$  are the exchange coefficients for  $\phi$ , and  $S_{\phi}$  is the source term.

#### 2.4 Solution Procedure

In the present computation, the time-averaged Navier-Stokes equations, the TKE equation, and the TKE dissipation rate equation are solved numerically by a control-volume finite-difference method [9, 14] together with the turbulence model equations, equation (4) for the k- $\varepsilon$  model or equation (11) for the ASM. All equations are in a generalised form of equation (13). The SIMPLE algorithm is utilised for pressure-velocity de-coupling and iteration [9, 14]. The hybrid, the upwind, the quadratic upstream interpolation for convective kinematics (QUICK) [8] and the second-order upwind (SOU) [12] schemes were used for discretising convection and diffusion transports on a staggered grid cell. The under-relaxation iterative TDMA line-by-line sweeping technique is used for solving the resultant finite-difference equations. The computation was carried out using a personal computer (Pentium III-550 MHz). About 20,000 iterations were needed to achieve satisfactory convergence for each calculation case, which requires about 3.0 hr of computer time.

#### III. SWIRLING FLOW OF AHMED (1997)

The performances of the k- $\varepsilon$  model and the ASM are compared for a turbulent swirling flow in a combustor of Ahmed (1997) [1], shown in Fig. 1. The details of the geometry and fluid properties are given in Table 1 below. A single air stream entered the test section through a secondary annulus and passed through an adjustable vane swirler. Experimental mean velocity profiles for u, v and w, turbulence intensities and the Reynolds stresses were

measured at downstream locations of the expansion corner. All data in radial profiles were obtained with a two-components LDV system.

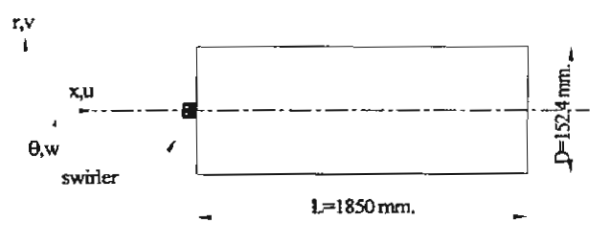


Fig. 1 Flow geometry and computational domain.

Table 1 Data for flow of Ahmed (1997)

Test section characteristics	
swirl vane angle (degree)	45
chamber length (m)	1.85
chamber dia. (m)	0.1524
Inlet flow conditions	
Reynolds number	200,000.
average velocity, Uo (m/s)	30.4

Since axial, radial and tangential velocities and turbulence intensities including shear stresses were provided at x/D = 0.0633 downstream of the inlet, computations are started at that location to reduce uncertain inlet conditions. In the present computation, performances of both the standard k- $\varepsilon$  model and the ASM are examined by comparing the predicted velocity profiles at ten locations, namely, x/D = 0.0633, 0.167, 0.25, 0.333, 0.417, 0.5, 0.583, 0.669, 0.833 and 1.0.

#### IV. RESULTS AND DISCUSSION

#### 4.1 Effects of Grid Densities and Numerical Schemes

The comparisons between the predicted results by the k- $\varepsilon$  turbulence model and the ASM and the measured data of the flow are presented in Figs. 2 through 7. The predicted axial, radial and tangential velocities are compared with the measurements, where solid or dash curves are represented for the calculated results while open circles for the measured data. The computational results are based on a 95x40 non-uniform grid with refinement in the vicinity of the slit. Grid independence of the numerical results was verified with a 120x60 finer grid. It is found that the differences for both the base grid and the finer grid in local flow properties are marginal. This suggests that grid independent solutions can be obtained with a 95x40 grid, which is used throughout the computations.

The axial, radial and tangential mean velocity profiles predicted with the k-ɛ model and four different numerical schemes are compared with the measured data in Fig. 2. It is found that predictions with the four schemes generally are in fairly good agreement with the measurements. However, in prediction with hybrid, QUICK and SOU, under-predicted tangential velocity profiles are seen in all locations while good agreement is found for axial and radial velocity profiles in comparison with experimental data. For the four numerical schemes, the FOU scheme performs the best agreement in prediction of tangential velocity but shows poorer agreement for axial and radial velocity profiles. Thus, in terms of the strength of the tangential velocity, only the FOU scheme is considered for computation of this flow.

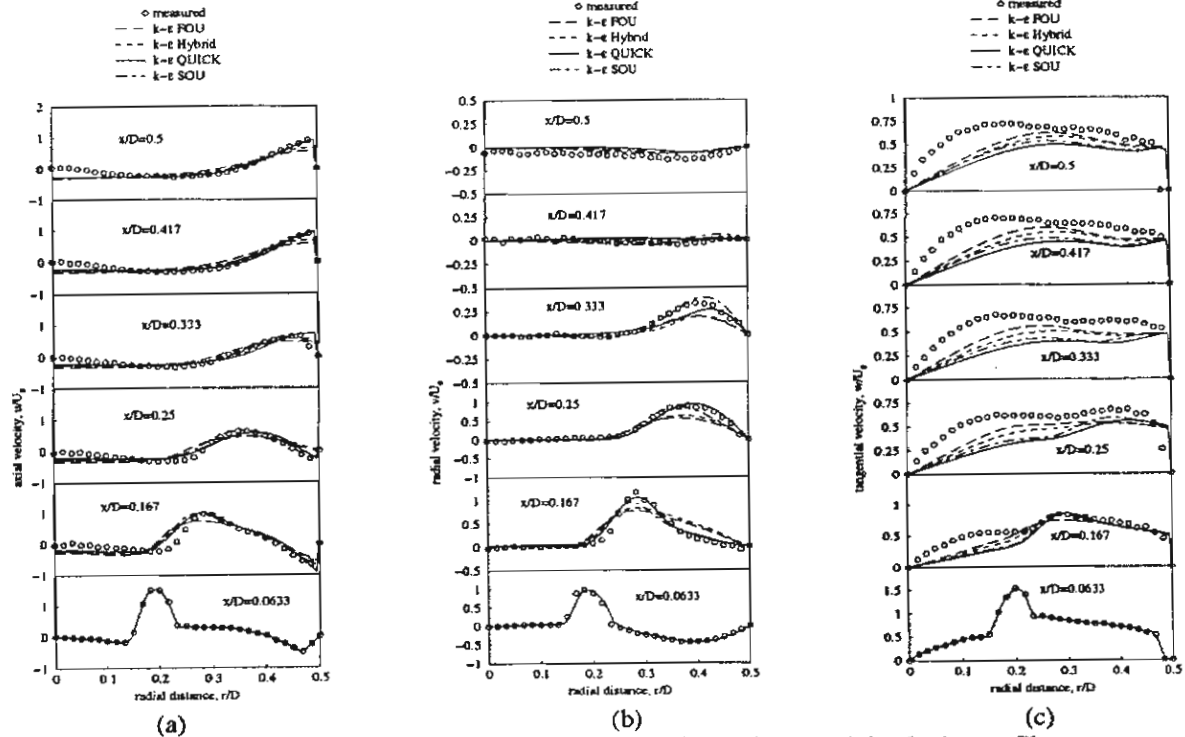


Fig. 2 Effect of numerical schemes on the axial, radial and tangential velocity profiles.

#### 4.2 Flow Field

Velocity Field. Predictions of velocity profiles using the k- $\varepsilon$  model and the ASM are compared with experimental data in Figs. 2a, 2b and 2c for the axial, radial and tangential velocity profiles respectively. For the radial profile of axial velocity in Fig. 2a, it is seen that the predicted profiles show no difference for both turbulence models and generally are in favorable agreement with measurements especially for  $x/D \ge 0.333$ . The ASM However, both turbulence models give under-predicted results in the core region. Predictions with the ASM show closer agreement with measurements than those with the k- $\varepsilon$  model in some locations as can be seen at x/D = 0.167 and 0.25 between r/D = 0.35 and r/D = 5. The results of Fig. 2a indicate that the predicted axial velocity recovers and progresses to uniformity at a faster rate than in the measurements.

Fig. 2b compares the radial profile of radial velocities predicted by the k- $\varepsilon$  model and the ASM with measurements. It is of interest to note that prediction with the ASM shows closer agreement with experimental data than that with the k- $\varepsilon$  model. The ASM results mimic very well the measurements while the k- $\varepsilon$  model gives underpredicted results, especially in the vicinity of the inlet. For the downstream region far away from the inlet (x/D > 0.417), both turbulence models yield similar results and agree well with the measurements.

The tangential velocity profiles predicted by the k- $\varepsilon$  model and the ASM along with the measurements are shown in Fig. 2c. It is worth noting that the tangential velocity predictions with the k- $\varepsilon$  model display a rapid decay to a forced vortex profile (solid-body rotation) while the experimental data correspond to a combined free and forced vortex profile. It is clear that the tangential velocity predictions do not agree with the measured data even for trends. Since the calculations were fairly free of numerical diffusion, discrepancies between the data and the predictions can be attributed to two sources: - improper boundary conditions at the inlet plane and deficiencies of the turbulence model.

All inlet values except the  $\varepsilon$  and the k, were obtained indirectly from the experiment. The values of  $\varepsilon$  were derived from a constant length-scale assumption and those of k from an approximation of total kinetic energy. To study the sensitivity of the inlet  $\varepsilon$  and k profiles to the flow field, calculations were made using different  $\varepsilon$  and k distributions, by increasing or decreasing their estimated values by a factor of 10. It was found that the calculated velocity was not affected significantly. The poor agreement between the predictions and measurements is, therefore, more likely to be due to the deficiencies of the turbulence model.

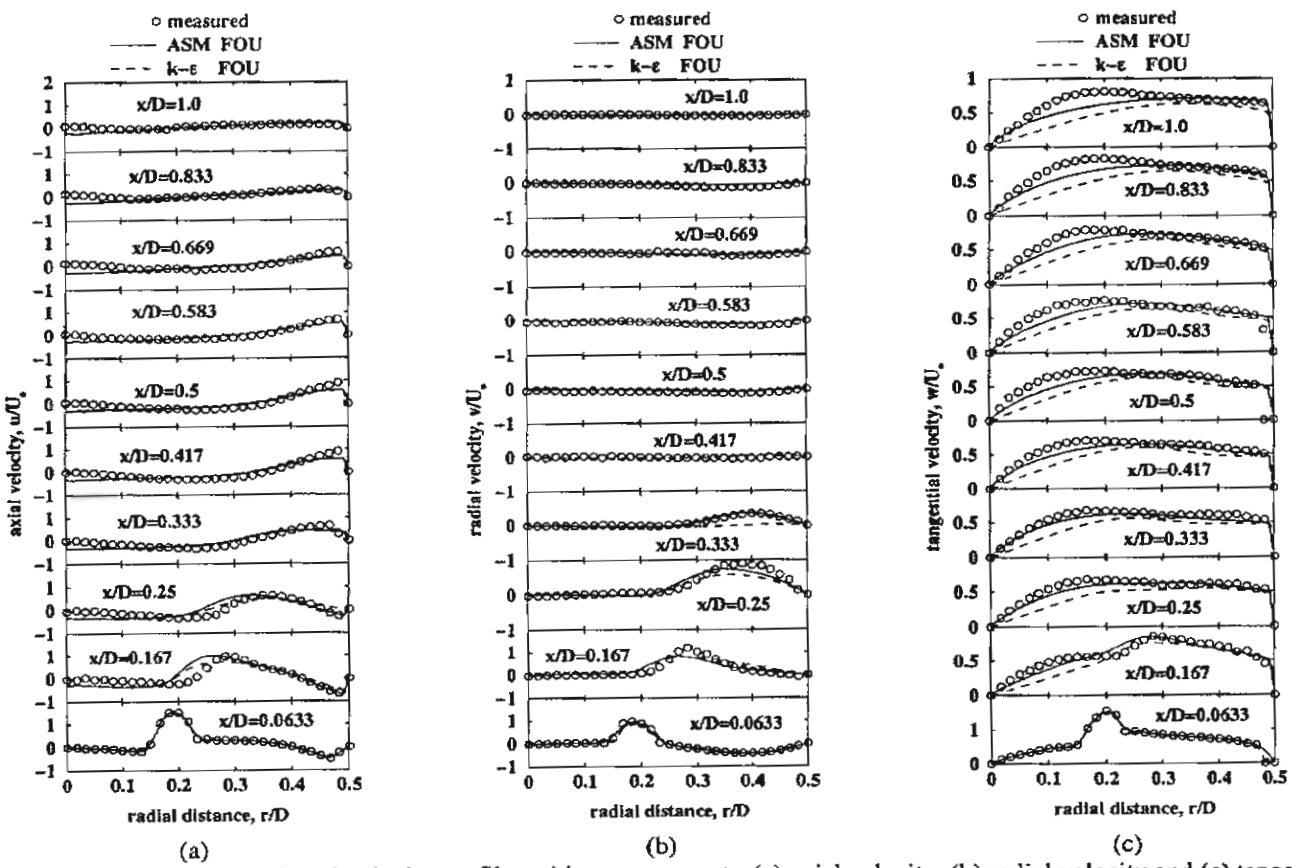


Fig. 3 Comparison of predicted velocity profiles with measurements; (a) axial velocity, (b) radial velocity and (c) tangential velocity profiles.

The use of ASM results in better overall agreement with the measurements than possible with the k- $\varepsilon$  model. The major difference between calculations with the two turbulence models is most clear in the recirculation region and in the tangential velocity profiles. The agreement between the calculation with the ASM and the experimental data is fairly good. The peak values and a combined forced and free (Rankine) vortex motion for the tangential velocity profiles are well predicted. The recirculation zone (IRZ) is, however, longer and wider than that with the k- $\varepsilon$  model.

Streamlines predicted by the ASM and the  $k-\varepsilon$  model are shown in Figs. 4 and 5 respectively. The contour plot of streamlines is in a range of x/D = 0 to 3 and r/D = 0 to 0.5, which has a high change of velocities. From the figures, there is no change of velocities at about x/D = 1.5 for the ASM and at some x/D = 3 for the  $k-\varepsilon$  model. Two

recirculation zones are identified; one is at the corner and the other, an internal recirculation zone (IRZ) or central toroidal recirculation, near the inlet. It is observed that the size of the recirculation zone calculated by the ASM is larger than that by the k- $\varepsilon$  model.

Vector plots of velocity predicted with the ASM and the k- $\varepsilon$  model are illustrated in Fig. 6 and Fig. 7 respectively. The plots for both turbulence model are also in a range of x/D = 0 to 3 and r/D = 0 to 0.5. It is clear to note that for the ASM, the centers of the corner recirculation and the central toroidal recirculation are, respectively, at about x/D = 0.1 and r/D = 0.42 and at x/D = 0.35 and r/D = 0.35. For the k- $\varepsilon$  model, they are at some x/D = 0.05 and r/D = 0.42 and at x/D = 0.3 and x/D = 0.3. In the inlet region, the reverse flow occurs for both turbulence models but the flow predicted by the ASM is longer than that by the k- $\varepsilon$  model as can be seen from the figures.

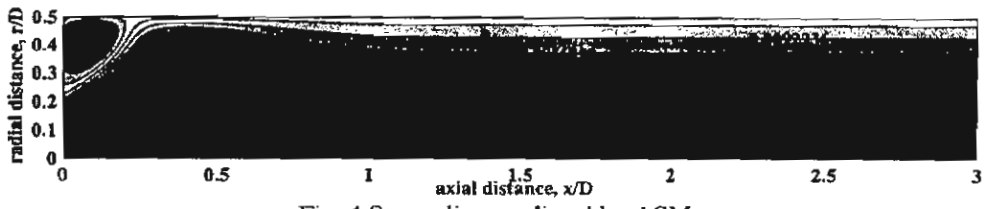


Fig. 4 Streamline predicted by ASM



Fig. 5 Streamline predicted by the  $k - \varepsilon$  model

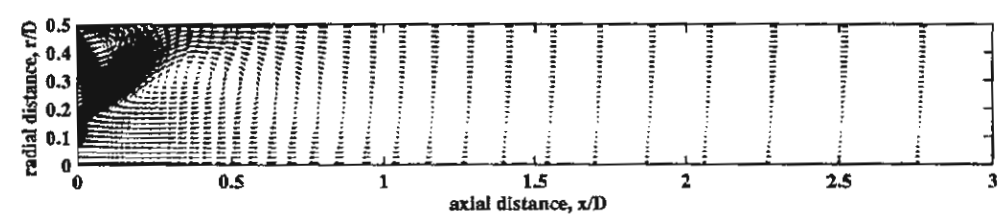


Fig. 6 Velocity vectors predicted by ASM

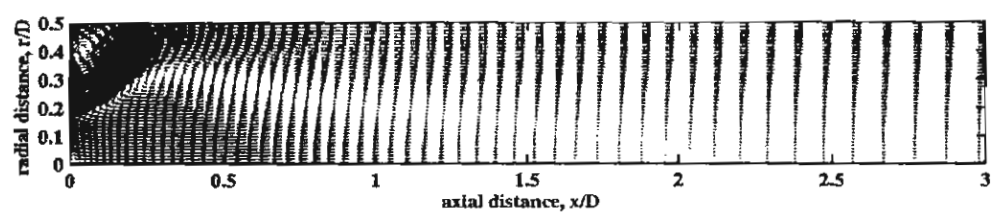


Fig. 7 Velocity vectors predicted by  $k - \varepsilon$  model

#### V. CONCLUDING REMARKS

The assessments of the k- $\epsilon$  model and the ASM have been carried out in a swirling incompressible flow. The conclusions from the validation study are as follows: The numerical procedure incorporating the ASM was tested for a swirling turbulent flow. Since the ASM represents better the anisotropy of the turbulence, the ASM results with the FOU scheme is in closer agreement with measurements than those with the k- $\epsilon$  model which predicts a fast decay of tangential velocity profiles to a solid-body rotation. The computations of the flow showed that the ASM performs better than the k- $\epsilon$  model in capturing the mean flow behaviour, superiority rooted in the response of the ASM to turbulence interaction.

#### VI. ACKNOWLEDGEMENTS

The authors would like to gratefully acknowledge the Thailand Research Fund (TRF) for financial support of this research.

#### VII. REFERENCES

- [1] Ahmed S.A, (1997), "Three Component Velocity Measurements of an Isothermal Confined Swirling Flow", Proc. Instn Mech. Engrs, Part G, J. of Aerospace Engineering, 211(G2), pp. 113-122.
- [2] Boysan, F, Ayers, W.H. and Swithenbank, J. (1982), A Fundamental Mathematical Modelling Approach to Cyclone Design, Trans. Inst. Chem. Eng., Vol.60, pp.222-230.
- [3] Chen, C.P. (1986), Calculation of Confined Swirling Jets, Commu. Appl. Numer. Methods, Vol.2, pp.333-338.
- [4] Gatski, T.B. (1996), Turbulent Flows: Model Equations and Solution Methodology, in Handbook of Computational Fluid Mechanics, Edited by Roger Peyret, Academic Press Ltd, London.

- [5] Gupta, A.K., Lilley, D.G., and Syred, N. (1984), Swirl Flows, Abacus Press, Turnbridge Wells, England.
- [6] Hogg, S. and Leschziner, M.A.(1989), Computation of Highly Swirling Confined Flow with a Reynolds Stress Turbulence Model, AIAA J., Vol.27, pp.57-63.
- [7] Jones, W.P. and Pascau, A. (1989), Calculation of Confined Swirling Flows with a Second Moment Closure, Trans. ASME J. of Fluid Engineering, Vol.111, Sept, pp.248-255.
- [8] Leonard, B.P. (1979), A Stable and Accurate Convective Modelling Procedure Based on Quadratic Upstream Interpolation, Comp. Meth. Appl. Mech. Eng., 19, pp.59-98.
- [9] Patankar, S.V. (1980), Numerical Heat Transfer and Fluid Flow, Hemisphere, Washington, D.C.
- [10] Patankar, S.V. and Spalding, D.B. (1970), Heat and Mass Transfer in Boundary Layers, Intertext Books, London.
- [11] Rodi, W.A. (1976), New Algebraic Relations for Calculating the Reynolds Stresses, Z. Angew. Math. Mech. (ZAMM), vol. 56, pp. T219-T221.
- [12] Shyy, W., Thakur, S., and Wright, J. (1992), Second Order Upwind and Central Difference Schemes for Recirculating Flow Computation, AIAA J., Vol.30, No.4,pp.931-932.
- [13] Sloan, D.G., Smith, P.J., and Smoot, L.D. (1986), Modeling of Swirl in Turbulent Flow System, Progr. Energy Combust. Sci., vol. 12, pp. 163-250.
- [14] Versteeg, H.K. and Malalasekera, W. (1995), An Introduction to Computational Fluid Dynamics: The Finite Volume Method, Longman Scientific & Technical, Longman Group Limited, Essex, England.
- [15] Wilcox, C.D. (1993), Turbulent Modelling for CFD, DCW Industries, Inc., California.
- [16] Zhang, J., Nieh, S. and Zhou, L. (1992), A New Version of Algebraic Stress Model for Simulating Strongly Swirling Turbulent Flows, J. Numerical Heat Transfer, Part B, Vol. 22, pp. 49-62.



July 29 - August 2, 2001 at the Westin Hotel, Savannah, Georgia















co-sponsored by











#### C CAT-21: WIRELESS ENERGY TRANSFER/SPACE SOLAR 2001-EI-14 Eco-Energy City Project - the Concept and the POWER SYSTEMS results of the research - Yoshihiro Ogisu Tuesday, July 31, 2001 2001-PI-05 An Efficient Time-Space Numerical Method For 8:30 - 11:30 AM Global Warming Studies - Takeo S. Saitoh and Organizers and Chairs: Dr. Frank Little, Texas A&M Shinichiro Wakashima University 2001-EI-08 Electric and Magnetic Fields Associated with Dr. Henry Brandhorst, Auburn University the Use of Electrical Power in the Workplaces in 2001-AT-05 Comparison of Space Solar Power Systems and Underdeveloped Countries - Ahmed Farag Terrestrial Photovoltaic Arrays - Finley R. Shapiro 2001-EI-09 Electromagnetic Fields Policy Implication For 2001-AT-44 Air-Launch Lunar Tourism with Beamed-Power Risk Assessment - Ahmed Farag Electrical Propulsion Costing - Simon Rowland 2001-EI-10 Power Frequency Electromagnetic Fields 2001-AT-56 Effects of Hypervelocity Impact on Solar Cell Management Technologies - Ahmed Farag Modules at High Voltage - Henry Brandhorst ES-3: THERMAL AND MECHANICAL ENERGY STORAGE CT-2: ADVANCED CYCLES II Tuesday, July 31, 2001 Tuesday, July 31, 2001 8:30 - 11:30 AM 8:30 - 11:30 AM 2001-ES-20 Evaluation and Improvement of Eddy Current 2001-CT-02 I/V Characteristic of ZnSe Schottyky Diodes -Position Sensors for Use in Magnetically Dirk M. Chiu Suspended Flywheel Systems — Timothy Dever 2001-CT-08 A Novel Integrated Gas/ Steam Cycle with Storage and Transport of "Cold" Using 2001-ES-24 Ericsson Bottoming Gas Turbine - Onkar Singh Clathrate Slurries: Fundamental Thermophysical Characteristics of Aqueous 2001-CT-11 Prediction of Performance of Simple Combined Gas/ Steam Cycle and Cogeneration Plants with Solution of TBAB - I. Tanasawa, S. Takao Different Means of Cooling - Sanjay Yadav, 2001-ES-44 Heat Balance of Long-Term Supercooled Mechanical Engg., Regional Institute of Thermal Energy Storage - Satoshi Hirano Technology, Jamshedpur, Jharkand, India. 2001-CT-13 Test and Demonstration Results of a New RE-3: HYDROGEN AND BIOMASS ENERGY Tuesday, July 31, 2001 Magnetically Coupled Adjustable Speed Drive -8:30 - 11:30 AM Kenneth Anderson 2001-RE-06 Hydrogen from Solar Energy: An Overview of 2001-CT-25 Fast Rise of Seebeck Coefficient in CdTe with Decreasing temperature: Theoretical Theory and Current Technological Status Explanation - Svetla Vackova Paul A. Erickson and D. Yogi Goswami, Department of Mechanical Engineering, University of Florida **ET-3: BATTERIES FOR TERRESTRIAL APPLICATIONS** Tuesday, July 31, 2001 2001-RE-03 On-Board Hydrogen Storage for Fuel Cell 8:30 - 11:30 AM Vehicles - Thomas Vernersson, Kristina Johansson, and Per Alvfors, Royal Institute of 2001-ET-12 Optimization of Nanostructured Hydrous Technology, Department of Chemical Engineering RuO2/ Carbon Supercapacitor - Kim Hansung, and Technology, Division of Energy Processes Bala Haran, Slavkov Dragan, Ralph E. White and Branko N. Popov 2001-RE-07 Premixed Combustion of Hydrogen/Methane Mixtures in a Porous Medium Burner 2001-ET-13 Optimization of Energy Density and Power Chung-fen Tseng Department of Mechanical Density of Li-ion Based Hybrid Devices - Bala Engineering, National Central University S. Haran, Anand Durairajan, Ralph E. White and 2001-RE-04 Biomass Briquetting Technology with Branko N. Popov Preheating - Sk Ahad Ali 2001-ET-16 Nickel-Hydrogen Battery Design for Terrestrial

#### 2001-ET-19 OSCR program for Primary Pouch Batteries -Christo Brand PF-2: POLICY AND GLOBAL ISSUES

Tuesday, July 31, 2001 8:30 - 11:30 AM

Organizer and Chair: William D. Jackson, HMJ Corp. 2001-PI-03 Structural Problems with the Danish CO2 Tax System - Jens Anderson

Applications - Jeff Dermott

2001-ET-17 45-Ah Lithium Ion cells for the Team Northern

Sun Solar Powered Car - Gregg Bruce

#### TM-2: SPACECRAFT AND AIRCRAFT THERMAL MANAGEMENT Tuesday, July 31, 2001 8:30 - 11:30 AM

Characteristics in a Rice Husk Fired Vortex

of Mechanical Engineering, King Mongkutis

Institute of Technology Ladkrabang, Bangkok

Combustor - Pongjet Promvonge, Department

Organizer and Chair: Dr. Michael K. Choi NASA Goddard Space Flight Center

2001-RE-17 Experimental Study of Combustion

2001-TM-16 Off-design Performance of a Heat Exchanger for Regenerative Aircraft Engines - S. Pasini, U. Ghezzi, and R. Andriani

Proceedings of IECEC'01
36th Intersociety Energy Conversion Engineering Conference
July 29-August 2, 2001, Savannah, Georgia

2001-RE-17

### EXPERIMENTAL STUDY OF COMBUSTION CHARACTERISTICS IN A RICE HUSK FIRED VORTEX COMBUSTOR

#### Pongjet Promvonge

Mechanical Engineering Department, Faculty of Engineering, King Mongkut's Institute of Technology Ladkrabang, Bangkok 10520, Thailand Email: kppongje@kmitl.ac.th

#### Kulthorn Silapabanleng

Former Associate Professor

Mechanical Engineering Department, Faculty of Engineering,
Chulalongkorn University,
Bangkok 10330, Thailand

#### **ABSTRACT**

This paper presents the study of combustion characteristics of rice husk fuel in an annular vortex combustor (VC). The temperature distributions for selected locations inside the combustor and the fly ash and smoke from its flue gas were measured and observed respectively. Measurements were made by setting a constant mass flow rate of rice husk to be 0.2 kg/min and by varying the equivalence ratio,  $\Phi$ , to be 0.8, 1.0 and 1.2. To study the effect of feeding secondary air on flame stability, three values of the ratio of volumetric flow rates of the secondary air to the total air,  $(\lambda)$ , were used and set to be 0.0, 0.2 and 0.4. The experiment shows the maximum temperature of about 1000° C in the upper chamber with less smoke of flue gas. Besides, emissions and the sizes of flyash particles from the exhaust stack can be controlled by the flow rate ratios of the secondary air to the total air, \( \lambda \). The VC shows an excellent performance, low emissions, high stabilization and ease of operation in firing the fine rice husk.

**Keywords:** annular vortex combustor, rice husk, biomass.

#### INTRODUCTION

The conventional sources of energy have been depleting at an alarming rate and the price of conventional energy is going up. Thus, the focus on alternative renewable sources of energy has been increasing and biomass is one of them that has been getting continued and increased attention. In general, paddy rice is one of the mostly produced crops throughout the world. Since it is not possible to take the whole of it as food, about 22% by weight of this paddy rice is generated as a waste, known as rice husk. It is estimated that over 60 million tons of rice husks are generated each year worldwide. Thailand generates 4.4-4.6 million tons of rice husks annually, which their thermal potentials are equivalent to 1.46-1.53 million tons of crude oil.

About 10% of rice husk are utilized as a source of heat energy in Thailand. It is creating waste management problem, especially in the rice milling sites. Therefore, an attempt to energy recovery from this rice husk waste by combustion technique may be worthwhile. With this the burning of rice husk by an annular vortex combustor (VC) can be considered.

There have been many reports published on various combustors using biomass materials or coals as a fuel. Singh et al. [1] designed a cyclonic rice husk furnace for drying a ton of paddy and its moisture was reduced from 35% to 14%d.b. Different furnace efficiencies were found for various rice husk feed and air flow rates. Tumambing [2] also investigated a rice husk furnace for drying paddy. Xuan et al. [3] studied two types of husk furnaces. One was a furnace with inclined grate and cylindrical combustion chamber with heat exchanging in the furnace upper part. Inlet air entered at the lower part of inclined grate and burnt the rice husk on grate. The other was a pneumatic-fed furnace (vortex type) including combustion chamber and rice husk feed system. Rice husk was fed into the combustion chamber with primary air and burnt and fell to the lower part of the furnace. The secondary air entered tangentially the chamber to create the vortex flow with a view to eliminating dust from flue gas. Soponronnarit et al [4] applied a rice husk fired furnace to a fluidized bed paddy dryer. An extensive study of a vortex combustor for burning dry ultrafine coal and coal water fuel was studied by Nieh and Fu [5]. A vortex combustor similar to [5] but using rice husk fuel instead was experimentally investigated by Promyonge et al. [6]. For above combustors burning rice husk fuel, effects of ash inside the combustors on combustion efficiency including its problem in elimination were reported.

This article deals with a preliminary study of combustion characteristics and temperature distributions in a vortex combustor burning rice husk fuel. Effect of feeding secondary air on flame stability, temperature control in the combustor, emissions, ashes and smokes from the exhaust stack are studied and observed for a guideline in design and improving the performance of the combustor.

Table 1 Composition of fine rice	husk
Carbon	38.0 %
Hydrogen	5.70 %
Oxygen	41.6 %
Nitrogen	0.69 %
Sulfur	0.06 %
Moisture	10.3 %
Ash	14.0 %
Density, kg/m <sup>3</sup>	100.00
Gross heat of combustion, kcal/kg	3,580.00
Stoichiometric air	4.850 kg/kg fuel

#### EXPERIMENTAL SETUP

The rice husk particles were milled and grinded, sieved up to about 1.3-mm size (between 1.19 and 1.41 mm), and stored in the laboratory under dry condition (10.3% of moisture content). The arrangement of experimental system of the combustor is shown in Fig. 1 below. The combustor was a concentric cylindrical pipe made of steel with castable refractory cement lining as insulation while the exhaust center pipe was made of stainless steel. It is 0.755-m high and 0.20-m

19. Cyclone

inside diameter (D) with multiple injection nozzles of 0.005-m diameter each for the secondary air  $(Q_2)$  as depicted in Fig. 2. The exhaust center pipe is 0.078 m in diameter.

The combustor was operated over a temperature range from 600 - 1000° C. A blower and two compressors were used for providing both primary and secondary combustion airs. Rice husk fuel was fed through a screw feeder and injected to the bottom chamber by pneumatic conveying via the primary air (Q1). Start up process was commenced by heating up the VC with LPG torch inserted at the lower air nozzle slot. The preheating took about 20 minutes for the chamber to raise its temperature to be about 400°C. Then feeding commenced through the hopper, slowly with the rice husk until 0.2 kg/min and kept constant. When the temperature in the chamber reached 700° C, stop of preheating with LPG was made. A thick, black smoke was seen at the beginning and slowly thinned out by adjusting the air/fuel (A/F) ratio. Excess air at various levels for equivalence ratio, defined as  $\Phi = (A/F)_{stai}/$  $(A/F)_{actual}$ , of 0.8, 1.0 and 1.2 was tried for each of  $\lambda$ . The temperatures were monitored at various selected locations with chromel-alumel (type K) thermocouples while volumetric flow rates of primary and secondary airs were measured by using orifice meters. Flue gas emissions were measured by a gas analyzer. All data collection was taken at steady state condition.

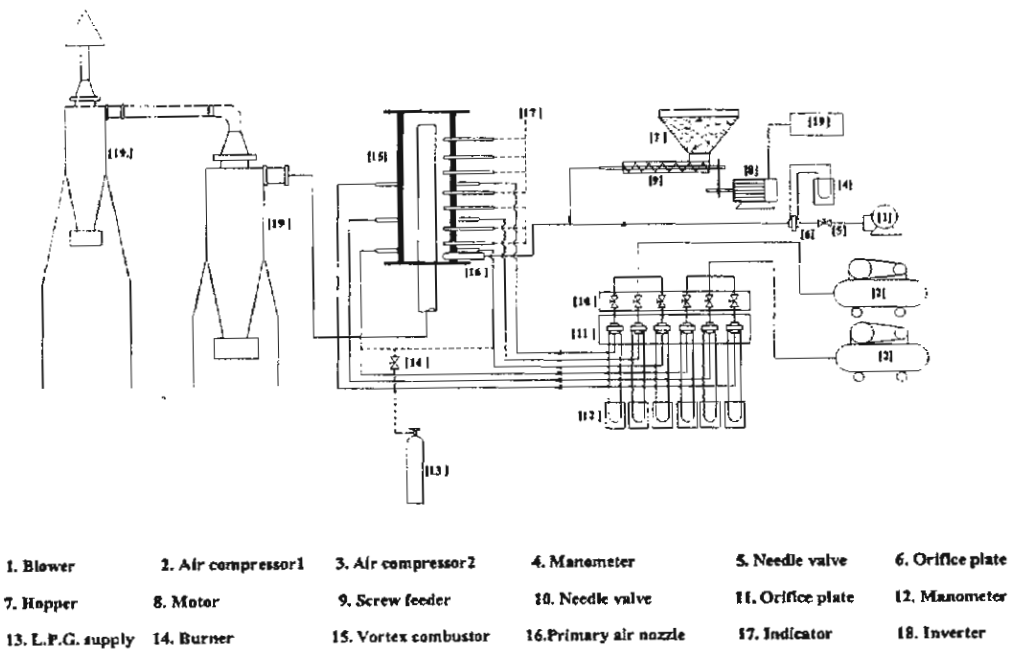


Fig. 1 Schematic diagram of experimental setup of combustion system.

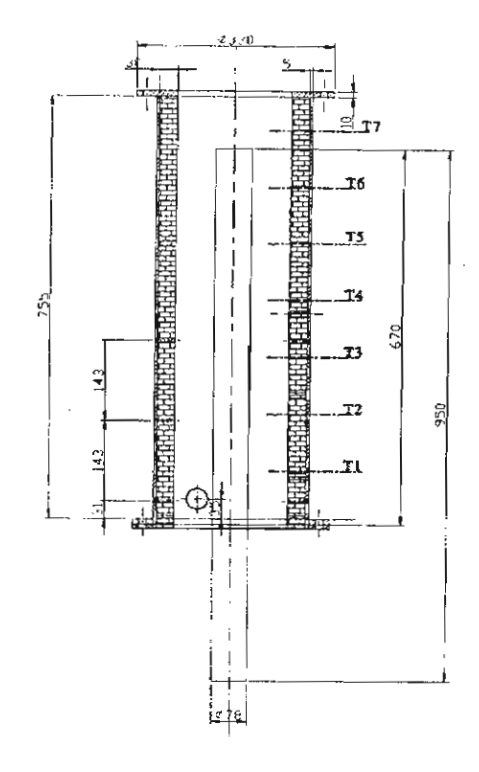


Fig. 2 Configuration of vortex combustor (unit in mm.)

#### **RESULTS AND DISCUSSION**

The VC was originally designed to accommodate various types of coal fuels as sources of heat. The VC responded significantly to the various fuels as expected. For rice husks, the level of equivalence ratio (or excess air) was varied to optimize the temperature inside the VC. The measurements of temperature were made at seven axial locations namely, x/D = 0.5, 1.0, 1.5, 2.0, 2.5, 3.0 and 3.5.

#### Effects of Equivalence Ratios

The radial profiles of temperature inside the VC for  $\Phi = 1.2$  (rich),  $\Phi = 1.0$  (stoich.) and  $\Phi = 0.8$  (lean) are presented in Figs. 3a, 3b and 3c respectively. The feed-rate of fine rice husk with 10.3% moisture content was 0.2 kg/min and kept constant throughout.

For  $\Phi=1.2$  and  $\lambda=0$ , Fig. 3a, it is found that the temperature profiles for all locations generally are not uniform. The temperature in the vicinity of the center pipe is higher than that near the chamber walls. Maximum temperature of about  $800^\circ$  C takes place in the top of chamber while lower temperature can be seen near the chamber wall. Unburned fuel and black smoke emission from the exhaust stack were observed for this case. This indicates the incomplete combustion (high CO concentration) or combustion reaction takes place very slowly.

Fig. 3b shows the temperature distributions for  $\Phi = 1.0$ . It can be seen that (for  $\lambda = 0$ ) the temperature profiles are nearly

uniform for all stations except at the top chamber. The maximum temperature above 800° C is found in the top annular space whereas the minimum temperature in the vicinity of the chamber walls at early station. This shows insufficient turbulence at the bottom chamber, which was due to too many rice husks, resulting in inadequate mixing and consequently the presence of fuel rich zones within the bottom space. This case yielded a less black smoke emission from the exit pipe.

The temperature distribution for  $\Phi=0.8$  is depicted in Fig. 3c. It is worth noting that the temperature profiles similar to the case for  $\Phi=1.0$ , are nearly uniform for all stations. The peak temperature of some  $800^{\circ}$  C is also seen in the top annular space while lowest temperature at the bottom one. The peak one for every station is found in the middle between the chamber and center pipe walls. The maximum temperature for this case has the lower value than the case for  $\Phi=1.0$ , as expected, since an increase in the excess air leads to decreasing temperature in the combustion system. White and thin smoke emission and small size of flyash particles are visible. This points out that complete combustion takes place for this case.

### Effects of Volumetric flow rate ratios of Secondary to total Airs ( $\lambda$ )

The ratio of volumetric flow rate of the primary air to the secondary air, defined as  $\lambda = Q_2/(Q_1+Q_2)$ , is an indication of the strength of the vortex of the flow. The increase in value of  $\lambda$  results in the higher tangential velocity component (strong vortex). This means that the impact of swirling phenomenon of the secondary air on the flow and temperature fields becomes more pronounced as the value of  $\lambda$  is increased. Comparison of the temperature distributions for  $\lambda = 0.0$ , 0.2 and 0.4 for various equivalence ratios is also presented in Fig. 3.

For  $\Phi = 1.2$ , it is obvious that adjusting of  $\lambda = 0.4$  leads to a flatter and higher temperature distribution curve than that of  $\lambda = 0.0$  and 0.2. The use of a value of  $\lambda$  can improve substantially the temperature distributions in the VC as can be seen in Fig. 3a. This indicates that for the rich mixture,  $\lambda$  should be used to help increase combustion efficiency.

When  $\Phi=1.0$ , it is interesting to note that the influence of  $\lambda$  on the temperature profiles shows slightly improvement on the first three stations at the bottom while significant improvement due to  $\lambda$  on the temperature profiles is found at other stations as illustrated in Fig. 3b. Again, use of  $\lambda$  leads to higher combustion temperature in the VC at about 20%.

As  $\Phi = 1.2$ , it is worth noting that effect of  $\lambda$  on the temperature distributions is seen at early stations while slightly influence on the top part of the VC as exhibited in Fig. 3c. Also, use of  $\lambda$  shows better combustion temperature obtained.

It is concluded that for all values of  $\Phi$ , use of  $\lambda$  results in significant improvement of temperature profiles and yields higher temperature of combustion in the VC. Besides, the increased swirling intensity leads to an abatement of particle elutriation, and to enlargement of recirculating region.

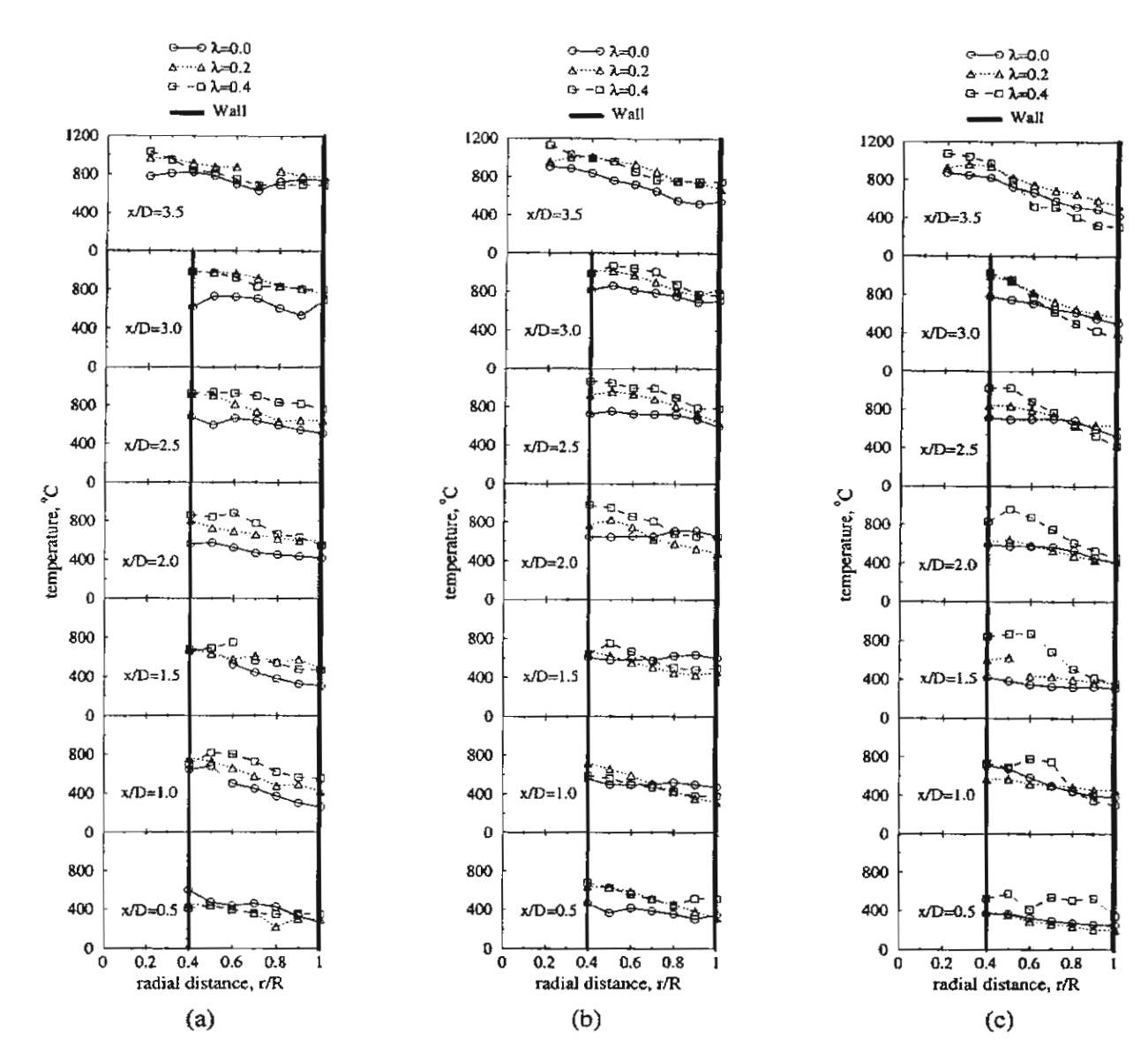


Fig. 3 Temperature distributions inside the combustor, (a)  $\Phi$  = 1.2, (b)  $\Phi$  = 1.0, and (c)  $\Phi$  = 0.8.

#### **Emissions of exhaust gas**

The flue gas emissions of CO, CO<sub>2</sub>, NO<sub>x</sub> and O<sub>2</sub> for various equivalence ratios and different  $\lambda$  are studied and presented in Figs. 4a, 4b 4c and 4d, respectively.

For CO emissions in Fig. 4a, it is interesting to note that the emissions of CO are reduced substantially when Φ is decreased (or lean mixture). The formation of CO is very low once λ is introduced for the three equivalence ratio cases. The emissions of CO<sub>2</sub> can be also reduced by increasing the excess air (or decreasing Φ). Nevertheless, the application of λ leads to the reduction of CO<sub>2</sub> as can be seen in Fig. 4b.

For  $NO_x$  emissions, Fig. 4c shows that lower equivalence ratio favours the formation of  $NO_x$ . Also, use of  $\lambda$  results in higher  $NO_x$  emissions. This can be attributed to higher temperature of combustion in the VC. The level of  $O_2$  emissions is presented in Fig. 4d. It is found that the  $O_2$  level increases for lower equivalence ratio and using  $\lambda$ .

#### CONCLUSIONS

The measurements of temperature distributions and flue gas emissions have been conducted during the combustion of fine rice husk in the VC. The conclusions derived from the results of these experiments are as follows: combustion of rice husk in the VC with equivalence ratio between 0.8 and 1.0 yields better combustion efficiency, flame stabilization, low emission and reliable furnace condition. For all equivalence ratios, use of

secondary air has a significant effect on the temperature distributions inside and helps reduce emissions and the size of flyash particle.

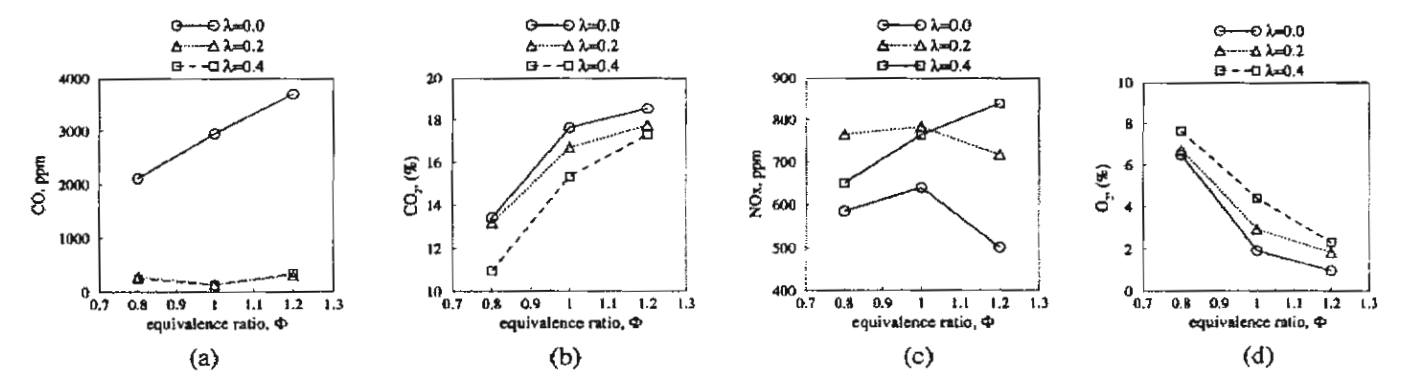


Fig. 4 Emissions of flue gas, (a) CO, (b) CO<sub>2</sub>, (c) NO<sub>K</sub>, and (d) O<sub>2</sub>.

#### **ACKNOWLEDGEMENTS**

The authors would like to acknowledge with appreciation, the Thailand Research Fund (TRF) for the financial support and the Mechanical Engineering Department, Mahanakorn University of Technology (MUT) for their support in this effort and the MUT undergraduate students for data collection.

#### REFERENCES

- Singh, R., Maherhweri, R.C., and Ojha, T.P., 1980, "Development of Husk Fired Furnace", The British Society for Research in Agricultural Engineering, India, pp. 109-120
- [2]. Tumambing, J.A., 1984, "Testing and Evaluation of Rice Hull-Fed Furnaces for Grain Drying", National Post Harvest Institute for Research and Extension, pp. 197-214.
- [3]. Xuan, N.V., Vinh, T., Anh, P.T. and Hien, P., 1995, "Development of Rice Husk Furnaces for Grain Drying",

- Proceeding of the International Conference on Grain Drying in Asia, 17-20 October, Bangkok, Thailand, pp.109-120.
- [4]. Soponronnarit, S., Prachayawarakorn, S. and Wangi, M., 1996, "Comercial Fluidized Bed Paddy Dryer", Proceedings of 10<sup>th</sup> International Drying Symposium (IDS'96), Krakow, Poland, 30 July-2 August, Vol. A, pp. 638-644.
- [5]. Nieh, S. and Fu, T.T., 1988, "Development of a Nonslagging Vortex Combustor (VC) for Space/Water Heating Applications", Proceeding of The 5<sup>th</sup> International Coal Conference, Pittsburgh, pp. 761-768.
- [6]. Promvonge, P., Vongsampigoon, L. and Piriyarungroj, N., 2000, "A Low Emission Annular Vortex Combustor Firing Rice Husk Fuel: Part II – Experimental Investigation", Proceeding of The First Regional Conference on Energy Technology Towards a Clean Environment, 1<sup>st</sup> – 2<sup>nd</sup> December, Chiang Mai, Thailand, pp. 279-284.



## สัมนาวิชาการวิศวกรรมเครื่องกล แห่งประเทศไทยครั้งที่ ๑๓



บทความทางวิชาการ เล่มที่ เป็น

จัดโดย
เครือข่ายวิศวกรรมเครื่องกล
ดำเนินงานโดย
ภาควิชาวิศวกรรมเครื่องกล
คณะวิศวกรรมศาสตร์
สถาบันเทคโนโลยีพระจอมเกล้า
เจ้าคุณทหารลาดกระบัง

Proceeding of the 13th National Mechanical Engineering Conference 2-3 December 1999, Royal Cliff Beach Resort Hotel, South Pattaya, Cholburi

#### Simulation of Turbulent Flow through a Circular Orifice

#### Pongjet Promyonge

Department of Mechanical Engineering, Faculty of Engineering, King Mongkut's Institute of Technology Ladkrabang, Bangkok 10520, Thailand. Email: kppongje@kmitl.ac.th

and

#### Kulthorn Silapabanleng

Department of Mechanical Engineering, Faculty of Engineering, Chulalongkorn University, Bangkok 10330, Thailand.

#### Abstract

The paper presents a numerical simulation of a steady turbulent airflow in a circular duct containing an orifice plate. A Finite Volume approach with a non-uniform and staggered grid system is employed in the present simulation. To account for the turbulence nature of the flow, the standard k-E turbulence model is incorporated in the time-averaged governing equations. Effects of numerical diffusion on the calculated results are also investigated by comparing between a second-orderdifferencing scheme for the convection transport and the first-order hybrid scheme. The calculated solutions are in close agreement with 3D LDA measurements. The computations of the flow reveal that the use of a secondorder scheme leads to more accurate results than that of a first-order scheme.

#### Introduction

The orifice meter is a device commonly used for measuring fluid flow in industrial processes such as metering flow in the natural gas industry. Although more accurate metering methods are available, the orifice plate continues to be preferred. The popularity of the orifice meter can be attributed primarily to its simplicity, relatively low cost and little maintenance requirements in comparison with other fluid meters. The orifice plate becomes the essential part of a fluid flow meter when installed in a pipe such that the fluid stream must negotiate the constriction.

By far the most common orifice plate installation is that of the concentric round orifice plate. In this type of arrangement the orifice is round and the plate is mounted between pipe flanges. The plate is positioned perpendicular to a fully developed pipe flow while at the same time the circular orifice is concentric with respect to the (circular) pipe interior. Other types of orifice plate exist, such as square orifices, series and non-concentric: Also, the inner edge of the orifice is machined in one of several different ways. Some orifice plates are square edged while others are rounded and beveled. This study is

concerned with the concentric, round, beveled orifice plate.

Most of the work thus far on orifice meters has focused almost entirely on the determination of discharge coefficients. There have been a handful of attempts to study in detail the flow field in the vicinity of the orifice plate. It is believed that knowledge concerning details of the orifice flow field will lead the way to improvements in metering accuracy. These improvements could come via improved determination and prediction of discharge coefficients.

This paper deals with the simulation of turbulent flow through an orifice plate with a view to increasing the knowledge of orifice meter flow. The mathematical model including the k- $\varepsilon$  turbulence model, numerical solution and other computational details is described. Comparisons of the calculated gas axial velocity with 3D LDV measured data [4] are made to evaluate the turbulence models and the numerical schemes used.

#### 2. Mathematical Modelling

#### 2.1 Governing Equations and Closures

For constant density, isothermal turbulent flows, the time-averaged incompressible Navier-Stokes equations in the Cartesian tensor notation can be written in the following form:

$$\frac{\partial}{\partial x_i} (\rho u_i) = 0 \tag{1}$$

$$\frac{\partial}{\partial x_i} (\rho u_i) = 0$$

$$\frac{\partial(\rho u_i u_j)}{\partial x_j} = -\frac{\partial \rho}{\partial x_i} + \frac{\partial}{\partial x_j} (\bar{t}_{ij} + \tau_{ij})$$
(2)

The mean viscous stress tensor is approximated as:

$$\bar{t}_{ij} = \mu \left( \frac{\partial u_i}{\partial x_j} + \frac{\partial u_j}{\partial x_i} \right) \tag{3}$$

where  $\mu$  is laminar viscosity. Due to the nonlinearity of equation (2), the averaging process employed introduces the unknown correlation the time-averaged Reynolds stress tensor,  $\tau_{ij}$  (=  $-\rho \overrightarrow{u_i u_j}$ ) that are obtained from

turbulence models [1, 2, 3, 10]. In the present study, the standard k-E turbulence model [1, 10] is adopted and the Reynolds stress is linearly related to the mean rate of strain by a scalar eddy viscosity. The standard version relates the turbulent eddy viscosity to the turbulence kinetic energy k and the dissipation rate  $\varepsilon$  through Boussinesq's approximation [8] as:

$$\tau_{ij} = -\frac{2}{3}\delta_{ij}(\rho k) + \mu_t(\frac{\partial u_i}{\partial x_j} + \frac{\partial u_j}{\partial x_i})$$
 (4)

where  $\mu_i$  is the turbulent eddy viscosity. In the k- $\epsilon$  model the turbulent viscosity is related to k and  $\varepsilon$  by

$$\mu_{t} = C_{\mu} \rho \frac{k^{2}}{\varepsilon} \tag{5}$$

The two turbulence quantities in equation (5), k and  $\varepsilon$ , are obtained from the following transport equations which are solved simultaneously with governing equations (1) and

$$\frac{\partial}{\partial x_j} (\rho u_j k) = \frac{\partial}{\partial x_j} \left( \frac{\mu_e}{\sigma_k} \frac{\partial k}{\partial x_j} \right) + G - \rho \varepsilon \tag{6}$$

$$\frac{\partial}{\partial x_{j}} \left( \rho u_{j} \varepsilon \right) = \frac{\partial}{\partial x_{j}} \left( \frac{\mu_{e}}{\sigma_{\varepsilon}} \frac{\partial \varepsilon}{\partial x_{j}} \right) + \frac{\varepsilon}{k} \left( C_{\varepsilon 1} G - C_{\varepsilon 2} \rho \varepsilon \right) \tag{7}$$

in which G represents the rate of generation of turbulent kinetic energy while  $\rho \varepsilon$  is its destruction rate, G is given

$$G = \mu_t \left[ \left( \frac{\partial u_i}{\partial x_j} + \frac{\partial u_j}{\partial x_i} \right) \frac{\partial u_i}{\partial x_j} \right]$$
 (8)

The boundary values for the turbulent quantities near the wall are specified with the wall function method [6]. The empirical constants  $C_{\mu}$ ,  $C_{\epsilon 1}$ ,  $C_{\epsilon 2}$ ,  $\sigma_{k}$ , and  $\sigma_{\epsilon}$  in the turbulent transport equations are assumed to have the values of 0.09, 1.44, 1.92, 1.0 and 1.3 [8, 10] respectively.

#### 2.2 Common Form for the Equations

All the governing partial differential equations can be re-organised and expressed in a standard form that includes the convection, diffusion, and source terms [5, 9] for 2-D axisymmetric flows as follows:

$$\frac{\partial}{\partial x} (\overline{\rho} u \phi) + \frac{1}{r} \frac{\partial}{\partial r} (r \overline{\rho} v \phi) - \frac{\partial}{\partial x} \left( \Gamma_{\phi x} \frac{\partial \phi}{\partial x} \right) - \frac{1}{r} \frac{\partial}{\partial r} \left( r \Gamma_{\phi r} \frac{\partial \phi}{\partial r} \right) = S_{\phi}$$
(8)

where  $\phi$  may stand for any variable including the velocity components,  $\Gamma_{\phi_x}$  and  $\Gamma_{\phi_r}$  are the exchange coefficients for  $\phi$ , and  $S_{\phi}$  is the source term.

Detailed expressions of  $\Gamma_{\phi_x}$ ,  $\Gamma_{\phi_r}$  and  $S_{\phi}$  for different  $\phi$ 's are summarised in Table 1 below.

#### -Nomenclature -

 $C_{\epsilon 1}, C_{\epsilon 2}$  constants in the dissipation rate equation C convection term

constant in the k-E turbulence model

D diffusion term; dimension

pipe or duct diameter

orifice diameter

G stress generation

D

turbulence kinetic energy

turbulence characteristic length scale

p mean pressure

inlet wall pressure  $p_{ia}$ 

outlet wall pressure Pout

radial co-ordinate; radius

pipe radius R

Reynolds number based on pipe diameter  $Re_D$ 

general source term; swirl number

viscous stress tensor

fluctuating velocities in direction xi

 $\rho u_i u_i$ Reynolds stresses

time-averaged velocity in x-direction

time-averaged velocity in r-direction

axial co-ordinate

#### **Greek Symbols**

Kronecker delta tensor  $\delta_{it}$ 

ε, dissipation

generalised dependent variable

exchange coefficient  $\Gamma_{\phi}$ 

ratio of pipe to orifice diameter (d/D)

dynamic viscosity, eddy-viscosity  $\mu, \mu,$ 

effective viscosity,  $(= \mu_i + \mu)$  $\mu_e$ 

ρ density

 $\sigma_{\phi}$ Schmidt or Prandtl numbers for the scalar \$\phi\$

Reynolds stress tensor  $\tau_{ii}$ 

#### Subscripts

effective e

turbulence

Cartesian indices i, j, k

#### Superscripts and Overbars

- fluctuating quantity in time-averaging
- mean quantity

Table 1 Summary of the governing equations.

Conservation of	ф	Гфх	Γ <sub>φr</sub>	$s_{\phi}$
Mass	1	0	0	0
x-momentum	и	$\mu_{\!\scriptscriptstyle o}$	$\mu_e$	$\frac{\partial}{\partial x} \left( \mu_{e} \frac{\partial \widetilde{u}}{\partial x} \right) + \frac{\partial}{r \partial r} \left( r \mu_{e} \frac{\partial \widetilde{v}}{\partial x} \right) - \frac{\partial}{\partial x} \left( \overline{p} + \frac{2}{3} \overline{\rho} k \right)$
r-momentum	ν	$\mu_e$	$\mu_e$	$\frac{\partial}{\partial x} \left( \mu_e \frac{\partial \tilde{u}}{\partial r} \right) + \frac{\partial}{r \partial r} \left( r \mu_e \frac{\partial \tilde{v}}{\partial r} \right) - \frac{\partial}{\partial r} \left( \overline{p} + \frac{2}{3} \overline{\rho} k \right) - \frac{2 \mu_e \tilde{v}}{r^2}$
Turbulent kinetic energy	k	$\mu J \sigma_k$	μ./σ <sub>k</sub>	G- hoarepsilon
TKE dissipation rate	ε	$\mu I \sigma_{\varepsilon}$	μ√σε	$(C_{\varepsilon 1}G - C_{\varepsilon 2} \rho \varepsilon) \frac{\varepsilon}{k}$

where 
$$\sigma_{k} = 1.0$$
,  $\sigma_{t} = 1.3$ ,  $C_{t1} = 1.44$ ,  $C_{t2} = 1.92$ ,  $\mu_{e} = \mu_{t} + \mu$ ,  $G_{k} = \mu_{e} \left\{ 2 \left[ \left( \frac{\partial \widetilde{u}}{\partial x} \right)^{2} + \left( \frac{\widetilde{v}}{r} \right)^{2} \right] + \left( \frac{\widetilde{v}}{\partial x} + \frac{\partial \widetilde{u}}{\partial x} \right)^{2} \right\}$ 

#### 2.3 Solution Procedure

In the present computation, the time-averaged Navier-Stokes equations, the TKE equation, and the TKE dissipation rate equation are solved numerically by a control-volume finite-difference method [5, 9] together with the the k- $\varepsilon$  model, equation (4). All equations are in a generalised form of equation (8). The SIMPLE algorithm is utilised for pressure-velocity de-coupling and iteration [5, 8]. The hybrid [9] and the second order upwind (SOU) [7] schemes were used for discretising convection and diffusion transports on a staggered grid cell. The underrelaxation iterative TDMA line-by-line sweeping technique is used for solving the resultant finitedifference equations. The computation was carried out using a PC (Pentium III - 450 MHz) computer. About 5,000 iterations were needed to achieve satisfactory convergence for each calculation case, which requires about 15 minutes of computer time.

#### Flow through an Orifice of Nail [4]

A flow in pipe with a circular orifice of Nail [4] was employed in the present simulation. A schematic configuration of the duct orifice is shown in Fig. 1 below. The pipe with a length of 9D has a diameter of 25.4 mm and the 3.2-mm thick orifice diameter is 12.7 mm. Profile measurements of centerline axial velocities, wall-static pressure, Reynolds stresses, and wall shear stresses were measured by using Laser Doppler anemometer (LDA). The flow had the Reynolds number (Re) of 1.84 x 10<sup>4</sup> and rate of mass flow of 1.356 x 10<sup>-2</sup> kg/s with temperature at 300K (see Table 2 below for specifications).

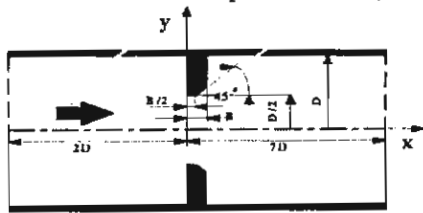


Fig. 1 Geometry of pipe with the orifice.

Table 2 Data for flow through an orifice plate [4].

Parameter	Magnitude	
Test section characteristics		
Pipe diameter (D), m	0.0254	
Orifice diameter (d), m	0.0127	
pipe length (L), m	1.8	
Inlet fluid properties (air)		
Mean axial velocity, m/s	5.6	
Temperature, K	300	
Reynolds number	$1.84 \times 10^4$	

#### 4. Results and Discussion

The comparisons between the predicted results by the k-\varepsilon turbulence model with different numerical schemes and the measured data of the flow are presented in Figs. 2 through 7. The predicted gas pressure and centerline axial velocities are compared with the measurements, where solid or dash curves are represented for the calculated results while open circles for the measured data.

The computational results are based on a 70x30 non-uniform grid with refinement in the vicinity of the orifice. Grid independence of the numerical results was verified with a 90x50 finer grid. It is found that the differences for both the base grid and the finer grid in local flow properties are marginal. This suggests that grid independent solutions can be obtained with a 70x30 grid, which is used throughout the computations. In order to reduce uncertainties in the inlet profiles of the mean flow field, the inlet boundary conditions were specified at x/D = -2.0 for which measured data was available, apart from the radial velocity  $\nu$  which is set to zero.

The distributions of centerline axial velocity predicted with the hybrid and the SOU schemes are compared with the measured data in Fig. 2. A closer examination reveals that predictions with both the

schemes are in generally good agreement with the measurements. However, for prediction with the hybrid scheme, under-predicted results are seen in the orifice region in comparison with experimental data. The use of the SOU leads to substantial improvement for this flow.

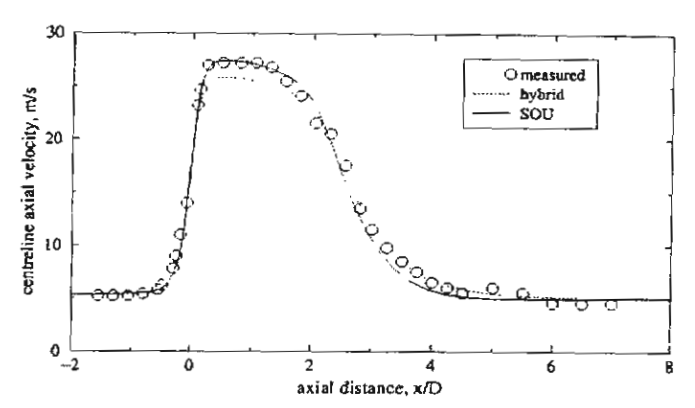


Fig. 2 Effects of numerical schemes on centerline axial velocity profiles with measurements.

Figure 3 compares the profiles of static pressure along the wall using the hybrid and the SOU schemes with the measurements. It is found that there is a high-pressure drop across the orifice. Predictions with both numerical schemes show favourable agreement in upstream region of the orifice. However, immediately after the orifice plate, the calculated wall pressure rises faster than the experiment shows. At downstream regions from the orifice, the SOU results mimic experimental data very well while the hybrid scheme ones are over-predicted. Again, the use of the SOU results in significant improvement for this flow

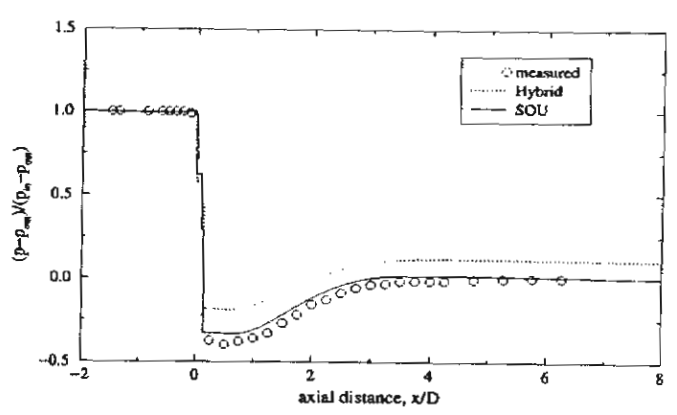


Fig. 3 Effects of numerical schemes on wall-static pressure profiles with measurements.

Streamlines predicted with the hybrid and SOU schemes are shown in Fig. 4 and Fig. 5 respectively. Two recirculation zones are found; one is at the corner upstream of the orifice and the other, a large recirculation zone, a downstream region one. The size of the recirculation zone calculated by the hybrid is slightly larger than that by the SOU. The center of recirculation predicted by the SOU is at about x/D = 1 and r/R = 0.7 while at about x/D = 0.85 and r/R = 0.7 is seen for the hybrid. The reattachment length, an important measure of the quality of numerical results, is well predicted ( $x_{r,exp} = 2.25D$ ,  $x_{r,calc} = 2.23D$  for SOU, and  $x_{r,calc} = 2.1D$  for hybrid).

Velocity vectors predicted by the hybrid and SOU schemes are depicted in Figs. 6 and 7 respectively. High velocities are observed in the core region in a range of x/D = 0 to 3 from downstream of the orifice.

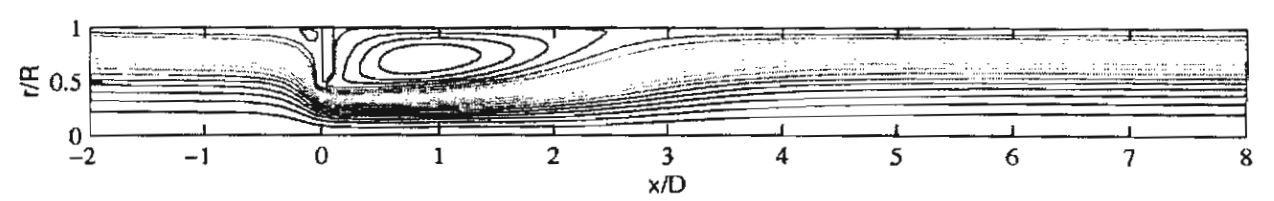


Fig. 4 Streamlines predicted by the hybrid scheme

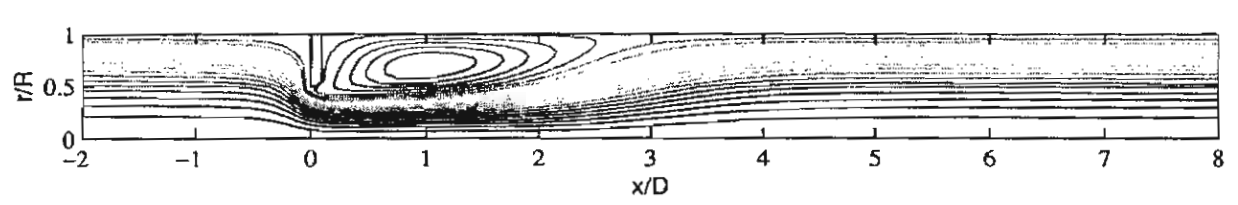


Fig. 5 Streamlines predicted by the SOU scheme

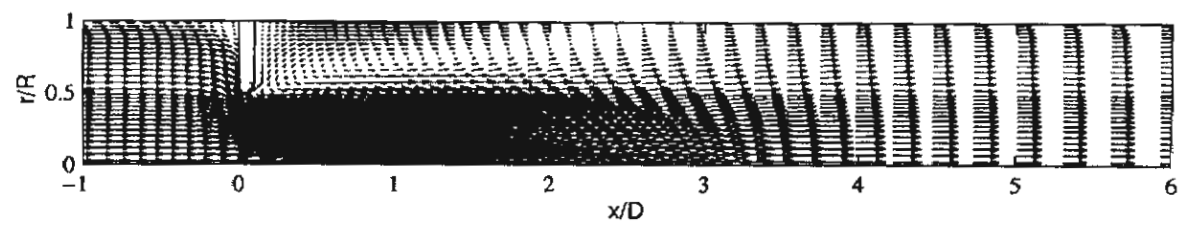


Fig. 6 Velocity vectors predicted by the hybrid scheme

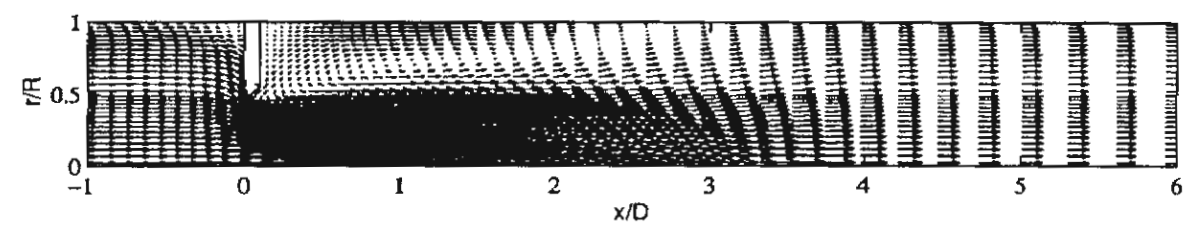


Fig. 7 Velocity vectors predicted by the SOU scheme

#### 5. Concluding Remarks

Simulations of turbulent flow through a circular orifice plate have been carried out by utilizing the k-ɛ model and two different numerical schemes. The predicted results of mean flow properties were compared with measurements. The conclusions from the investigation can be drawn as follows:

- The predicted centerline axial velocity and wall-static pressure profiles by the hybrid and SOU schemes are in generally good agreement with measurements.
- The SOU shows a significant improvement over the hybrid scheme and both schemes give slightly overpredicted results in the core region and slightly underpredicted near the walls in comparison with measurements.

#### 6. Acknowledgements

The authors would like to gratefully acknowledge the Thailand Research Fund for financial support of this research.

#### 7. References

 Gatski, T.B. (1996), Turbulent Flows: Model Equations and Solution Methodology, in Handbook of Computational Fluid

- Mechanics, Edited by Roger Peyret, Academic Press Ltd, London.
- Hogg, S. and Leschziner, M.A.(1989a), Computation of Highly Swirling Confined Flow with a Reynolds Stress Turbulence Model, AIAA J., Vol.27, pp.57-63.
- Jones, W.P. and Pascau, A. (1989), Calculation of Confined Swirling Flows with a Second Moment Closure, Trans. ASME J. of Fluid Engineering, Vol.111, Sept, pp.248-255.
- Nail, G.H. (1991), A Study of 3-dimensional flow through orifice meters, Ph.D. Dissertation, Texas A&M University.
- Patankar, S.V. (1980), Numerical Heat Transfer and Fluid Flow, Hemisphere, Washington, D.C.
- 6. Patankar, S.V. and Spalding, D.B. (1970), Heat and Mass Transfer in Boundary Layers, Intertext Books, London.
- Shyy, W., Thakur, S.,and Wright, J. (1992), Second Order Upwind and Central Difference Schemes for Recirculating Flow Computation, AIAA J., Vol.30, No.4, pp.931-932.
- Sloan, D.G., Smith, P.J., and Smoot, L.D. (1986), Modeling of Swirl in Turbulent Flow System, Progr. Energy Combust. Sci., vol. 12, pp. 163-250.
- Versteeg, H.K. and Malalasekera, W. (1995), An Introduction to Computational Fluid Dynamics: The Finite Volume Method, Longman Scientific & Technical, Longman Group Limited, Essex, England.
- Wilcox, C.D. (1993), Turbulent Modelling for CFD, DCW Industries, Inc., California.

The Fifth Annual Mational Symposium on Computational Science and Engineering

# ANSCSE 2001

Organizers:

National Electronics and Computer Technology Center

June 19 - 20, 2001

Bangkok Convention Center (BCC); Central Plaza

#### Numerical Simulation of Isothermal Swirling Turbulent Flow in a Combustor

P. Promvonge<sup>1</sup>, L. Vongsarnpigoon<sup>2</sup> and K. Silapabanleng<sup>3</sup>
<sup>1</sup>Dept. of Mechanical Engineering, Faculty of Engineering,
King Mongkut's Institute of Technology Ladkrabang,
Bangkok 10520, Thailand. Email: <a href="mailto:kppongje@kmitl.ac.th">kppongje@kmitl.ac.th</a>

<sup>2</sup>Dept. of Mechanical Engineering, Faculty of Engineering, Mahanakorn University of Techonology, Bangkok 10530, Thailand.

<sup>3</sup>Dept of Mechanical Engineering, Faculty of Engineering, Chulalongkorn University, Bangkok 10330, Thailand.

#### **Abstract**

The paper presents the simulation of strongly swirling confined flow in a combustor with an algebraic Reynolds stress model (ASM). The k- $\epsilon$  turbulence model was also employed in the present simulation for comparison. For the flows compared, the predicted results of gas tangential and axial velocities based on this model are in good agreement with measurements. The computation shows that the ASM is superior to the k- $\epsilon$  model in capturing the stabilising effect of the swirl.

Keywords: swirl, turbulent flow, algebraic stress model.

#### 1. Introduction

Swirl flows have been of considerable interest over the past decades because of their occurrence in industrial applications, such as furnaces, utility boilers, internal combustion engines, gas turbine combustors and dust collectors [2, 5]. Swirl has been used in combustion systems to enhance the flame stability, the mixing and heat transfer besides prolonging the fuel residence time and abating the pollutants. This is because under appropriate conditions, swirl can be employed to induce a central recirculation zone. The recirculating flow generates additional turbulence in the shear layer between the reverse flow and the surrounding forward flow and helps stabilize the flame in combustors. Swirling turbulent flows are physically complex in nature due to the effect of a swirl-turbulence interaction. The turbulence structure in swirling turbulent flows is generally highly non-isotropic and nonhomogeneous.

Computation of swirling flows is a difficult and challenging task. Large velocity gradients appear in these flows, so numerical problems and turbulence modelling play a significant role in their analysis. The commonly used, the k- $\varepsilon$  model may not be suitable for simulating swirling turbulent flows [3, 6, 7]. It is also found that the use of modified k- $\varepsilon$  models or even the non-linear k- $\varepsilon$  model [13] leads to no significant improvement of the predictions in swirling flows. The second-order moment closure models, i.e., the Reynolds stress model (RSM) and the algebraic Reynolds stress model provide better methods for the simulation of swirling turbulent flows [6, 7]. The RSM is regarded as a most logical approach to the turbulence closure problem, which does not need any ad hoc modification for extra strain rates. However, in the prediction of swirling flows with the RSM, it is necessary to solve a total of 11 governing differential equations of elliptic type: a continuity equation, three momentum equations, an  $\varepsilon$ -equation, and six equations for the Reynolds stresses. This leads

to much extra computational effort to solve six Reynolds stress transport equations simultaneously [6, 7] and much attention needs to be paid to numerical stability and inlet boundary conditions. It is for this reason that a simplified algebraic Reynolds stress turbulence model [16] in axisymmetric cylindrical co-ordinates is employed for simulating strongly swirling flows.

In this paper, the formulation of the present model, the procedure of numerical solution based on the present ASM and the validation results of the proposed model are described in detail. The validation was conducted through successive comparisons of the calculated gas tangential, radial and axial velocities with the test data measured in a cold flow combustor.

#### 2. Mathematical Formulation

#### 2.1 Governing Equations

The phenomenon under consideration is governed by the steady two-dimensional axisymmetric form of the continuity and the time-averaged incompressible Navier-Stokes equations. In the Cartesian tensor system these equations can be written in the following form:

$$\frac{\partial}{\partial x_i}(\rho u_i) = 0 \tag{1}$$

$$\frac{\partial(\rho u_i u_j)}{\partial x_i} = -\frac{\partial p}{\partial x_i} + \frac{\partial}{\partial x_j} (\bar{t}_{ij} + \tau_{ij})$$
(2)

where  $\rho$ ,  $u_i$ , p and  $x_i$  are the density, mean velocity tensor, mean pressure and coordinate tensor respectively. The mean viscous stress tensor,  $\overline{t_i}$ , is approximated as:

$$\bar{t}_{ij} = \mu \left( \frac{\partial u_i}{\partial x_j} + \frac{\partial u_j}{\partial x_i} \right) \tag{3}$$

where  $\mu$  is laminar viscosity. The time-averaged Reynolds stress tensor,  $\tau_{ij} = -\rho \overrightarrow{u_i u_j}$ , in the above equation is not known and thus, models are needed to express it in terms of the solution variables. In the present study, two turbulence models are used, namely the k- $\varepsilon$  model and an algebraic stress model (ASM). The k- $\varepsilon$  model has been reviewed in references [4, 15] and it will be described briefly. The standard k- $\varepsilon$  model version relates the turbulent eddy viscosity to the turbulence kinetic energy k and the dissipation rate  $\varepsilon$  through Boussinesq's approximation as:

$$\tau_{ij} = -\frac{2}{3}\delta_{ij}(\rho k) + \mu_i(\frac{\partial u_i}{\partial x_i} + \frac{\partial u_j}{\partial x_i})$$
 (4)

where  $\mu_t = \rho C_{\mu} k^2 / \varepsilon$  is the turbulent eddy viscosity and  $\varepsilon$  is the dissipation rate of turbulence kinetic energy (TKE). The modelled equation of the TKE, k is given by:

$$\frac{\partial}{\partial x_{j}} (\rho u_{j} k) = \frac{\partial}{\partial x_{j}} \left( \frac{\mu_{e}}{\sigma_{k}} \frac{\partial k}{\partial x_{j}} \right) + G - \rho \varepsilon \tag{5}$$

in which  $\mu_e = \mu_t + \mu$  is effective viscosity. Similarly the dissipation rate of TKE is given by the following equation:

$$\frac{\partial}{\partial x_{j}} \left( \rho u_{j} \varepsilon \right) = \frac{\partial}{\partial x_{j}} \left( \frac{\mu_{\epsilon}}{\sigma_{\varepsilon}} \frac{\partial \varepsilon}{\partial x_{j}} \right) + \frac{\varepsilon}{k} \left( C_{\epsilon 1} G - C_{\epsilon 2} \rho \varepsilon \right) \tag{6}$$

where G is the rate of generation of the TKE while  $\rho \varepsilon$  is its destruction rate. G is given by:

$$G = \mu_{e} \left[ \left( \frac{\partial u_{i}}{\partial x_{j}} + \frac{\partial u_{j}}{\partial x_{i}} \right) \frac{\partial u_{i}}{\partial x_{j}} \right]$$
 (7)

The boundary values for the turbulent quantities near the wall are specified with the wall function method [10].  $C_{\mu} = 0.09$ ,  $C_{\text{E}i} = 1.44$ ,  $C_{\text{E}2} = 1.92$ ,  $\sigma_{k} = 1.0$ , and  $\sigma_{\epsilon} = 1.3$  are empirical constants [4, 15] in the turbulence transport equations. Reynolds-averaged transport equations can be solved for  $\tau_{ii}$ , [4, 15] the modelled equations for which are:

$$\frac{\partial \tau_{ij}}{\partial t} + \frac{\partial (u_k \tau_{ij})}{\partial x_k} = -G_{ij} - \Phi_{ij} + D_{ij} + \varepsilon_{ij}$$
(8)

where

$$G_{ij} = \text{local production} = \rho P_{ij} = -\left(\rho \overrightarrow{u_i u_k} \frac{\partial u_j}{\partial x_k} + \rho \overrightarrow{u_j u_k} \frac{\partial u_i}{\partial x_k}\right)$$

$$\Phi_{ij} = \text{local pressure strain} = -C_1 \frac{\rho \varepsilon}{k} \left(\overrightarrow{u_i u_j} - \frac{2}{3} k \delta_{ij}\right) - C_2 \left(G_{ij} - \frac{2}{3} G \delta_{ij}\right)$$

$$D_{ij} = \text{net diffusive transport} = -\frac{\partial}{\partial x_k} \left(\frac{\mu_e}{\sigma_T}\right) \frac{\partial \overrightarrow{u_i u_j}}{\partial x_k}$$

$$\varepsilon_{ij} = \text{local dissipation tensor} = \frac{2}{3} \rho \varepsilon \delta_{ij}$$

in which  $C_1 = 2.5$ , and  $C_2 = 0.55$  are model constants.

#### 2.2 Algebraic Reynolds Stress Model (ASM)

For simplicity in solving the six Reynolds stresses, Rodi's approximation [11] is used in this study and the Reynolds stress transport can be expressed in algebraic form as follows:

$$\frac{D\tau_{ij}}{Dt} - D_{ij} = \frac{\tau_{ij}}{\rho k} (\frac{Dk}{Dt} - D_k) \tag{9}$$

Substitution of eqs. (5) and (8) into eq. (9) gives the desired algebraic expression for  $\tau_{ij}$ :

$$-G_{ij} - \Phi_{ij} + \frac{2}{3} \delta_{ij} \rho \varepsilon = \frac{\tau_{ij}}{\rho k} (G - \rho \varepsilon)$$
 (10)

The ASM expressions can thus be rewritten as:

$$\rho \overrightarrow{u_i u_j} = \frac{2}{3} \delta_{ij} \rho k + \frac{\lambda k}{\varepsilon} \left( G_{ij} - \frac{2}{3} \delta_{ij} G \right)$$
(11)

where the empirical constant  $\lambda$ , was found to be 0.135, [16] is defined as:

$$\lambda = \frac{1 - C_2}{C_1 - 1 + \frac{G}{\rho \varepsilon}} \tag{12}$$

#### 2.3 Common Form for the Equations

All the governing equations can be re-organised and expressed in a standard form that includes the convection, diffusion, and source terms for 2-D axisymmetric flows as follows:

$$\frac{\partial}{\partial x}(\rho u\phi) + \frac{1}{r}\frac{\partial}{\partial r}(\rho v r\phi) - \frac{\partial}{\partial x}\left(\Gamma_{\phi x}\frac{\partial \phi}{\partial x}\right) - \frac{1}{r}\frac{\partial}{\partial r}\left(r\Gamma_{\phi y}\frac{\partial \phi}{\partial r}\right) = S_{\phi}$$
(13)

where  $\phi$  may stand for any variable including the velocity components,  $\Gamma_{\phi_x}$  and  $\Gamma_{\phi_r}$  are the exchange coefficients for  $\phi$ , and  $S_{\phi}$  is the source term.

#### 2.4 Solution Procedure

In the present computation, the time-averaged Navier-Stokes equations, the TKE equation, and the TKE dissipation rate equation are solved numerically by a control-volume finite-difference method [9, 14] together with the turbulence model equations, equation (4) for the k- $\varepsilon$  model or equation (11) for the ASM. All equations are in a generalised form of equation (13). The SIMPLE algorithm is utilised for pressure-velocity de-coupling and iteration [9, 14]. The hybrid, the upwind, the quadratic upstream interpolation for convective kinematics (QUICK) [8] and the second-order upwind (SOU) [12] schemes were used for discretising convection and diffusion transports on a staggered grid cell. The under-relaxation iterative TDMA line-by-line sweeping technique is used for solving the resultant finite-difference equations. The computation was carried out using a personal computer (Pentium III-550 MHz). About 20,000 iterations were needed to achieve satisfactory convergence for each calculation case, which requires about 3.0 hr of computer time.

#### 3. Swirling Flow of Ahmed (1997)

The performances of the k- $\varepsilon$  model and the ASM are compared for a turbulent swirling flow in a combustor of Ahmed (1997) [1], shown in Fig. 1. The details of the geometry and fluid properties are given in Table 1 below. A single air stream entered the test section through a secondary annulus and passed through an adjustable vane swirler. Experimental mean velocity profiles for u, v and w, turbulence intensities and the Reynolds stresses were measured at downstream locations of the expansion corner. All data in radial profiles were obtained with a two-components LDV system.

Since axial, radial and tangential velocities and turbulence intensities including shear stresses were provided at x/D = 0.0633 downstream of the inlet, computations are started at that location to reduce uncertain inlet conditions. In the present computation, performances of both the standard k- $\varepsilon$  model and the ASM are examined by comparing the predicted velocity profiles at ten locations, namely, x/D = 0.0633, 0.167, 0.25, 0.333, 0.417, 0.5, 0.583, 0.669, 0.833 and 1.0.

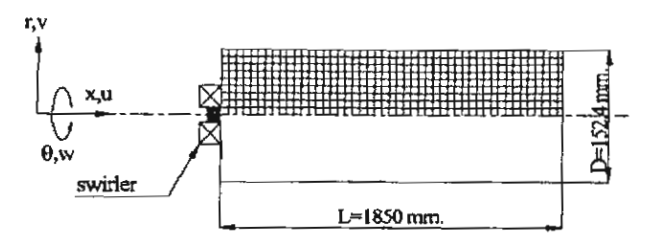


Fig. 1 Flow geometry and computational domain.

#### Table 1 Data for flow of Ahmed (1997)

Test section characteristics	
swirl vane angle (degree)	45
chamber length (m)	1.85
chamber dia. (m)	0.1524
Inlet flow conditions	
Reynolds number	200,000.
average velocity, U <sub>0</sub> (m/s)	30.4

#### 4. Results and Discussion

#### 4.1 Effects of Grid Densities and Numerical Schemes

The comparisons between the predicted results by the k-\varepsilon turbulence model and the ASM and the measured data of the flow are presented in Figs. 2 through 7. The predicted axial, radial and tangential velocities are compared with the measurements, where solid or dash curves are represented for the calculated results while open circles for the measured data. The computational results are based on a 95x40 non-uniform grid with refinement in the vicinity of the slit. Grid independence of the numerical results was verified with a 120x60 finer grid. It is found that the differences for both the base grid and the finer grid in local flow properties are marginal. This suggests that grid independent solutions can be obtained with a 95x40 grid, which is used throughout the computations.

The axial, radial and tangential mean velocity profiles predicted with the k-ɛ model and four different numerical schemes are compared with the measured data in Fig. 2. It is found that predictions with the four schemes generally are in fairly good agreement with the measurements. However, in prediction with hybrid, QUICK and SOU, under-predicted tangential velocity profiles are seen in all locations while good agreement is found for axial and radial velocity profiles in comparison with experimental data. For the four numerical schemes, the FOU scheme performs the best agreement in prediction of tangential velocity but shows poorer agreement for axial and radial velocity profiles. Thus, in terms of the strength of the tangential velocity, only the FOU scheme is considered for computation of this flow.

#### 4.2 Flow Field

Predictions of velocity profiles using the k- $\varepsilon$  model and the ASM are compared with experimental data in Figs. 2a, 2b and 2c for the axial, radial and tangential velocity profiles respectively. For the radial profile of axial velocity in Fig. 2a, it is seen that the predicted profiles show no difference for both turbulence models and generally are in favorable agreement with measurements especially for  $x/D \ge 0.333$ . The ASM However, both

turbulence models give under-predicted results in the core region. Predictions with the ASM show closer agreement with measurements than those with the k- $\epsilon$  model in some locations as can be seen at x/D = 0.167 and 0.25 between r/D = 0.35 and r/D = 5. The results of Fig. 2a indicate that the predicted axial velocity recovers and progresses to uniformity at a faster rate than in the measurements.

Fig. 2b compares the radial profile of radial velocities predicted by the k- $\varepsilon$  model and the ASM with measurements. It is of interest to note that prediction with the ASM shows closer agreement with experimental data than that with the k- $\varepsilon$  model. The ASM results mimic very well the measurements while the k- $\varepsilon$  model gives under-predicted results, especially in the vicinity of the inlet. For the downstream region far away from the inlet (x/D > 0.417), both turbulence models yield similar results and agree well with the measurements.

The tangential velocity profiles predicted by the k- $\varepsilon$  model and the ASM along with the measurements are shown in Fig. 2c. It is worth noting that the tangential velocity predictions with the k- $\varepsilon$  model display a rapid decay to a forced vortex profile (solid-body rotation) while the experimental data correspond to a combined free and forced vortex profile. It is clear that the tangential velocity predictions do not agree with the measured data even for trends. Since the calculations were fairly free of numerical diffusion, discrepancies between the data and the predictions can be attributed to two sources: - improper boundary conditions at the inlet plane and deficiencies of the turbulence model.

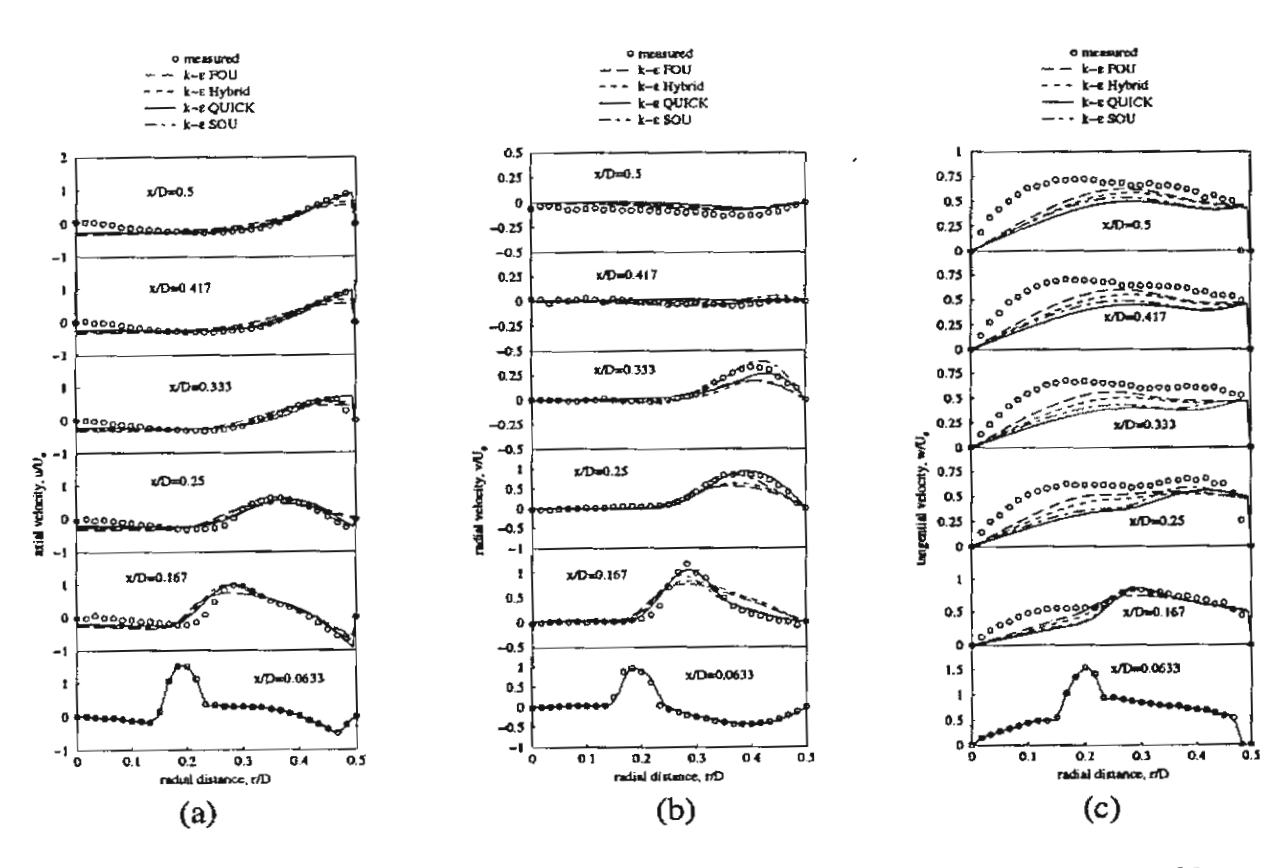


Fig. 2 Effect of numerical schemes on the axial, radial and tangential velocity profiles.

All inlet values except the  $\varepsilon$  and the k, were obtained indirectly from the experiment. The values of  $\varepsilon$  were derived from a constant length-scale assumption and those of k from an

approximation of total kinetic energy. To study the sensitivity of the inlet  $\varepsilon$  and k profiles to the flow field, calculations were made using different  $\varepsilon$  and k distributions, by increasing or decreasing their estimated values by a factor of 10. It was found that the calculated velocity was not affected significantly. The poor agreement between the predictions and measurements is, therefore, more likely to be due to the deficiencies of the turbulence model. The use of ASM results in better overall agreement with the measurements than possible with the k- $\varepsilon$  model. The major difference between calculations with the two turbulence models is most clear in the recirculation region and in the tangential velocity profiles. The agreement between the calculation with the ASM and the experimental data is fairly good. The peak values and a combined forced and free (Rankine) vortex motion for the tangential velocity profiles are well predicted. The recirculation zone (IRZ) is, however, longer and wider than that with the k- $\varepsilon$  model.

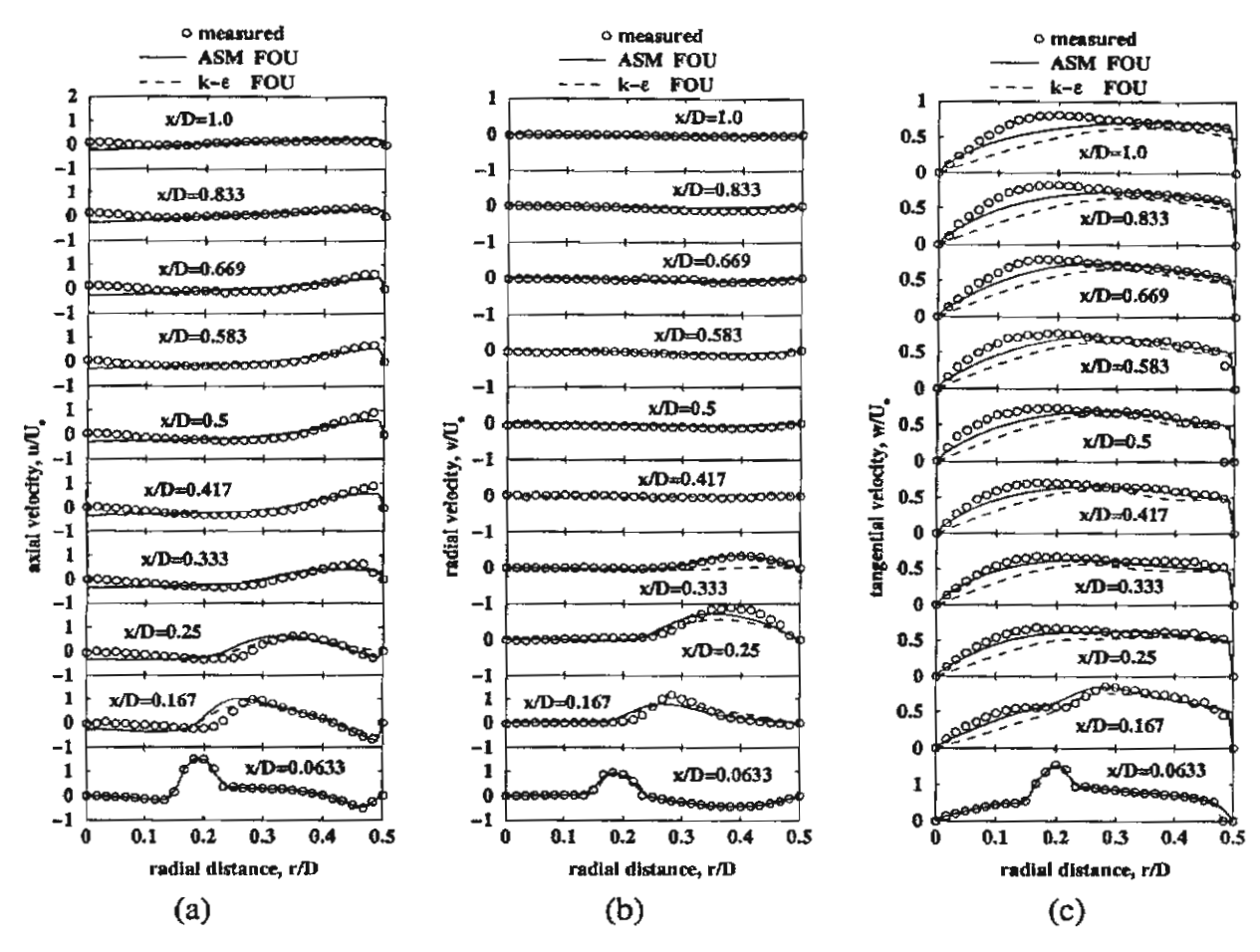


Fig. 3 Comparison of predicted velocity profiles with measurements; (a) axial velocity, (b) radial velocity and (c) tangential velocity profiles.

Streamlines predicted by the ASM and the k- $\varepsilon$  model are shown in Figs. 4 and 5 respectively. The contour plot of streamlines is in a range of x/D = 0 to 3 and r/D = 0 to 0.5, which has a high change of velocities. From the figures, there is no change of velocities at about x/D = 1.5 for the ASM and at some x/D = 3 for the k- $\varepsilon$  model. Two recirculation zones are identified; one is at the corner and the other, an internal recirculation zone (IRZ) or central